Physiology of the Extended Amygdala

by

Darrell Haufler

A dissertation submitted to the

Graduate School – Newark

Rutgers, The State University of New Jersey

in partial fulfillment of the requirements

for the degree of

Doctor of Philosophy

Graduate Program in Behavioral and Neural Sciences

written under the direction of

Denis Paré

and approved by

_____

_____

_____

_____

_____

Newark, New Jersey

October, 2017

ABSTRACT OF THE DISSERTATION

Physiology of the extended amygdala

By Darrell Haufler

Dissertation Director: Prof. Denis Paré

Based on anatomical similarities, it has been argued that the amygdala, bed nucleus of the stria terminalis (BNST) and adjacent components of the basal forebrain constitute a single system, termed the extended amygdala, which plays a critical role in emotions. In the first part of this thesis, I studied the role of BNST in the genesis of conditioned fear by recording neurons in the anterolateral (AL) and anteromedial (AM) regions of BNST in rats. During habituation, few neurons were responsive to the conditioned stimulus (CS). After fear conditioning, 20% of BNST-AL neurons developed inhibitory responses to the CS. In BNST-AM, 26% of neurons developed positive CS responses. Activity of BNST-AM and AL neurons during contextual fear paralleled their CS responsiveness, suggesting they exert opposite influences on fear output networks. During these experiments, I observed a hitherto unreported rhythm at ~140 Hz (termed *high frequency oscillations* or HFOs) in the local field potential of BNST. The second part of my thesis characterized HFOs, revealing a systematic dependence on behavioral state, a pronounced relationship to extended amygdala unit activity, coherence between distant sites, and coupling with lower frequency gamma activity. However, the origin, and nature of the HFO-gamma relationship remained unclear. This was explored in the last part of my thesis. I found that

HFOs and gamma are related through a generic phenomenon, manifest throughout the brain, whereby novel rhythms arise when signals combine in the presence of a non-linearity.

Acknowledgements and Dedication

I would like to thank my committee members: Bart Krekelberg, James Tepper, Joan Morrell, and Elizabeth Bauer, as well as all CMBN faculty and staff with whom I've had the privilege of working. To the animal facility staff: A special thank you for taking good care of my rats. I am grateful to the Natural Sciences and Engineering Research Council of Canada and the Rutgers BNS Program whose financial support made this work possible.

It has been greatly enriching working alongside my colleagues in the Paré-lab and throughout CMBN. To everyone who looked over my shoulder while I learnt a new technique, gave feedback on my work, or helped to realize a nascent idea: Thank you for your patience and for not holding back criticism. Denis, you let me explore many unknown paths and you had an uncanny knack for getting me back on track when I hit a dead end. Our discussions and arguments brought out my best.

I dedicate this thesis to my parents, Walter and Suzanne, who nourished the interests that started me on this journey, and my wife GP who helped me see it through.

Preface

The work described in Chapter II resulted from a collaboration between myself and Frank Nagy. The references of the papers that form Chapters II-IV are:

Haufler D, Nagy FZ, Paré D (2013) Neuronal correlates of fear conditioning in the bed nucleus of the stria terminalis. *Learning and Memory,* **20**:633-41.

Haufler D, Paré D (2014) High frequency oscillations are prominent in the extended amygdala. *Journal of Neurophysiology*, **112**:110-9.

Haufler D, Paré D (2017) *De novo* emergence of brain oscillations through nonlinear signal integration. *In preparation.*

During my doctoral studies, I also contributed to the following papers not included in this thesis:

Headley DB, DeLucca MV, Haufler D, Paré D (2015) Incorporating 3D-printing technology in the design of head-caps and electrode drives for recording neurons in multiple brain regions. *Journal of Neurophysiology,* **113**:2721-32.

Lee SC, Amir A, Headley DB, Haufler D, Paré D (2016) Basolateral amygdala nucleus responses to appetitive conditioned stimuli correlate with variations in conditioned behavior. *Nature Communications*, **7**:12275.

Lee SC, Amir A, Haufler D, Paré D (2017) Differential recruitment of competing valence-related amygdala networks during anxiety. Forthcoming in *Neuron*.

Table of Contents

List of Tables

List of Illustrations

List of Abbreviations

ACh	acetylcholine
AON	anterior olfactory nucleus
AW	active waking
BLA	basolateral amygdala
BM	basomedial amygdala
BNST	bed nucleus of the stria terminalis
CeA	central nucleus of the amygdala
CeL	lateral division of the central nucleus of the amygdala
CeM	medial division of central nucleus of the amygdala
CR	conditioned response
CS	conditioned stimulus
CSD	current source density
EBMA	extreme behavioral manifestations of anxiety
EPM	elevated plus maze
GABA	gamma aminobutyric acid
$GABA_AR$s	ionotropic gamma aminobutyric acid receptors
HFO	high frequency oscillation
IL	infralimbic prefrontal cortex
PL	prelimbic cortex
ING	interneuron network gamma
IPAC	interstitial nucleus of the posterior limb of the anterior commissure
LFP	local field potential
mAChRs	muscarinic acetylcholine receptors
mGluRs	metabotripic glutamate receptors
nAc	nucleus accumbens
NBM	nucleus basalis magnocellularis
OFC	orbitofrontal cortex
pII	phase interaction information
PING	principal cell-interneuron network gamma
PTSD	post-traumatic stress disorder
QW	quiet waking
REM	rapid eye movement sleep

SI	substantia innominata
SLEAc	sublenticular extended amygdala central division
SLEAm	sublenticular extended amygdala medial division
SWS	slow-wave sleep
UR	unconditioned response
US	unconditioned stimulus

CHAPTER I

Introduction

1.1 OVERVIEW

The theoretical physicist Werner Heisenberg wrote: “We have to remember that what we observe is not nature herself, but nature exposed to our method of questioning”. The series of questions asked throughout my PhD centered around activity in the extended amygdala and how it is shaped. As I describe below, they led from an established behavioral paradigm to a novel view of the structure of neural activity.

When I began my doctoral studies, my goal was to shed light on the role of the bed nucleus of the stria terminalis (BNST) in the genesis of fear and anxiety. The first data chapter reflects this objective. In this study, I recorded BNST neurons in rats subjected to a classical fear conditioning paradigm. However, over the course of these experiments, I noticed a rhythm at ~140 Hz in the local field potential (LFP) of the BNST. This rhythm, which we termed high frequency oscillations (HFOs), had never been described in the BNST and it intrigued me. This led me to conduct a series of experiments aiming to characterize HFOs, as described in the second data chapter of this thesis. Although these studies revealed that HFOs entrain the activity of a high proportion of BNST neurons, HFOs exhibited a number of unusual properties that could not be easily accounted for by standard mechanisms. During the next three years, I tested various hypotheses for HFO genesis to no avail. As described in the third data chapter of this thesis, this led to an altogether novel mechanism accounting for certain properties of HFOs. Moreover, this mechanism, and the

tools developed to study it, seem widely applicable to activity throughout the brain.

This introduction is organized as follows. In the first part I will summarize the current state of knowledge regarding the role of the BNST and related structures in the genesis of fear and anxiety. This section will set the stage for the first data chapter of my thesis. The second part of the introduction will focus on the genesis of field potentials and neuronal oscillations so that readers can more easily understand the context of the second and third data chapters.

1.2 FEAR, AMYGDALA, AND BNST

1.2.1 Early roots

In the early 1900's, Kluver and Bucy reported that ablation of the temporal lobes in monkeys resulted in strange behavioral changes (Kluver and Bucy, 1939). These included the diminished fear responses, indiscriminate responding to all presented stimuli, the seeking of sexual gratification undiscerningly, and ingestion of non-food objects. Although most of these changes were later observed following lesions largely restricted to the amygdala (reviewed in Gloor, 1960), it became generally believed in the field that damage to the amygdala was responsible for the loss of fear whereas the other behavioral aberrations resulted from the lesion of neighboring structures. This notion was strengthened by parallel studies implicating the amygdala in the genesis of learned and innate fear (Kellicut and Schwartzbaum, 1963; Blanchard and Blanchard, 1972; LeDoux, 1993). Soon, Pavlovian fear conditioning became the dominant

laboratory model to study how animals associate innate fear responses to new stimuli or contexts.

1.2.2 The role of the amygdala and BNST in conditioned fear

In classical (or Pavlovian) fear conditioning, an initially neutral conditioned stimulus (CS) comes to elicit conditioned fear responses (CRs) after pairing with a noxious unconditioned stimulus (US). In *cued* fear conditioning, the CS is a salient sensory stimulus such as a pure tone, burst of white noise, or bright light, whereas in *contextual* fear conditioning, the CS is the ensemble of the sensory cues present in the environment where conditioning takes place. However, even in cued fear conditioning, animals also learn about the context where they are trained such that later exposure to the context elicits low levels of fear.

Early findings suggested that conditioned fear memories depend on a simple circuit located entirely in the amygdala: a convergence of information about the CS and US arrives at neurons of the lateral amygdala (LA), and leads to the strengthening of synapses conveying CS inputs. Subsequent presentations of the CS would elicit defensive behaviors via projections of LA to the central amygdala (CeA), and from there to brainstem and hypothalamic networks involved in the genesis of fear responses (reviewed in LeDoux, 1995).

Consistent with this model, it was found that CeA lesions abolish conditioned fear to discrete CSs. However, CeA lesions had inconsistent effects on the expression of contextual fear with some studies reporting that CeA lesions reduce contextual freezing (Sullivan et al., 2004; Goosens and Maren, 2001,

2003), whereas others did not (Fanselow and Kim, 1994; Walker et al., 2009; Pitts et al., 2009).

Based on the observations that BNST lesions impair contextual fear but not cued fear unless the CS is very long (reviewed in Gungor and Paré, 2016), Walker, Miles, and Davis (2009) suggested that the amygdala and BNST play complementary roles in fear and anxiety. They proposed that BNST generates sustained anxiety-like responses to diffuse or non-specific environmental threats whereas CeA mediates defensive behaviors in response to imminent danger. Before considering the value of this model, I briefly review the anatomy and connectivity of the amygdala and BNST.

1.2.3 Anatomy of the amygdala and BNST

1.2.3.1 Amygdala. The amygdala consists of many interconnected nuclei usually divided into three groups: the basolateral complex (BLA), the centromedial nuclear group, and a group of cortical regions (Pape & Paré, 2010, Sah et al, 2003). The BLA is nonlaminar but contains cell types closely resembling cortical neurons: a majority of glutamatergic cells with spiny dendrites and a minority of aspiny GABAergic local-circuit cells. The BLA consists of the lateral, basolateral and basomedial nuclei (LA, BL and BM respectively) and is the primary input site of the amygdala for sensory information. The centromedial nuclear group resembles the striatum in that GABAergic neurons constitute the principal cell type (Pape & Paré, 2010, Sah et al, 2003). It consists of two nuclei, the medial and central amygdala (MeA and CeA), with the latter including medial

and lateral subdivisions (CeM and CeL respectively). Most amygdala projections to the brainstem involved in fear expression originate in CeM.

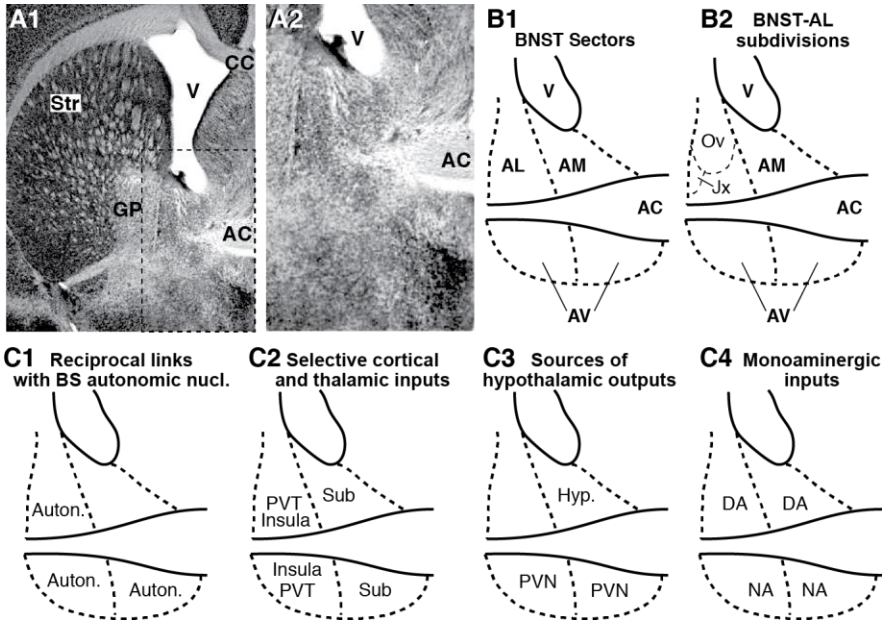

Figure 1. Structure and main connections of BNST. **A.** Anterior BNST at low (1) and high (2) magnification. Coronal sections processed to reveal NeuN immunoreactivity. **B.** Nomenclature. **C.** Connections. Two major fiber bundles, the intra-BNST segment of the stria terminalis (ST) and the anterior commissure (AC) naturally divide the anterior part of BNST in three sectors: Dorsal to the AC, are the AL and AM sectors, located lateral and medial to the ST, respectively. Ventral to the AC, is the AV region. In contrast with BNST-AL, BNST-AM receives little or no CeA inputs (see references in main text), it does not project to brainstem autonomic centers (**C1)** and it is innervated by largely distinct cortical areas and thalamic nuclei (**C2**). Moreover, its hypothalamic projections are comparably massive (**C3**). Although the connectivity of the lateral and medial portions of BNST-AV is similar to that of BNST-AL and AM, respectively, it must be considered separately because of its heavy noradrenergic innervation, among the densest in the brain (**C4**), as well as its strong projections to the ventral tegmental area (VTA) and paraventricular nucleus of the hypothalamus (PVN). Abbreviations: AC, Anterior commissure; Auton, Autonomic centers; BS, Brainstem; CC, Corpus callosum; DA, Dopamine; GP, Globus pallidus; Hyp, Hypothalamus; Jx, Juxtacapsular; NA, Noradrenaline; Ov, Oval; PVN, Paraventricular nucleus of hypothalamus; PVT, Paraventricular nucleus of thalamus; Sub, Subiculum; Str, Striatum; V, Ventricle. Reproduced with permission from Gungor and Paré (2016).

1.2.3.2 BNST structure. Although its name suggests otherwise, BNST is a group of nuclei. However, there is considerable controversy regarding their location and number (Moga et al., 1989 and Ju and Swanson, 1989a,b). Posterior BNST nuclei are thought to regulate reproductive behaviors (Simerly, 2002) and will not be discussed further here. Fear and anxiety researchers have

focused on the anterior part of BNST (LeDoux et al., 1988) since it is the principal termination region of CeA inputs (Krettek and Price, 1978a). Although many have identified multiple subnuclei in the anterior region of BNST, they are too small to be selectively targeted during *in vivo* experiments and, generally, neighboring nuclei have similar connections. Thus, in our laboratory, we have adopted a regional subdivision of BNST based on connectivity. Using this criterion, we divide BNST in three regions: an anterolateral sector (AL), an anteromedial sector (AM), and an anteroventral sector (AV). See Figures 1 and 2 for a summary of these connections.

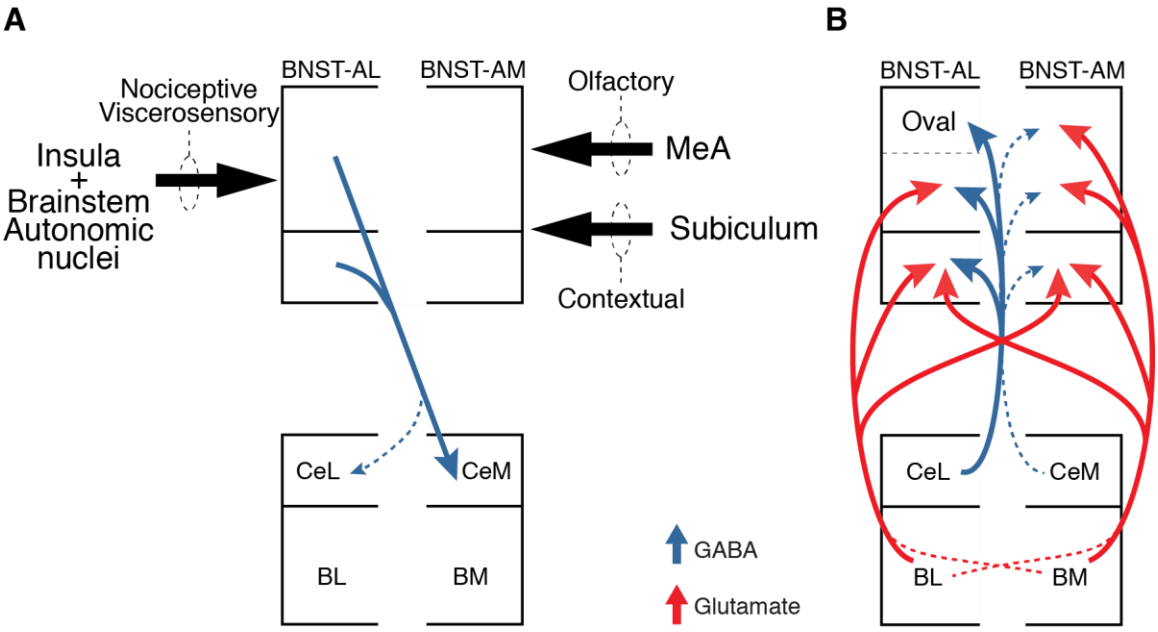

Figure 2. Reciprocal connections between the amygdala and the anterior part of BNST. (**A**) BNST projections to the amygdala. Dominant sensory inputs are also indicated by black arrows. Abbreviations: MeA, medial nucleus of the amygdala. (**B**) Amygdala projections to BNST. Reproduced with permission from Gungor and Paré (2016).

1.2.3.3 BNST cell types. Most BNST-A cells, including projection neurons, are GABAergic (Cullinan et al., 1993; Sun and Cassell, 1993; Polston et al., 2004; Poulin et al., 2009). These cells express different combinations of various

peptides (Gray and Magnuson, 1987; Ju et al., 1989b; Moga et al., 1989). This is the case for CRF cells located in the dorsal region of BNST-AL, termed the oval nucleus (Sakanaka et al., 1987; Phelix and Paull, 1990). Besides the main group of GABAergic cells, BNST-AM and AV also contain a small number of glutamatergic neurons (Poulin et al., 2009), a subset of which project to the brainstem (Kudo et al., 2012).

1.2.3.4 Intrinsic connectivity of BNST. BNST cells form connections with neurons located in the same or other BNST regions (Dong and Swanson, 2003, 2004, 2006a-c; Turesson et al., 2013). Inhibitory *intra-regional connections* are more important than glutamatergic ones except in BNST-AV (Turesson et al., 2013). Depending on the nuclei involved, *inter-regional connections* can be reciprocal or asymmetric, inhibitory or involving a mixture of glutamatergic and GABAergic connections (Turesson et al., 2013). For instance, BNST-AL outputs to other anterior BNST regions are purely GABAergic and much stronger than connections in the opposite direction. Thus, when the activity of GABAergic BNST-AL neurons is reduced, BNST-AM cells might be disinhibited.

1.2.3.5 Role of the BNST-AL region. Several lines of evidence suggest that BNST-AL exerts anxiolytic influences. Among them, stimulation of BNST-AL *lowers* corticosterone levels (Dunn, 1987) whereas lesions of BNST-AL *enhance* stress-induced gastric erosions (Henke, 1984). In addition, intra-BNST infusions of calcitonin gene-related peptide, which inhibit BNST-AL neurons (Gungor and Paré, 2014), cause an enhancement of *fos* expression in the targets of BNST-AL while increasing acoustic startle (Sink et al., 2011). These findings appear to

contradict the widespread notion that through the CRF neurons found in its oval nucleus, BNST-AL exerts anxiogenic effects. Indeed, infusions of CRF in BNST induces signs of anxiety (Sahuque et al., 2006) and stressors enhance CRF mRNA expression in BNST-AL and AV, suggesting that CRF cells are recruited during stress (Daniel and Rainnie, 2015). In support of this idea, chemo- and optogenetic inhibition of CRF cells decrease manifestations of anxiety (Pleil et al., 2015; Kim et al., 2013). However, it remains unclear how CRF cells are recruited by stressors to begin with: As the oval nucleus is devoid of inputs from the amygdala, how are CRF cells informed of environmental contingencies? Indeed, most of the inputs thought to convey information about contexts (from subiculum) and predators (from medial amygdala) target other BNST sectors (Cullinan et al., 1993; McDonald et., 1999; Dong et al., 2001a), Instead, the oval nucleus mainly receives viscerosensory inputs from the insula (McDonald et al., 1999; Reynolds et al., 2005) and autonomic nuclei of the brainstem (Saper and Loewy, 1980; Schwaber et al., 1982). In principle, the anxiogenic influence of BNST-AL CRF cells depends on CRF effects in BNST itself or in its brainstem targets (Gray and Magnuson, 1987, 1992). However, somatic expression of CRF-R1 mRNA was reported to be low in BNST (Potter et al., 1994; van Pett et al., 2000; Dabrowska et al., 2013). As to CRF's post-synaptic effects, various mechanisms, in many cases with opposite consequences, have been reported (Kash et al., 2008; Nobis et al., 2011; Silberman et al., 2013; Ide et al., 2013; Nagano et al., 2015) and thus it is not clear how CRF generates anxiety.

1.2.3.6 Role of the BNST-AM region. In contrast with the connections of BNST-AL, those of BNST-AM are well suited for generating anxiety. In particular, most of the signals required for the recruitment of BNST by threatening stimuli, namely sensory inputs from the BLA, contextual information from the subiculum, and olfactory inputs from the medial amygdala end in BNST-AM (Cullinan et al., 1993; McDonald et al., 1999; Dong et al., 2001a). Moreover, BNST-AM strongly projects to the ventromedial hypothalamus (VMH), which is known to generate aggressive and defensive behaviors (Gross and Canteras, 2012; Silva et al., 2013; Lee et al., 2014; Wang et al., 2015). Interestingly, the core of VMH, which contains VMH's output cells, receives glutamatergic inputs from amygdala, particularly BM (Petrovich et al., 1996), whereas BNST-AM projects to the shell of VMH (Dong and Swanson, 2006a). Because the shell of VMH contains GABAergic neurons that inhibit core neurons (Fu and van den Pol, 2008), the BM and BNST-AM might act synergistically to enhance the excitability of VMH core neurons, the former through a direct excitation and the latter through disinhibition.

However, the above model stands in sharp contrast with two recent studies where it was found that BM and BNST-AM exert an anxiolytic influence (Kim et al., 2013; Adikhari et al., 2015). Given that the common projection of BM and BNST-AM to the VMH and the projections of BM to CeM, this conclusion is puzzling. However, it is possible that these paradoxical conclusions resulted from the misinterpretation of predatory or active avoidance behaviors for decreased levels of anxiety in the elevated plus maze or open field.

1.2.4 Interactions between BNST and the amygdala.

Most sensory afferents to BNST reach it indirectly, through the major glutamatergic inputs it receives from the basal nuclei of the amygdala (BL and BM; Krettek and Price, 1978a; Weller and Smith, 1982; Dong et al., 2001a). This massive input likely plays a pivotal role in regulating how organisms respond to their environment. According to the model proposed by Davis and colleagues (Walker et al., 2009), basal amygdala nuclei would convey threat signals to BNST and CeA in parallel. In turn, neurons in CeM would be activated rapidly, recruiting brainstem fear networks. By contrast, the recruitment of BNST would not only depend on BM and BL inputs, but also on CRF afferents arising in CeL. Consequently, the activation of BNST would be delayed with respect to CeM's, causing the slow and longer lasting emergence of anxiety-like states in response to sustained but diffuse threats. This hypothesis also stipulates that once BNST has been activated, it inhibits CeM, precluding involvement of the later in anxiety-like states. As discussed below, there is evidence for and against this model.

On the positive side, CeA lesions were generally not found to interfere with aversive responses to unconditioned threats like predator odors (Fendt et al., 2003) or bright lights (Waker and Davis, 1997). Moreover, the expression of conditioned fear responses to contexts or long CSs was generally not blocked by CeA lesions (Fanselow and Kim, 1994; Pitts et al., 2009; Walker et al., 2009; however, see Sullivan et al., 2004; Goosens and Maren, 2001). At odds with the model however, it was found that the difference in freezing between sham and

BNST-lesioned animals during exposure to a threatening context is constant even though the model predicts augmenting differences with time (Hammack et al., 2015).

In further opposition with the model, it was found that intra-BNST infusions of muscimol enhance fear-potentiated startle (Meloni et al., 2006), not only indicating that BNST participates in the processing of discrete CSs but also that it tonically inhibits CeA or a common target. Consistent with this, Duvarci et al. (2009) found that excitotoxic BNST lesions enhance the specificity of conditioned fear to discrete cues.

Overall, the available evidence indicates that while BNST is not essential for the expression of conditioned defensive behaviors to discrete CSs, it seems equally clear that BNST regulates how such cues are processed. Consistent with this, BNST does project to the amygdala (Sun and Cassell, 1993; Dong et al., 2001b; Bienkowski and Rinaman, 2013). In particular, the anterolateral and anteroventral sectors of BNST send robust projections to CeM (mainly GABAergic; Gungor et al., 2016), and to a lesser extent, to CeL. Moreover, CeL, but less so CeM, project back to BNST-AL.

In my first data chapter, I will further test the Walker et al. model by recording BNST neurons in rats subjected to a differential auditory fear conditioning paradigm.

1.3. GENESIS OF FIELD POTENTIALS AND NEURONAL OSCILLATIONS

1.3.1 Genesis of field potentials.

Key to understanding neuronal oscillations is the genesis of field potentials. Due to the electrical properties of neuronal membranes, transmembrane currents occurring mainly through voltage- or ligand-gated ionic channels cause spatially non-uniform changes in intracellular potential, resulting in further current flow between regions that have different potentials (Hubbard et al., 1969). As current flows longitudinally within neurons, some leaks through the membrane back to the extracellular environment, closing the current loop. Because of the resistive properties of the extracellular space, this situation sets up an electric field so that extracellular electrodes near the originating vs. return currents detect potentials of opposite polarities, often referred to as a dipole.

While voltage-gated currents can contribute to extracellular field potentials, particularly if many neurons fire synchronously, synaptic activity is usually the main contributor (Buzsaki et al, 2012). The extracellular potentials generated by synaptic inputs to different cells sum linearly. That is, potentials of the same polarity add up whereas potentials of opposite polarity cancel each other. In structures where neurons have randomly oriented dendrites, much cancellation occurs. By contrast, in cortex where neurons exhibit a regular morphological polarization, the layered arrangement of afferents favors the summation of extracellular potentials, a situation termed open field. As a result, the potentials generated by open fields tend to be larger and can be recorded at

significant distances from their site of origin, a phenomenon termed volume conduction.

1.3.2 Neuronal oscillations.

Oscillations are highly conspicuous features of neurophysiological data. Recording from the olfactory bulb of anesthetized rabbits, Adrian (1950) characterized two modes of activity corresponding to what would now be considered the low and high gamma range: Oscillations directly evoked by olfactory stimulation in the frequency range of 50 - 60 Hz, and spontaneous or *intrinsic* oscillations in the range of 70 - 100 Hz. Under light anesthesia and during presentation of an odorant, the intrinsic activity showed continuous interruption by the evoked pattern (50 – 60 Hz) upon each inhalation of the animal. The intrinsic activity was present even following the destruction of the olfactory epithelium and disconnection from the forebrain. Adrian speculated that if the evoked activity reflected the maximum frequency of the direct olfactory pathway (known through the work of Cajal), the intrinsic activity must have a different origin, suggesting what are now known to be interneurons:

> Although the mitral cells certainly take part in this activity there is some reason to suppose that it originates in cells of another type, possibly the smaller “cells with short axons” (Cajal) which are arranged in layers below the mitral cells. (Adrian, 1950).

Since the work of Adrian, many different neural oscillations have been described in a variety of brain structures (Buzsaki and Draguhn, 2004). Each is differentially expressed across behavioral states with unique implications for normal and pathological brain function. The cellular basis of many oscillations is well understood. Well-characterized examples include theta activity in the hippocampus during paradoxical sleep and exploratory behavior (Buzsaki, 2002), spindles in the thalamus and cortex during deep slow-wave sleep (SWS; Steriade et al., 1993), and gamma oscillations in the olfactory bulb (Laurent, 2002) and in various cortical and subcortical regions (Headley & Paré, 2013).

1.3.2.1 General properties of oscillations. Neuronal oscillations arise from the interplay between the intrinsic properties of neurons (Llinas, 1988; Whittington and Traub, 2003) and the architecture of the network in which they are embedded (Steriade and Llinas, 1988). Supporting the idea that these rhythms fulfill critical signaling functions, neural oscillations are well conserved across mammalian species (Buzsaki et al., 2013) and in some cases, phyla (Kay, 2015). Indeed, oscillations provide an energy efficient way to coordinate interactions within and between networks by creating alternating periods of increased and decreased neuronal excitability. As a result, oscillations allow for the selective routing of information and the flexible formation of cell assemblies based on phase (Buzsaki and Draguhn, 2004; Fries, 2015; Sejnowski and Paulsen, 2006).

Oscillations range widely in frequency (~0.1-300 Hz). Generally, lower frequency rhythms recruit larger networks than faster rhythms (Steriade et al.

1993; Konig et al., 1995). Also, the power of the faster oscillations typically changes as a function of the phase of the slower ones (Bragin et al., 1995; Steriade et al., 1996). Although the amplitude of oscillations generally decreases as their frequency increases (Nunez and Srinivasan, 2006), in specific networks and functional contexts some rhythms deviate from this global trend and become more pronounced (Gray et al., 1989; Singer, 1999). Depending on the brain region and behavioral state, oscillations of distinct frequencies predominate, but many can coexist and interact in the same or different networks (Buzsaki and Draguhn, 2004). At any given moment, LFPs exhibit a continuously evolving mixture of oscillatory components, which are thought to reflect interactions between different local circuit elements with different oscillatory propensities.

1.3.2.2 State-dependent changes in neuronal oscillations.

During wakefulness and paradoxical sleep, LFPs recorded from a variety of structures (e.g. neocortex, amygdala, striatum) exhibit high frequency low amplitude oscillations, referred to as gamma oscillations. In contrast, during slow-wave sleep (SWS), high amplitude slow waves prevail. During SWS, low frequency components (<1-4 Hz), sometimes termed slow oscillations or delta oscillations are particularly conspicuous (Steriade, 1997). These oscillations are comprised of a depth-negative phase that coincides with augmented firing in cortical cells, and a depth-positive phase during which neurons are silent. This oscillation is also observed in a number of subcortical structures (e.g. thalamus,

striatum) (Steriade et al., 1993; Wilson and Kawaguchi, 1996) as a result of cortical inputs (Timofeev et al., 1996).

Another oscillation observed during SWS are sleep spindles, which consist of short periods (1-2 s) of oscillations at 7-14 Hz that recur every 3-10 s in much of the neocortex (Dempsey and Morison, 1942). Spindles arise from interactions between thalamocortical cells and reticular thalamic neurons (Steriade, 1997). In addition, faster oscillations in the beta and gamma range are also observed during the excitatory (depth-negative) phase of the slow oscillation (Steriade et al., 1996). However, these faster rhythms appear much more prominent during wakefulness and rapid eye movement sleep when the slow rhythms vanish.

During paradoxical sleep, arousal, and locomotion, the LFP in the hippocampus exhibits a prominent oscillation in the 6-10 Hz range theta range (Buzsaki et al., 1983), which is associated with rhythmic amplitude modulation of gamma waves (Bragin et al., 1995; Chrobak and Buzsaki, 1996, 1998). Hippocampal theta depends on inputs from the medial septum (Petsche et al., 1962) and entorhinal cortex (Buzsaki, 2002). In contrast, during SWS, hippocampal LFPs are dominated by high amplitude slow waves of various frequencies as well as brief large amplitude potentials (sharp waves) which are associated with a transient increase in the amplitude of very fast oscillations (~200 Hz) termed ripples (Buzsaki et al., 1992; Ylinen et al., 1995). Sharp waves and ripples also occur when animals are immobile or engaged in consummatory behaviors.

Since different states of vigilance have different oscillatory correlates in the neocortex and hippocampus, and considering that these structures project to the amygdala and BNST, these structures are in a good position to express both sets of rhythms. Consistent with this, it was reported that during slow-wave sleep, the BLA exhibits the slow/delta oscillations but no spindles (Collins et al., 2001). The slow oscillations are associated with large changes in firing probability, precluding the possibility that they are volume conducted from adjacent cortical areas. Moreover, during REM sleep and fear expression, the BLA shows theta oscillations, which also entrain neuronal firing (Paré and Gaudreau, 1996). Last, gamma oscillations have also been observed in the BLA (Bauer et al., 2007; Popescu et al., 2009; Stujenske et al., 2014). In contrast, no information was available regarding BNST oscillations when I began my doctoral studies.

Below, I briefly review the properties of the fast rhythms that will figure prominently in the last two data chapters of my thesis.

1.3.2.3 Gamma oscillations. In addition to the olfactory bulb, several structures show alternating periods of low and high frequency gamma oscillations. Low gamma in the CA1 region of the hippocampus is coherent with low gamma oscillations in CA3, and this activity is thought to originate locally in the hippocampus because CA3 slice preparations can generate similar activity following activation of mAChRs. In contrast, high gamma oscillations in CA1 are coherent with the entorhinal cortex (EC), and the CA1 activity is thought to depend on rhythmic synaptic input from the EC (Colgin et al, 2009; Zemankovics

et al, 2013). In the striatum, low gamma dominates during active waking and shows highest coherence with the piriform cortex. In contrast, high gamma is unrelated to piriform activity and is coherent with the frontal cortex (Berke, 2009). In both hippocampus and striatum, fast spiking interneurons, thought to consist largely of parvalbumin positive (PV+) basket cells, fire in synchrony with gamma oscillations (Tukker et al, 2007). Hippocampal slices can generate gamma oscillations in response to various pharmacological manipulations. By mimicking cholinergic afferents from the medial septum, activiation of mAChRs on CA3 pyramidal cells elicits a form of low gamma that is sensitive to AMPA and $GABA_AR$ antagonists (Fellous and Sejnowski, 2000; Fisahn et al. 1998). In contrast, gamma generated through activation of mGluR and kainate receptors, thought to be mainly expressed by interneurons, is only sensitive to $GABA_AR$ antagonists (Whittington et al, 1995; Fisahn et al, 2004).

Based on these hippocampal slice experiments, computational models of these two different modes of gamma have been developed: *Principal cell-interneuron network gamma* (PING) depends both excitatory and inhibitory cell types, while *interneuron network gamma* (ING) only depends on the latter (Whittington et al, 2000). As this thesis focuses on BNST and related structures, most of which have an inhibitory principal cell type, the ING model would seem to be the candidate mechanism for the fast oscillations observed. Robust oscillations via ING are promoted by fast membrane kinetics, the inclusion of action potential propagation delays between neurons, and dendritic gap junctions between reciprocally connected inhibitory cells (Bartos et al., 2007). In the

hippocampus, basket cells are thought to be a primary contributor to gamma oscillations because they are mutually connected, fire at high frequencies phase locked to gamma, exhibit an intrinsic resonance at the appropriate frequency, and are coupled by gap junctions (Bartos et al., 2007).

1.3.2.4 Very high frequency oscillations. In addition to gamma oscillations and sharp wave ripples, other high-frequency rhythms have been described. The following will not deal with ultra-fast rhythms seen in epileptic tissue but focus on a rhythm that figures prominently in my second and third data chapters: high-frequency oscillations (HFOs) at 130-150 Hz. HFOs are observed more readily in inbred rat strains unless subjects are administered N-methyl-D-aspartate (NMDA) receptor antagonists, in which case HFOs also become conspicuous in outbred strains. The state induced by partial NMDA receptor blockade is considered a model of schizophrenia (Gonzalez-Burgos and Lewis, 2012). Indeed, schizophrenia symptoms develop in healthy humans when ketamine or phencyclidine are administered (Javitt and Zukin, 1991; Uhlhaas and Mishara, 2007). In rodents, the same treatments cause a sustained enhancement of HFOs in the extended amygdala and nearby structures (Hunt and Kasicki, 2013). Interestingly, this effect is mimicked by hallucinogenic drugs (Goda et al., 2013) and blocked by atypical antipsychotics (Hunt et al., 2015).

When I began my doctoral studies, very little was known about HFOs, in part because they had only been studied with LFP recordings restricted to nucleus accumbens. Accordingly, the second data chapter of my thesis examines the properties of HFOs using unit and LFP recordings in BNST and

related structures. Through the course of these experiments, we noticed that HFOs and gamma oscillations are closely related but conventional mechanisms could not account for this relation. This led me to consider a novel mechanism for the genesis of oscillations, which will be described in the third data chapter.

CHAPTER II

Neuronal correlates of fear conditioning in the bed nucleus of the stria terminalis

Lesion and inactivation studies indicate that the central amygdala (CeA) participates in the expression of cued and contextual fear whereas the bed nucleus of the stria terminalis (BNST) is only involved in the latter. The basis for this functional dissociation is unclear because CeA and BNST form similar connections with the amygdala and brainstem fear effectors. To address this question, we recorded neurons in the anterolateral (AL) and anteromedial (AM) regions of BNST in rats subjected to auditory fear conditioning. During habituation, few neurons were responsive to the conditioned stimulus (CS). After fear conditioning, 20% of BNST-AL neurons developed inhibitory responses to the CS. In BNST-AM, 26% of neurons developed positive CS responses. The behavior of BNST-AM and AL neurons during contextual fear paralleled their CS responsiveness: more BNST-AM neurons fired at higher rates during contextual freezing than movement whereas the opposite was seen in BNST-AL cells. These findings point to regional differences in the activity of BNST-AL and AM in relation to learned fear, raising the possibility that they exert opposite influences on fear output networks. However, given the similar behavior of BNST-AM and AL neurons in relation to cued and contextual fear, it remains unclear why lesion and inactivation of BNST differentially affect these two types of fear. Either neurons in a different BNST sector, not explored here, show a different activity profile in relation to the two forms of fear or inactivation/lesion studies inadvertently affected a structure adjacent to BNST, which is involved in contextual fear.

The bed nucleus of the stria terminalis (BNST) and the central amygdala (CeA) are major components of an anatomical entity named the extended amygdala (Alheid and Heimer 1988; de Olmos and Heimer 1999). This notion stems from similarities in the morphology and transmitter content of BNST and CeA neurons (reviewed in McDonald 2003), shared inputs from the basolateral amygdala (Krettek and Prince 1978ab; Paré et al. 1995; Savender et al. 1995; Dong et al. 2001a) as well as common projections to brainstem nuclei that generate various aspects of fear/anxiety responses (Hopkins and Holstege 1978; Sofroniew 1983; Veening et al. 1984; Holstege et al. 1985; Dong et al. 2000, 2001b; Dong and Swanson 2003, 2004, 2006a-c).

Despite these anatomical similarities however, BNST and CeA appear to play different roles. For instance, local drug infusion (Kim et al. 1993; Wilensky et al. 2006), lesion (Hitchcock and Davis 1987, 1991; LeDoux et al. 1988; Campeau and Davis 1995; Jimenez and Maren 2009), optogenetic (Ciocchi et al. 2010) and unit recording studies (Duvarci et al. 2011) suggest that CeA is required for the rapid expression of conditioned fear responses to discrete sensory cues (however see Koo et al. 2004; Pitts et al. 2009), functions that are left intact by BNST lesions (Walker and Davis 1997; Gewirtz et al. 1998; Sullivan et al. 2004). Instead, BNST lesions interfere with the development of longer “anxiety-like” states in response to more diffuse environmental contingencies, responses that often persist after the threat has vanished (reviewed in Walker et al. 2003; Sullivan et al. 2004; Duvarci et al. 2009). In particular, BNST lesions were reported to disrupt corticosterone and freezing responses to contextual stimuli

that were previously associated with aversive outcomes (Sullivan et al. 2004). Importantly, dissociation between CeA and BNST functions is not only seen in aversive learning paradigms but also in response to some unconditioned stimuli (Fendt 2003).

Given their common inputs from the basolateral amygdala and overlapping projections to fear effector neurons, the basis for the functional dissociation between BNST and CeA is unclear. To shed light on this question, we recorded anterior BNST neurons in freely moving rats subjected to an auditory fear conditioning paradigm.

RESULTS

Nomenclature used to designate different BNST subregions

As shown in **figure 1**, all our recordings were obtained dorsal to the anterior commissure, in the anterior third of BNST. Previously, this BNST region was divided in multiple subnuclei based on cytoarchitectural and immunohistochemical criteria (Ju and Swanson 1989; Ju et al. 1989). However, due to the difficulty of unambiguously identifying these subnuclei in sections stained with cresyl violet, we simply divided our recording sites in two groups, based on their position relative to the intra-BNST component of the stria terminalis. Indeed, this fiber bundle separates the anterior BNST in two large sectors: medial (BNST-AM) and lateral (BNST-AL). The correspondence between these two regions and the subnuclei identified by Swanson and colleagues is as follows. BNST-AL corresponds to Swanson's oval,

juxtacapsular, and anterolateral subnuclei. BNST-AM corresponds to Swanson's anterodorsal subnucleus. Note that in more recent publications (Dong and Swanson 2006), Swanson also terms the latter region BNST-AM.

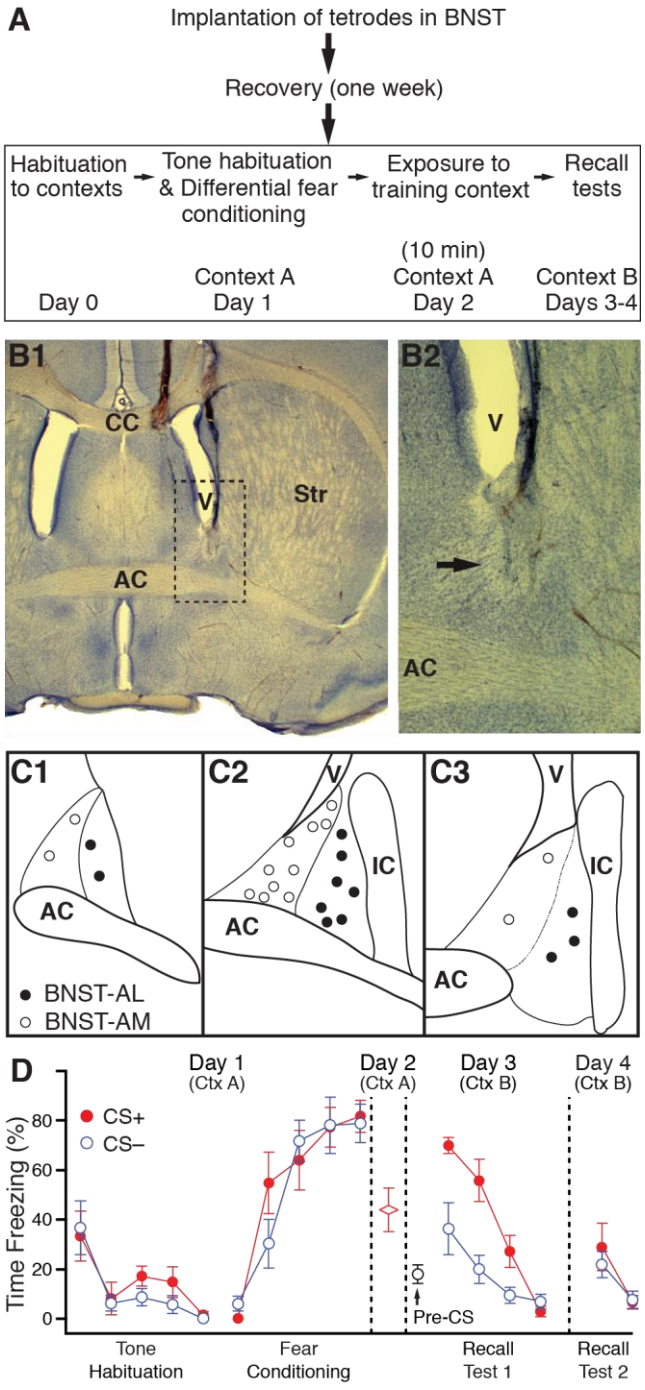

Figure 1. Experimental paradigm, location of recording sites, and behavioral results. (**A**) Experimental paradigm. After implantation of tetrodes in BNST and recovery from surgery, rats were subjected to a differential auditory fear conditioning paradigm. On day 0, rats were habituated to the training contexts A and B. On day 1, in context A, they were first habituated to the CS+ and CS- and then subjected to fear conditioning session where the two CSs were presented an equal number of time in random order with only the CS+ co-terminating with a footshock. On day 2, they were exposed to the training context A with no tone presentations to assess contextual fear. On days 3-4, to recall tests were conducted in context 5. (**B**) Histological verification of recording site. (**B1**) Photomicrograph showing a coronal section at the level of BNST-A. Arrow points to small electrolytic lesion performed at the conclusion of the experiment to mark a recording site. The area enclosed in the dashed rectangle is expanded in **B2**. Abbreviations: AC, anterior commissure; CC, corpus callosum; Str, striatum, V, ventricle. (**C**) Location of well positioned tetrodes. Three antero-posterior levels arranged from the most rostral (**C1**) to the most caudal (**C3**). Filled and empty circles represent tetrode placements in BNST-AL and AM, respectively. (**D**) Percent time (average +/- sem) the rats (n = 8) spent freezing during the CS^{+} (red circles), CS^{-} (blue circles) or during exposure to the training context (red diamond) in various phases of the behavioral protocol (x-axis). For Day 1, we plot freezing to individual CSs. For Days 3-4, blocks of 5 CSs were used to compute the averages. Empty black circle indicates pre-CS freezing during recall test 1. Note that 5 minutes elapsed between placement of the rats in context B and presentation of the first CS. Pre-CS freezing was measured the last four minutes of this period.

Database

Histological verification of recording sites (**Fig. 1B-C**) revealed that tetrodes reached their intended targets (BNST-AL and/or AM) in seven of the eight rats. Units recorded with misplaced tetrodes were excluded from the analyses. Overall, samples of 47 to 56 BNST-AL and 65 to 105 BNST-AM units were recorded on each day of the conditioning protocol. The locations of well-positioned tetrodes are shown in **figure 1C**. Electrodes were not moved during the behavioral protocol unless units were lost overnight across all tetrodes within a bundle. In such rare cases, the tetrode bundle was lowered 60 µm. Although the electrodes were generally not moved, spike shapes varied from day to day in a proportion of units. Therefore, below it is assumed that different cells were recorded on each day.

Impact of differential fear conditioning

After electrode implantation and recovery from surgery, rats were trained on cued (auditory) fear conditioning while recording BNST activity. As summarized in **figure 1A**, the behavioral protocol included habituation to the training contexts (**Fig. 1A**, Day 0) followed the next day by habituation to the auditory CS^+ and CS^-, and then differential fear conditioning in context A (**Fig. 1A**, Day 1). Twenty-four hours later, contextual fear memory was assessed in context A for 10 minutes (no CS; **Fig. 1A**, Day 2). Finally, two recall tests of cued fear memory were performed on consecutive days in context B (**Fig. 1A**, Days 3 and 4).

Figure 1D illustrates the percent time rats spent freezing during the various phases of the behavioral protocol. Red and blue circles represent freezing to the CS^+ and CS^-, respectively. The red diamond represents contextual freezing in context A. Relative to the last CS^+ and CS^- of habituation, fear conditioning caused a significant increase in freezing levels to the CS^+ (CS^+ 5, 81.9 ± 6.5%) and CS^- (CS^- 5, 78.9 ± 7.8%, paired t-tests, $p < 0.001$). The next day, in the absence of auditory stimuli, the rats exhibited robust freezing to the training context (A, 43.9 ± 8.8%, red diamond). On day 3, rats showed little freezing prior to presentation of the auditory stimuli (pre-CS freezing: 17.9 ± 3.8%; black circle) in context B. However, the first few CS^+ elicited large increases in freezing (CS^+ 1-5: 69.9 ± 3.2%) that gradually diminished with additional CS^+ presentations (CS^+ 16-20: 2.8 ± 2.2%, paired t-test, $p<0.001$). Although discrimination between to CS^+ and CS^- was imperfect, freezing to the CS^- (CS^- 1-5, 36.3 ± 10.5%) was significantly lower than to the CS^+ (paired t-test, $p = 0.002$). On Day 4, the first few CS^+ presentations again elicited freezing (CS^+ 1-5: 28.8 ± 9.5%) that extinguished with additional presentations of the CS^+ (CS^+ 6-10: 6.6 ± 2.7%).

Overall, these results suggest that the differential auditory fear conditioning paradigm used in this study led to the formation of a fear memory to the training context and CS^+. Although discrimination between the CS^+ and CS^- was imperfect, fear responses to the CS^+ were clearly stronger than to the CS^- during the first recall test.

Cellular correlates of cued fear memory in BNST-AL and AM

To analyze training-induced changes in auditory responsiveness, we first computed the firing rate of each unit in 5 sec bins, from 20 s before to 120 s after the onset of the CS^+ and CS^-. We obtained separate averages for the habituation phase (trials 3-5), the first two and last three CS^+ and CS^- of training, as well as the first and last five CS^+ and CS^- of the two recall tests. For each average, we then z-scored the data to firing rate variations seen in the pre-CS period. Next, to determine whether a CS-evoked change in firing rate was significant, we separately averaged the z-scores of each cell during the six 5-s bins of the CS^+ or CS^- and assessed whether it differed from the baseline period by ±1.96 z or more (yielding a significance threshold of $p \leq 0.05$). The results of these analyses are shown in figures 2-6, including group analyses and individual examples of significantly responsive cells.

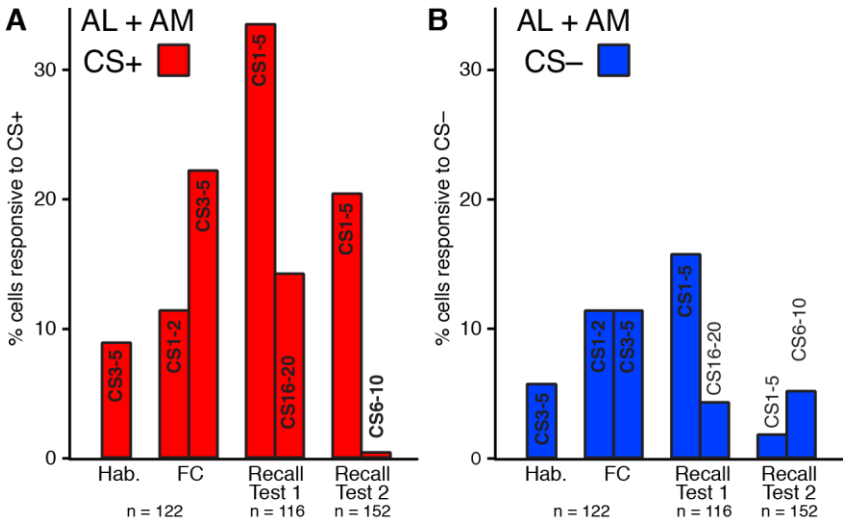

Figure 2. Differential fear conditioning alters the responses of BNST neurons in a CS-specific manner. Proportion of BNST cells (AL and AM combined) with significant responses (increased or decreased) to the CS^+ (**A**) or CS^- (**B**) during the various phases of the behavioral protocol (x-axis). The number of recorded cells is indicated at the bottom of the graphs.

Figure 2 illustrates the proportion of cells responsive to the CS^+ (**Fig. 2A1**) or CS^- (**Fig. 2A2**) in the different phases of the behavioral protocol, combining the results obtained in BNST-AL and AM. The proportion of

responsive cells changed depending on the phase of the behavioral protocol. To determine if these changes were statistically significant, we used a chi-square test. This analysis revealed a significant dependence ($p < 0.0001$) between response type to the CS^+ (response, no response) and behavioral phase (habituation, CS^+ 1-2 or 3-5 of training, first 5 or last 5 CS^+ of the two recall tests).

Paralleling our behavioral observations, the proportion of cells responsive to the CS^+ (**Fig. 2A**) and CS^- (**Fig. 2B**) was low during habituation, and it increased significantly as a result of fear conditioning (chi-square test, habituation vs. CS^+ 3-5 of training, $p = 0.003$). The proportion of responsive cells was significantly higher for the CS^+ than the CS^- at the end of training (chi-square test, $p = 0.015$). Without exception, all cells with significant responses to the CS^- were also responsive to the CS^+ and the two CSs elicited responses of the same polarity (see below). Interestingly, the proportion of CS^+-responsive cells increased further from the end of fear conditioning to the first recall test two days later (chi-square test, $p = 0.03$) and was significantly higher than that to the CS^- (chi-square test, $p = 0.001$). Additional presentation of the CS^+ during the two recall tests caused a progressive reduction in the proportion of CS^+-responsive cells such that it became statistically indistinguishable from that seen during habituation by the end of the second recall test.

In the analyses presented so far, we considered all cells with significant responses, whether these responses consisted of an increase or a decrease in firing rate. We now consider the polarity of their responses. However, because the proportion of cells with significant responses to the CS^- was low (Fig. 2B), the

following analyses will focus on CS+-evoked activity.

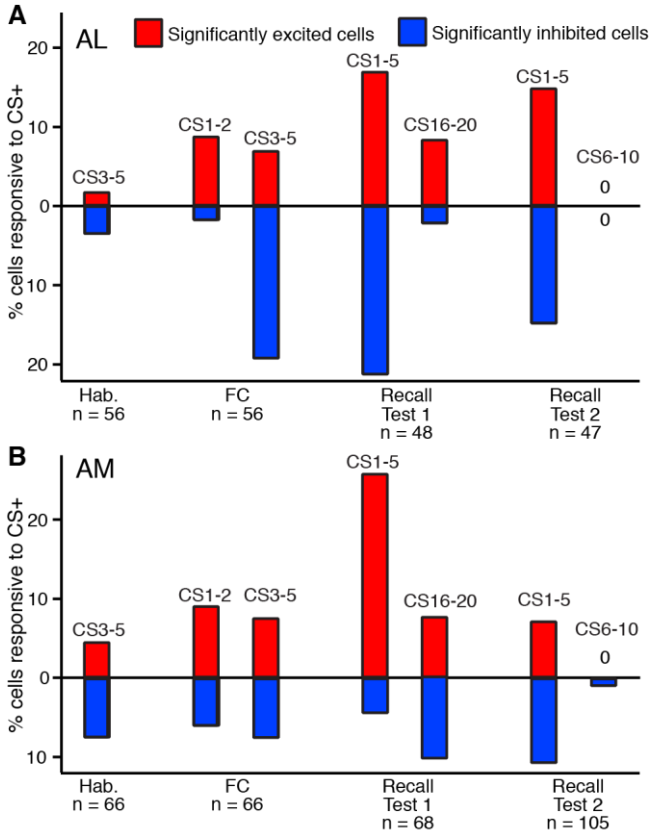

Figure 3. Opposite polarity of changes in CS responsiveness in BNST-AL vs. AM neurons. Proportion of BNST-AL (**A**) and AM (**B**) cells with significant excitatory (red) or inhibitory (blue) responses to the CS+ during the various phases of the behavioral protocol (x-axis). The number of recorded cells is indicated at the bottom of the graphs.

As shown in **figure 3**, the relative incidence of cells with inhibitory (blue; "Off-cells") vs. excitatory (red, "On-cells") responses to the CS+ differed between BNST-AL and AM. In BSNT-AL (**Fig. 3A**), fear conditioning caused a large increase in the proportion of Off-cells (CS+ 1-2 vs. 3-5 of training, chi-square test, $p = 0.0022$) with little change in the incidence of On-cells. Two days later, during the first 5 CS+ of the recall test, the incidence of Off-cells remained similarly high whereas the proportion of On-cells augmented. However, the latter change did not reach significance. With additional presentations of the CS+, roughly equal but decreasing proportions of cells showed inhibitory and excitatory responses.

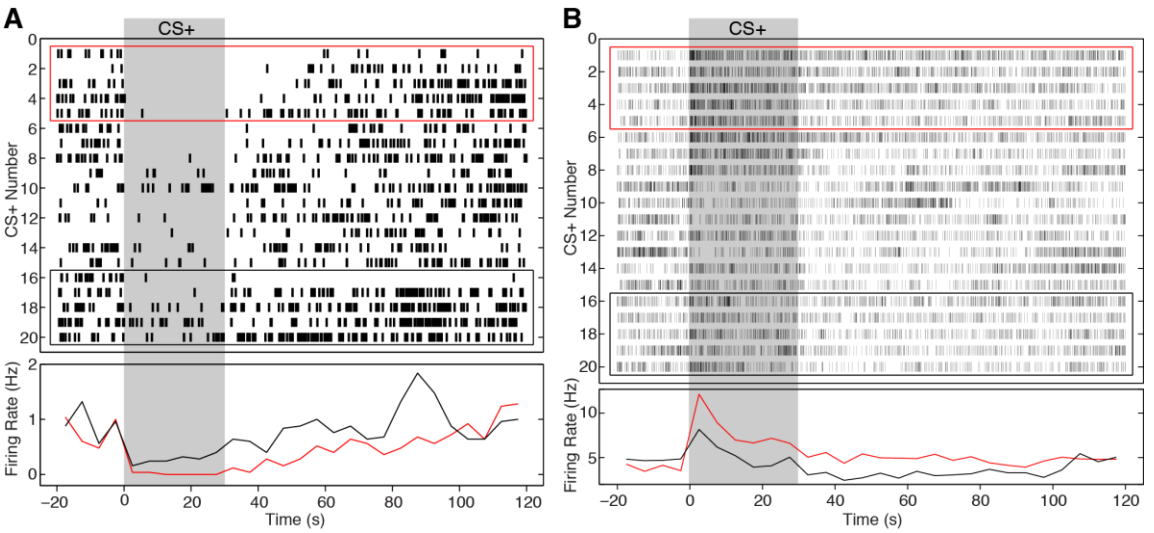

Figure 4. Examples of BNST neurons with inhibitory and excitatory CS^+ responses at recall. (**A**) BNST-AL cell with inhibitory response to the CS^+. (**B**) BNST-AM neurons with excitatory responses to the CS^+. In the **top panel** of **A** and **B**, each of the twenty horizontal lines shows the activity of the cell from the first (top) to the last (bottom) CS^+ (gray shading) of recall test 1. Each vertical tick represents one action potential. The bottom panel shows the average firing rate of the same cells during the first (red) and last (black) five CS^+.

Figure 4A illustrates a representative example of BNST-AL neuron with inhibitory responses to the CS^+ during the first recall test. In the top panel, each of the twenty lines shows the activity of the cell from the first (top) to the last (bottom) CS^+ (gray shading) of recall test 1. The bottom panel shows the average firing rate of the same cell during the first (red) and last (black) five CS^+ of the first recall test. The first five CS^+ elicited a sustained decrease in firing rate, essentially silencing the cell for the entire duration of the CS^+. Across all BNST-AL cells with inhibitory responses to the CS^+, the firing rate during the first five CS^+ of recall test 1 decreased to 27.3 ± 10.8% of baseline. Additional presentations of the CS^+ caused a reduction of the CS^+-evoked inhibition (CS^+16-20, to 48.5 ± 12.1% of baseline; paired t-test, p = 0.00011).

In contrast with the results obtained in BNST-AL, the proportion of BNST-AM units with inhibitory or excitatory responses to the CS^+ did not change on the

training day (compare CS^+ 1-2, vs. 3-5 of training in **Fig. 3B**). Two days later, during the first 5 CS^+ of the recall test, a large and significant increase in the incidence of On-cells was observed (CS^+ 3-5 of training vs. CS^+ 1-5 of recall test 1, chi-square test, p = 0.0021) with little change in the proportion of Off-cells. Additional presentations of the CS^+ reduced the incidence of On-cells.

Figure 4B illustrates a representative example of BNST-AM neuron with excitatory responses to the CS^+ during recall test 1. Typical for these cells, the increase in firing rate elicited by the CS^+ peaked during the first 5 sec of the CS and then decreased later on. Also typical for these cells, addition presentations of the CS^+ during the recall test, caused a reduction of their responses (from 137.6 ± 6.5% of baseline to 105.7 ± 4.2% during the first 5 and last 5 CS^+, respectively; paired t-test, p = 0.00055).

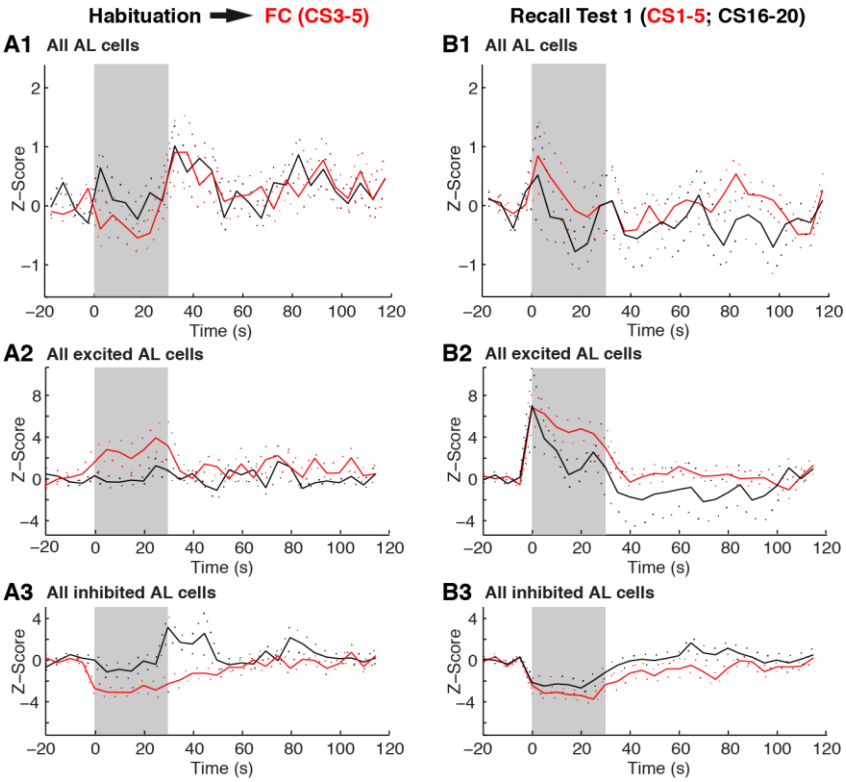

Figure 5. Grand average of the responses of BNST-AL neurons to the CS^+ (gray shading) (**A**) during habituation (black) and at the end of training (red) as well as (**B**) during the recall test (red and black: first and last 5 CS^+, respectively). In **A1** and **B1**, all available BNST-AL cells were included in the averages, whereas the averages shown in panels 2 and 3 were restricted to cells with significant excitatory or inhibitory responses, respectively. Dotted lines represent the SEM.

In the chi-square analyses presented in figures 2-3, we reported on the incidence cells with significant responses to the CSs. A limitation of this approach when comparing two cell groups is that it ignores the magnitude of the changes in responsiveness. To address this potential confound, we next compared the average responses of BNST-AL (**Fig. 5**) and AM (**Fig. 6**) cells from habituation to the end of training (left) and during the recall test (right). Separate averages are provided (from top to bottom) for all cells combined, On-cells, and Off-cells.

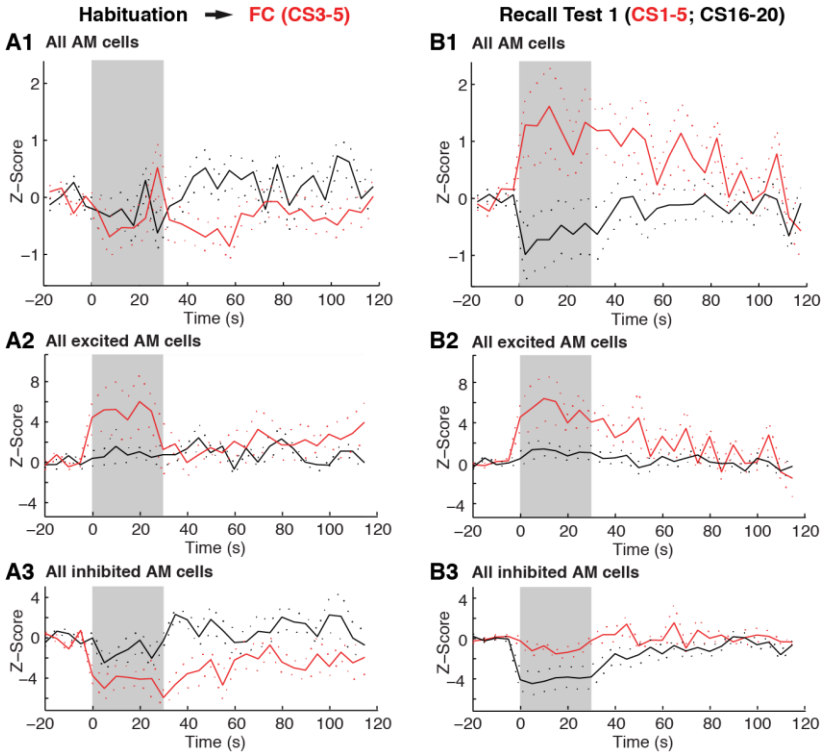

Figure 6. Grand average of the responses of BNST-AM neurons to the CS^+ (gray shading) (**A**) during habituation (black) and at the end of training (red) as well as (**B**) during the recall test (red and black: first and last 5 CS^+, respectively). In **A1** and **B1**, all available BNST-AM cells were included in the averages, whereas the averages shown in panels 2 and 3 were restricted to cells with significant excitatory or inhibitory responses, respectively. Dotted lines represent the SEM.

Comparing the average behavior of BNST-AL and AM neurons during the recall test (**Figs. 5B** and **6B**, respectively) reveals striking differences that are consistent with the incidence analyses presented in figure 3. Due to response heterogeneity among BNST-AL neurons (**Fig. 5B2, C2**), no significant change in CS responsiveness is seen in the grand average of all BNST-AL neurons from

the beginning (red) to the end (black) of the first recall test. This contrasts with the grand average of all BNST-AM neurons (**Fig. 6B1**) where, due to the prevalence of On-cells (**Fig. 6B2**), a significant increase in activity is apparent at the onset of the recall test (**Fig. 6B1**, red). Unexpectedly, that neuronal responses of BNST-AL cells to the CS^+ persisted to some extent at the end of the recall test (trials 16-20; (Fig. 5B2,3), when freezing had fully extinguished (Fig 1D). This observation might be interpreted as evidence of a persistent associative memory in BNST, which could rekindle fear after extinction.

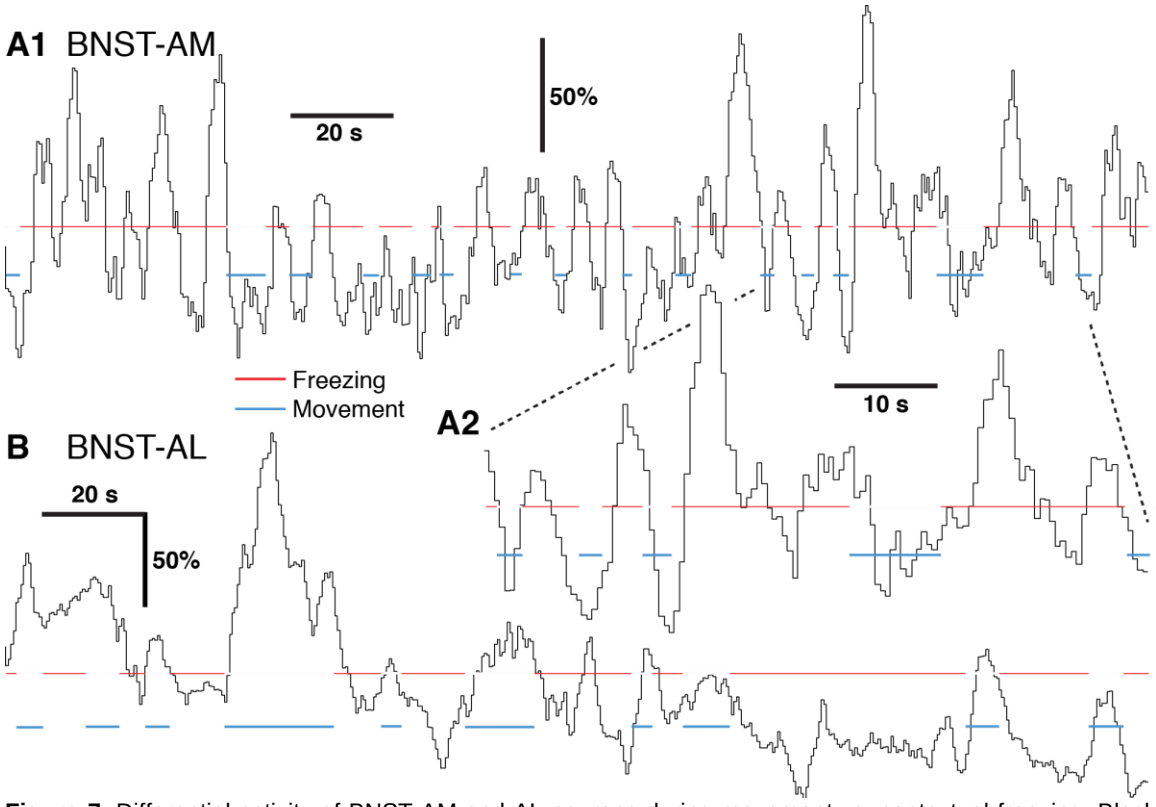

Figure 7. Differential activity of BNST-AM and AL neurons during movement vs. contextual freezing. Black traces depict normalized fluctuations in firing rate during periods of freezing (red lines) and movement (blue lines). (**A**) Fluctuations in the firing rate of five simultaneously recorded BNST-AM cells, expressed as percent of average. A portion of **A1** (dashed lines) is shown with an expanded time base in **A2**. (**B**) Fluctuations in the firing rate of three simultaneously recorded BNST-AL cells, expressed as percent of average. In **A** and **B**, prior to averaging, the firing rates of individual cells was normalized to the average of the entire period so as to give and equal weight to the data obtained in each cell. Note that to optimize the temporal resolution of the behavioral measurements, the exact onset and offset times of visually identified periods of freezing and movement were determined using frame-by-frame analysis of the video recordings. Data depicted in A and B was obtained in different rats.

Comparison of firing rates, patterns, and spike shapes between CS^+-responsive and unresponsive BNST neurons

In contrast with other brain structures such cortex (Markram et al. 2004) or striatum (Tepper and Bolam 2004), where the distinctive neurochemical, morphological, and electrophysiological properties of projection cells and interneurons are well known, there is no such clarity in the BNST. A majority of BNST cells are GABAergic/peptidergic and a minority are glutamatergic (Day et al. 1999; Poulin et al. 2009; Kudo et al. 2012). Given the pattern of results obtained in retrograde tracing studies (Day et al. 1999; Herman et al. 2004; Kudo et al. 2012), it is likely that a large proportion of the GABAergic cells and at least some of the glutamatergic neurons are projection cells. Similarly, although electrophysiological studies have distinguished three main cell types in BNST-AL (Hammack et al. 2007; Hazra et al. 2011; Rodriguez-Sierra et al. 2013), it remains unclear whether all or a subset of each class correspond to projection cells or interneurons. Nevertheless, in an attempt to determine whether distinct cell types respond differently to the CS^+, we next compared the properties of neurons with significant vs. non-significant responses to the CS+ during the recall test (CS^+1-5).

Although the spontaneous firing rates of BNST cells ranged widely (from near zero to 32 Hz), most BNST-AL and AM neurons had low firing rates (AL, 82% < 4 Hz; AM, 84% < 4 Hz), with no overall difference in the firing rate of the cells recorded at these two sites (2.22 ± 0.54 Hz) and BNST-AM (3.14 ± 0.82 Hz; Wilcoxon Rank-Sum test, p=0.43). To determine whether there was a

relationship between the CS^+ responsiveness of BNST-AL or AM neurons (excited, inhibited, no response) and their firing properties (baseline firing rate or spike duration), we computed Kruskal-Wallis one-way ANOVAs. For baseline firing rates, both ANOVAs reached significance (AL, $p = 0.035$; AM, $p = 0.004$). Post-hoc Wilcoxon Rank-Sum tests with Bonferroni correction of the significance level revealed that there was a trend for BNST-AM On-cells to have higher baseline firing rates (5.4 ± 1.5 Hz) than Off-cells (0.6 ± 0.3 Hz, $p = 0.07$) or unresponsive neurons (2.7 ± 0.8 Hz, $p = 0.05$). For BNST-AL cells, none of the post-hoc comparisons approached significance. However, it was clear that BNST-AL cells had significantly lower baseline firing rates than BNST-AM On cells ($p = 0.022$). With spike duration, the ANOVA did not reach significance for BNST-AM cells ($p = 0.39$) but it did for BNST-AL cells ($p = 0.023$). Post-hoc Wilcoxon Rank-Sum tests revealed that there was a trend for BNST-AL Off cells to generate spikes of longer duration (0.52 ± 0.08 ms) than unresponsive cells (0.39 ± 0.03 ms; $p = 0.08$). Finally, since earlier patch clamp studies reported that a major physiological class of BNST neurons generate low-threshold spike bursts (Hammack et al. 2007; Hazra et al. 2011; Rodriguez-Sierra et al. 2013), we compared the incidence of bursting and non-bursting neurons among On-cells, Off-cells, and unresponsive neurons of BNST-AL or AM but found no significant differences ($p \geq 0.3$).

Cellular correlates of contextual fear memory in BNST-AL and AM

Because prior behavioral studies have revealed that BNST lesions reduce

contextual fear (Sullivan et al. 2004; Duvarci et al. 2009), we next studied the activity of BNST-AL (n = 38) and AM (n = 69) neurons during the 10-min exposure to the training context on day 2, when the rats exhibited high levels of contextual freezing (**Fig. 1D**, red diamond). We observed that most BNST-AM cells fired at a higher rate during freezing than movement whereas BNST-AL cells tended to show the opposite pattern of activity. Representative examples of BNST-AM and AL neurons with respectively higher and lower activity during behavioral freezing than movement are provided in **figure 7A** and **B**, respectively.

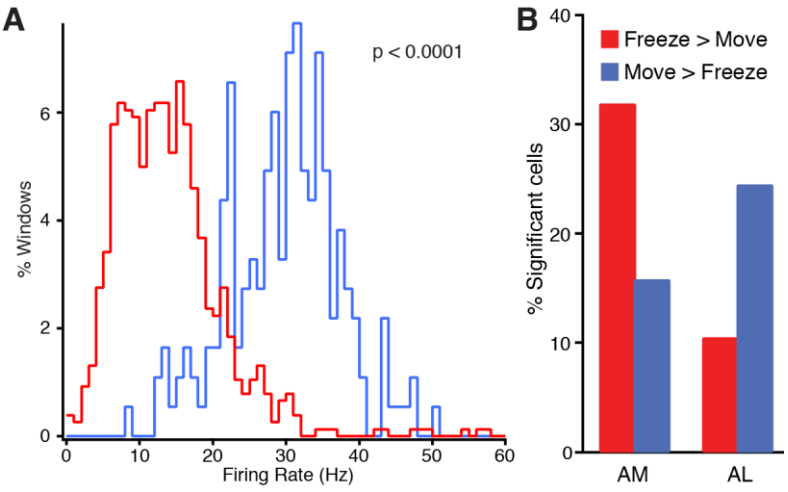

Figure 8. Analysis of fluctuations in firing rates during movement vs. freezing. (**A**) Frequency distributions of firing rates during freezing (red) or movement (blue) for a BNST-AL cell. The spike train of the cell was first smoothed with a Gaussian kernel with a standard deviation of 0.25 s. The resulting rate estimate was then sampled at 0.5 s intervals and frequency distributions of firing rates were computed. (**B**) Incidence of BNST-AM (left) and AL (right) cells with significantly higher firing rates during freezing (red) or movement (blue).

To address this quantitatively, we compared the firing rate of each cell during multiple epochs of freezing vs. movement. The spike trains was first smoothed with a Gaussian kernel with a standard deviation of 0.25 s. The resulting rate estimate was then sampled at 0.5 s intervals and periods of freezing and movement were compared using an unpaired t-test, in each cell independently (**Fig. 8A**). As shown in **figure 8B**, a similar proportion of BNST-AM (47.8% or 33 of 69) and AL cells (36.8% or 14 of 38) fired at significantly

different rates in epochs of high vs. low fear. However, paralleling the pattern of results seen with responses to the CS^+, the majority of significant BNST-AM cells (66.6% or 22 of 33) fired at higher rates during freezing than movement whereas most significant BNST-AL cells did the opposite (71.4% or 10 of 14; Fisher exact, $p = 0.015$). Yet, there were no significant differences in the baseline firing rates (measured during wakefulness in the home cage) of neurons with higher vs. lower firing rates during freezing among or between BNST-AL or AM neurons (Wilcoxon Rank-Sum tests, $p \geq 0.12$).

Although prior lesion studies suggest that BNST plays an important role in the genesis of contextual freezing, it remains possible that the differences in firing rates described above do not relate to the affective state of the rats but to another factor such as proprioceptive feedback. To address this possibility, we compared the spontaneous firing rates of BNST-AL and AM neurons while the animals were in a neutral transfer cage prior to placement in context A (10 min epochs). In this environment, rats were generally active. Periods of immobility were almost always followed by a shift in their behavioral state to slow-wave sleep (SWS). This shift was easy to identify because it coincided with a dramatic increase in the power of large amplitude slow oscillations ≤ 4 Hz in the local field potentials.

Thus, using the same approach as in the above, we compared firing rates during movement vs. immobility, but excluding periods of overt SWS. Respectively 33.3% and 39.3% of BNST-AL and AM neurons were found to have significantly different firing rates in the two conditions. However, the proportion of

cells with higher firing rates in one condition or the other did not differ significantly (Fisher exact: AM, $p = 0.23$; AL, $p = 0.43$).

DISCUSSION

We have studied the behavior of anterior BNST neurons during cued and contextual fear. The interest of this question stems from earlier work indicating that BNST and CeA, despite forming similar connections with the basolateral amygdala (BLA) and brainstem fear effectors, are differentially involved in contextual vs. cued fear. Surprisingly, while we observed regional differences in BNST activity in relation to fear, the pattern of results was similar for contextual and cued fear. The significance of these findings is considered below.

Prior lesion and inactivation studies on the role of BNST in contextual and cued fear

There is consensus that BNST is involved in the genesis of contextual, but not cued fear. Reversible inactivation (Walker and Davis 1997) as well as electrolytic (Gewirtz et al. 1998; Sullivan et al. 2004; Waddell et al. 2006; Luyten et al. 2011) or neurotoxic (LeDoux et al. 1988; Hammack et al. 2004; Duvarci et al. 2009) lesions of BNST impair the expression of contextual but not cued fear, unless the CS is very long (Waddell et al. 2006) or the temporal relationship between the CS and US is ambiguous (Walker et al. 2009). However, more recent reports using techniques that allow selective manipulations of different BNST regions (Kim et al. 2013) or of different cell types within these regions

(Jennings et al. 2013) revealed that BNST is functionally heterogeneous. Consistent with this notion, some early studies suggested that BNST activity, while not required for generating learned fear to cues, exerts a tonic inhibitory influence on fear output networks. Indeed, intra-BNST infusions of muscimol was found to *enhance* fear potentiated startle (Meloni et al. 2006). Also, presentation of a fear-eliciting CS together with a conditioned inhibitor was found to *increase* fos expression in BNST relative to animals only presented with the CS (Campeau et al. 1997). Last, intra-BNST infusions of calcitonin gene-related peptide (CGRP) was reported to enhance startle and increase Fos expression in CeA (Sink et al. 2011). However, a patch-clamp study found that CGRP potentiates GABAergic inhibition in neurons of BNST-AL (Gungor and Paré 2012), the BNST region receiving CGRP inputs from the parabrachial nucleus (Gustafson and Greengard 1990; Dobolyi et al. 2005). Since most BNST neurons are GABAergic (Esclapez et al. 1993; Poulin et al. 2009), these results suggest the startle enhancement produced by intra-BNST infusions of CGRP is due to the inhibition of BNST-AL neurons and consequent disinhibition of CeA.

Activity of BNST-neurons in relation to cued and contextual fear

Overall, the findings reviewed above support the view that BNST exerts a dual influence over fear expression. On the one hand, BNST supports contextual fear; on the other, there is evidence that BNST, most likely its anterolateral region, exerts an inhibitory influence over fear output networks. As described below, we propose that this apparent contradiction reflects regional heterogeneity

in the anterior BNST. Indeed, the present study revealed that BNST-AL and AM neurons display a different activity profile in relation to learned fear. First, during cued fear conditioning, BNST-AL neurons acquired *inhibitory* responses to the CS (Off-cells). Two days later, during the recall test, the proportion of Off-cells remained high but an additional subset of cells developed positive responses to the CS (On-cells). In contrast, the CS responsiveness of BNST-AM neurons did not change during training. However, during the recall test two days later, we observed a large increase in the incidence of cells with *excitatory* responses to the CS. Importantly, BNST-AL and AM neurons also displayed an opposite activity profile in relation to contextual fear. Indeed, when rats were exposed to the training context the day after fear conditioning, a third of BNST-AM neurons fired at significantly *higher* rates during freezing than movement. Few BNST-AM cells showed the opposite behavior. By contrast, in BNST-AL, neurons with *lower* firing rates during freezing prevailed, consistent with the pattern of CS responsiveness described above.

These findings point to regional differences in the activity of BNST-AL and AM in relation to learned fear, raising the possibility that they exert opposite influences on fear output networks. Several factors likely underlie these differences, including regionally heterogeneous amygdala projections to BNST as well as the intrinsic BNST network. Indeed, the amygdala sends strong but neurochemically diverse projections to BNST: GABAergic/peptidergic inputs from CeA and glutamatergic inputs from BLA (Krettek and Price 1978b; Dong et al. 2001a; McDonald, 2003). Importantly, CeA contributes stronger projections to

BNST-AL than AM (Dong et al. 2001a). Conversely, a major component of BNST-AL, the oval nucleus, is largely devoid of BLA inputs (Dong et al. 2001a). In addition, a recent in vitro study on the intrinsic connections of BNST reported that BNST-AL neurons receive inhibitory inputs from other BNST neurons (Turesson et al. 2013). Thus, CS-related BLA inputs might excite BNST cells that send GABAergic projections to neurons of the oval nucleus, causing a feedforward inhibition. This inhibition of BNST-AL neurons might be reinforced by CeA inputs, which are much stronger to BNST-AL than AM (Dong et al. 2001a).

Consistent with the above, there is a correspondence between the CS responsiveness of neurons in the lateral (CeL) and medial (CeM) sectors of CeA and BNST. In particular, most CS responsive CeM neurons exhibit positive responses to the CS (Ciocchi et al. 2010; Duvarci et al. 2011), as in BNST-AM. In contrast, as in BNST-AL, CeL responses to the CS are heterogeneous, with different CeL neurons exhibiting inhibitory or excitatory responses (Ciocchi et al. 2010; Duvarci et al. 2011). Perhaps not coincidentally, the incidence of CeL Off-cells does not increase during training, but after a consolidation period (Duvarci et al. 2011). In parallel, an inflation of CS-evoked responses develops in BLA (Amano et al. 2011). At present, the cellular interactions leading to these time-dependent changes in CS responsiveness remain unclear. However, given the strong interconnections existing between BLA, CeA, and BNST neurons, a causal relation is likely. Also, considering the dramatic impact of medial prefrontal lesions on the expression of learned fear (Sierra-Mercado et al. 2011) and the

preferential innervation of BNST-AM by prelimbic afferents (reviewed in McDonald 1999), it is probable that prefrontal inputs also play a role.

Preferential BNST contribution to contextual fear

The impetus for the present study was to determine why BNST lesion and inactivation interfere with contextual but not cued fear given that BNST and CeA contribute similar projections to brainstem fear effector neurons. Yet, we found that BNST-AM and AL neurons show a similar differential activity profile in relation to cued and contextual fear. These findings raise the following possibilities. First, it is conceivable that neurons in a different BNST sector, not explored in the present study, show a different activity profile in relation to the two forms of fear. Second, it is possible that earlier inactivation or lesion studies inadvertently affected a structure adjacent to BNST, which is involved in contextual fear. Consistent with this possibility, recent findings implicate components of the septal region in the regulation of fear and anxiety (Yamaguchi et al. 2103). Additional experiments will be required to settle this question.

MATERIALS AND METHODS

Procedures were approved by the Institutional Animal Care and Use Committee of Rutgers University, in compliance with the Guide for the Care and Use of Laboratory Animals (DHHS). Our subjects were male Lewis rats (310-360 g, Charles River Laboratories, New Field, NJ) maintained on a 12 h light/dark

cycle. They were housed individually with *ad libitum* access to food and water. Prior to the experiments, they were habituated to the animal facility and handling for one week.

Surgery

Eight rats were anesthetized with a mixture of isoflurane and O_2, and administered atropine sulfate (0.05 mg/kg, i.m.) to aid breathing. In aseptic conditions, rats were mounted in a stereotaxic apparatus with nonpuncture ear bars. A local anaesthetic (bupivacaine, sc) was injected in the region to be incised. Fifteen minutes later, the scalp was incised and a craniotomy was performed above BNST. Then, movable bundles of four tetrodes (nichrome microwires, 20-µm inner diameter, impedance 100-300kΩ following gold plating) were stereotaxically aimed to the lateral and medial parts of the anterior portion of BNST (BNST-AL and BNST-AM, respectively). Tetrode tip positions within a bundle were staggered to facilitate histological reconstructions. The rats were allowed one week to recover from the surgery and then acclimated to handling for two additional days.

Behavioral protocol

The rats were subjected to a differential fear conditioning paradigm (**Fig. 1A**). Fear conditioning and recall testing occurred in different contexts (context A and B). For fear conditioning (context A), rats were placed in a rodent conditioning chamber with a metal grid floor (Coulbourn Instruments, Lehigh

Valley, PA) that was enclosed within a sound attenuating chamber, dimly illuminated by a single house light. For testing recall, the chamber contained a black plexiglass floor washed with peppermint soap (context B).

On day-0, rats were habituated to context A and B for 20 min each. Before and after each context exposure, the animals were placed in their home cage. On day-1, we performed a tone habituation session (5 presentations of the CS^+ and the CS^-; each 30 s in duration, white-noise or 2 kHz, 80 dB). The identity of the CS^+ and CS^- was varied across animals and they were presented in a random order. The CS^- served as a non-associative control. Following habituation, the rats received presentations of 5 CS^+ and 5 CS^-, with the CS^+ co-terminating with a footshock (US, 0.5 mA, 1s). On day-2, to test for contextual fear memory, rats were placed in context A for 10 min with no presentations of the CS^+ or CS^-. On day-3, in context B, recall of cued fear was tested with twenty additional presentations of the CS^- and CS^+. Another recall test was performed on day-4 (ten additional presentations of the CS^+ and CS^-). In all phases, five minutes elapsed between placement of the rats in context A or B and presentation of the first CS. The duration of the CS was always 30 sec and the inter-CS intervals varied between 3 and 4 minutes. This long interval was selected so that during the recall tests, freezing elicited by one CS would have subsided by the time the next CS is presented. However, note that during fear conditioning, once the first US was administered, rats froze at various times, including during the CSs and inter-CS intervals. Much of this freezing likely represents a non-associative response to the recent US exposure. Behavior was

recorded by a video-camera and scored off-line. Time spent freezing (immobility, with the exception of breathing) was measured by an experienced observer with a stopwatch. Contextual freezing was also measured using a custom Matlab script that compared absolute differences in luminosity values between corresponding pixels in successive video frames. Prior to carrying out this analysis, the frames were filtered with a two-dimensional median base filter to remove the so-called “salt-and-pepper” noise in luminosity values of nearby pixels. To detect freezing, we used a uniform threshold of luminosity variations (10% of maximal seen during locomotor activity) that had to be observed in at least 30 consecutive frames (or 1 sec). This automated approach closely matched the results obtained with visual scoring ($r = 0.9$).

Unit recording, clustering, and analysis

BNST unit recordings were performed during all the phases of the behavioral protocol described above. The signals were sampled at 40-kHz and stored on a hard drive. The data was first high-passed filtered using a median-based filter, then thresholded to extract spikes. We then ran PCA on the spikes and the first three components were clustered using KlustaKwik (http://klustakwik.sourceforge.net/). Spike clusters were then refined manually using Klusters (Hazan et al. 2006). The reliability of cluster separation was verified by inspecting auto- and cross-correlograms. Units with unstable spike shapes during a given recording session were excluded from the analyses.

To determine whether cells generated spike bursts akin to those

generated by the Type-II BNST-AL and AM neurons reported in previous in vitro patch-clamp studies (Hammack et al. 2007; Hazra et al. 2011; Rodriguez-Sierra et al. 2012), we fit the tail of the inter-spike interval (ISI) distribution (interval > 100 ms) to an exponential distribution, the form expected for a random (non-bursting) process. If the observed rate of ISIs < 20 ms was significantly greater than expected from the exponential approximation extrapolated from high to small interval values, the cell was classified as a bursting neuron.

To determine spike duration, we first selected the tetrode channel where, for a given cell, action potentials had the largest peak to trough amplitude. We then measured the spikes' half-amplitude duration as the time required for the action potential to rise from, and return to, half of its maximum amplitude (see Bartho et al. 2004).

Statistical analyses

To assess whether CS-evoked responses were significant, we first computed the firing rate of each unit in 5 sec bins, from 20 s before to 120 s after the onset of the CS^+ and CS^-. Separate averages were obtained for the habituation phase, the first two and last three CS^+ and CS^- of training, as well as the first and last five CS^+ and CS^- of the two recall tests. The data of each average was then z-scored to firing rate variations seen in the pre-CS period. A CS-evoked change in firing rate was deemed significant, when the six 5-s bins of the CS^+ or CS^- differed from the baseline period by ±1.96 z or more. This corresponds to a significance threshold of $p \leq 0.05$. To assess whether the

proportion of responsive cells changed significantly depending on the phase of the behavioral protocol, we used a chi-square test that analyze whether there was a dependence between response type (response, no response) and behavioral phase (habituation, CS^+ 1-2 or 3-5 of training, first 5 or last 5 CS^+ of the two recall tests. It should be noted that there were no significant differences in the effectiveness of the white noise vs. 2 kHz tone in eliciting significant responses from BNST-AL and AM cells during habituation. Indeed, a chi-square test revealed no significant dependence between response type (increased firing, decreased firing, no response) and the type of auditory stimulus (white noise or 2 kHz tone) ($\chi^2 = 1.03$, $p = 0.59$). In addition, the magnitude of significant excitatory or inhibitory responses elicited by the two auditory stimuli did not differ (paired t-tests, $p = 0.4256$ and $p = 0.1786$ respectively).

Histology

At the end of the experiments, the animals were deeply anesthetized and recording sites marked with small electrolytic lesions (20 µA between a tetrode channel and the animals' tail for 15 sec). One day later, the rats were then perfused-fixed through the heart, their brains extracted, cut on a vibrating microtome and the sections counterstained with cresyl violet. An example of histologically identified recording site is shown in **figure 1B**.

REFERENCES

Alheid GF, Heimer L. 1988. New perspectives in basal forebrain organization of special relevance for neuropsychiatric disorders: the striatopallidal, amygdaloid, and corticopetal components of substantia innominata. *Neuroscience* **27:** 1-39.

Barthó P, Hirase H, Monconduit L, Zugaro M, Harris KD, Buzsáki G. 2004. Characterization of neocortical principal cells and interneurons by network interactions and extracellular features. *J Neurophysiol* **92:** 600-608.

Campeau S, Davis M. 1995. Involvement of subcortical and cortical afferents to the lateral nucleus of the amygdala in fear conditioning measured with fear-potentiated startle in rats trained concurrently with auditory and visual conditioned stimuli. *J Neurosci* **15:** 2312-2327.

Ciocchi S, Herry C, Grenier F, Wolff SB, Letzkus JJ, Vlachos I, Ehrlich I, Sprengel R, Deisseroth K, Stadler MB, Müller C, Lüthi A. 2010. Encoding of conditioned fear in central amygdala circuits. *Nature* **468:** 277-282.

Campeau S, Falls WA, Cullinan WE, Helmreich DL, Davis M, Watson SJ. 1997. Elicitation and reduction of fear: behavioural and neuroendocrine indices and brain induction of the immediate-early gene c-fos. *Neuroscience* **78:** 1087-1104.

Day HE, Curran EJ, Watson SJ, Akil H. 1999. Distinct neurochemical populations in the rat central nucleus of the amygdala and bed nucleus of the stria terminalis: evidence for their selective activation by interleukin-1beta. *J Comp Neurol* **413**: 113–28.

De Olmos JS, Heimer L. 1999. The concepts of the ventral striatopallidal system and extended amygdala. *Ann N Y Acad Sci* **877:** 1-32.

Dobolyi A, Irwin S, Makara G, Usdin TB, Palkovits M. 2005. Calcitonin gene related peptide containing pathways in the rat forebrain. *J Comp Neurol* **489:** 92-119.

Dong HW, Swanson LW. 2003. Projections from the rhomboid nucleus of the bed nucleus of the stria terminalis: implications for cerebral hemisphere regulation of ingestive behaviors. *J Comp Neurol* **463:** 795-9.

Dong HW, Swanson LW. 2004. Organization of axonal projections from the anterolateral area of the bed nuclei of the stria terminalis. *J Comp Neurol* **468:** 277-298.

Dong HW, Swanson LW. 2006a. Projections from bed nuclei of the stria terminalis, anteromedial area: cerebral hemisphere integration of

neuroendocrine, autonomic, and behavioral aspects of energy balance. *J Comp Neurol* **494:** 142-178.

Dong HW, Swanson LW. 2006b. Projections from bed nuclei of the stria terminalis, magnocellular nucleus: implications for cerebral hemisphere regulation of micturition, defecation, and penile erection. *J Comp Neurol* **494:** 108-141.

Dong HW, Swanson LW. 2006c. Projections from bed nuclei of the stria terminalis, dorsomedial nucleus: implications for cerebral hemisphere integration of neuroendocrine, autonomic, and drinking responses. *J Comp Neurol* **494:** 75-107.

Dong HW, Petrovich GD, Swanson LW. 2000. Organization of projections from the juxtacapsular nucleus of the BST: a PHAL study in the rat. *Brain Res* **859:** 1-14.

Dong HW, Petrovich GD, Swanson LW. 2001a. Topography of projections from amygdala to bed nuclei of the stria terminalis. *Brain Res Brain Res Rev* **38:** 192-246.

Dong HW, Petrovich GD, Watts AG, Swanson LW. 2001b. Basic organization of projections from the oval and fusiform nuclei of the bed nuclei of the stria terminalis in adult rat brain. *J Comp Neurol* **436:** 430-455.

Duvarci S, Bauer EP, Paré D. 2009. The bed nucleus of the stria terminalis mediates inter-individual variations in anxiety and fear. *J Neurosci* **29:** 10357-10361.

Duvarci S, Popa D, Paré D. 2011. Central amygdala activity during fear conditioning. *J Neurosci* **31:** 289-294.

Esclapez M, Tillakaratne N, Tobin AJ, Houser CR. 1993. Comparative localization of two forms of glutamic acid decarboxylase with nonradioactive in situ hybridization methods. *J Comp Neurol* **331:** 339-362.

Fendt M, Endres T, Apfelbach R. 2003. Temporary inactivation of the bed nucleus of the stria terminalis but not of the amygdala blocks freezing induced by trimethylthiazoline, a component of fox feces. *J Neurosci* **23:** 23-28.

Gewirtz JC, McNish KA, Davis M. 1998. Lesions of the bed nucleus of the stria terminalis block sensitization of the acoustic startle reflex produced by repeated stress, but not fear-potentiated startle. *Prog Neuropsychopharmacol Biol Psychiatry* **22:** 625-648.

Gungor NZ, Paré D. 2012. In vitro study of CGRP effects suggests that BNST-AL

neurons exert an anxiolytic influence. *Soc for Neurosci abstract* 603.16.

Gustafson EL, Greengard P. 1990. Localization of DARPP-32 immunoreactive neurons in the bed nucleus of stria terminalis and central nucleus of amygdala: co distribution with axons containing tyrosine hydroxylase, vasoactive intestinal polypeptide, and calcitonin gene related peptide. *Exp Brain Res* **1990:** 447-458.

Hammack SE, Mania I, Rainnie DG. 2007. Differential expression of intrinsic membrane currents in defined cell types of the anterolateral bed nucleus of the stria terminalis. *J Neurophysiol* **98**: 638–56.

Hazan L, Zugaro M, Buzsaki G. 2006. Klusters, NeuroScope, NDManager: a free software suite for neurophysiological data processing and visualization. *J Neurosci Methods* **155:** 207-216.

Hazra R, Guo J-D, Ryan SJ, Jasnow AM, Dabrowska J, Rainnie DG. 2011. A transcriptomic analysis of type I-III neurons in the bed nucleus of the stria terminalis. *Mol Cell Neurosci* **46**: 699–709.

Hitchcock JM, Davis M. 1987. Fear-potentiated startle using an auditory conditioned stimulus: effect of lesions of the amygdala. *Physiol Behav* **39:** 403-408.

Hitchcock JM, Davis M. 1991. Efferent pathway of the amygdala involved in conditioned fear as measured with the fear-potentiated startle paradigm. *Behav Neurosci* **105:** 826-842.

Holstege G, Meiners L, Tan K. 1985. Projections of the bed nucleus of the stria terminalis to the mesencephalon, pons, and medulla oblongata in the cat. *Exp Brain Res* **58:** 379-91.

Hopkins DA, Holstege G. 1978. Amygdaloid projections to the mesencephalon, pons and medulla oblongata in the cat. *Exp Brain Res* **32:** 529-547.

Jennings JH, Sparta DR, Stamatakis AM, Ung RL, Pleil KE, Kash TL, Stuber GD. 2013. Distinct extended amygdala circuits for divergent motivational states. *Nature* **496:** 224-228.

Jimenez SA, Maren S. 2009. Nuclear disconnection within the amygdala reveals a direct pathway to fear. *Learn Mem* **16:** 766-768.

Ju G, Swanson LW. 1989. Studies on the cellular architecture of the bed nuclei of the stria terminalis in the rat: I. Cytoarchitecture. *J Comp Neurol* **280:** 587-602.

Ju G, Swanson LW, Simerly RB. 1989. Studies on the cellular architecture of the

bed nuclei of the stria terminalis in the rat: II. Chemoarchitecture. *J Comp Neurol* **280:** 603-621.

Kim M, Campeau S, Falls WA, Davis M. 1993. Infusion of the non-NMDA receptor antagonist CNQX into the amygdala blocks the expression of fear-potentiated startle. *Behav Neural Biol* **59:** 5-8.

Kim Sung-Yon, Adhikary A, Lee SY, Marshel JH, Kim CK, Mallory CS, Lo M, Pak S, Mattis J, Lim BK, Malenka RC, Warden MR, Neve R, Tye KM, Deisseroth K. 2013. Assembling behavioral states: divergent neural pathways recruit separable anxiety features. *Nature* **496:** 219-223.

Koo JM, Han JS, Kim JJ. 2004. Selective neurotoxic lesions of basolateral and central nuclei of the amygdala produce differential effects on fear conditioning. *J Neurosci* **24:** 7654-7662.

Krettek JE, Price JL. 1978a. A description of the amygdaloid complex in the rat and cat with observations on intra-amygdaloid axonal connections. *J Comp Neurol* **178:** 255-280.

Krettek JE, Price JL. 1978b. Amygdaloid projections to subcortical structures within the basal forebrain and brainstem in the rat and cat. *J Comp Neurol* **178:** 225-254.

Kudo T, Uchigashima M, Miyazaki T, Konno K, Yamasaki M, Yanagawa Y, Minami M, Watanabe M. 2012. Three types of neurochemical projection from the bed nucleus of the stria terminalis to the ventral tegmental area in adult mice. *J Neurosci* **32**: 18035–46.

LeDoux JE, Iwata J, Cicchetti P, Reis DJ. 1988. Different projections of the central amygdaloid nucleus mediate autonomic and behavioral correlates of conditioned fear. *J Neurosci* **8:** 2517-2529.

Markram H, Toledo-Rodriguez M, Wang Y, Gupta A, Silberberg G, Wu C. 2004. Interneurons of the neocortical inhibitory system. *Nat Rev Neurosci* **5**: 793-807, 2004.

McDonald AJ. 2003. Is there an amygdala and how far does it extend? An anatomical perspective. *Ann NY Acad Sci* **985:** 1-21.

Meloni EG, Jackson A, Gerety LP, Cohen BM, Carlezon WA Jr. 2006. Role of the bed nucleus of the stria terminalis. BST. in the expression of conditioned fear. *Ann N Y Acad Sci* **1071:** 538-41.

Paré D, Smith Y, Paré JF. 1995. Intra-amygdaloid projections of the basolateral and basomedial nuclei in the cat: Phaseolus vulgaris-leucoagglutinin anterograde tracing at the light and electron microscopic level. *Neuroscience* **69:** 567-583.

Pitts MW, Todorovic C, Blank T, Takahashi LK. 2009. The central nucleus of the amygdala and corticotropin-releasing factor: insights into contextual fear memory. *J Neurosci* **29:** 7379-7388.

Poulin JF, Arbour D, Laforest S, Drolet G. 2009. Neuroanatomical characterization of endogenous opioids in the bed nucleus of the stria terminalis. *Prog Neuropsychopharmacol Biol Psychiatry* **33:** 1356-65.

Rodríguez-Sierra OE, Turesson HK, Paré D. 2013. Contrasting distribution of physiological cell types in different regions of the bed nucleus of the stria terminalis. *J Neurophysiol*, in press.

Savander V, Go CG, LeDoux JE, Pitkänen A. 1995. Intrinsic connections of the rat amygdaloid complex: Projections originating in the basal nucleus. *J Comp Neurol* **361:** 345-368.

Sierra-Mercado D, Padilla-Coreano N, Quirk GJ. 2011. Dissociable roles of prelimbic and infralimbic cortices, ventral hippocampus, and basolateral amygdala in the expression and extinction of conditioned fear. *Neuropsychopharmacology* **36:** 529-538.

Sink KS, Walker DL, Yang Y, Davis M. 2011. Calcitonin gene-related peptide in the bed nucleus of the stria terminalis produces an anxiety-like pattern of behavior and increases neural activation in anxiety-related structures. *J Neurosci* **31:** 1802-10.

Sofroniew MV. 1983. Direct reciprocal connections between the bed nucleus of the stria terminalis and dorsomedial medulla oblongata: evidence from immunohistochemical detection of tracer proteins. *J Comp Neurol* **213:** 388-405.

Sullivan GM, Apergis J, Bush DE, Johnson LR, Hou M, Ledoux JE. 2004. Lesions in the bed nucleus of the stria terminalis disrupt corticosterone and freezing responses elicited by a contextual but not by a specific cue-conditioned fear stimulus. *Neuroscience* **128:** 7-14.

Tepper JM, Bolam JP. 2004. Functional diversity and specificity of neostriatal interneurons. *Curr Opin Neurobiol* **14**: 685–92.

Turesson HK, Rodriguez-Sierra O, Paré D. 2013. Intrinsic connections in the anterior part of the bed nucleus of the stria terminalis. *J Neurophysiol* **109:** 2438-50.

Veening JG, Swanson LW, Sawchenko PE. 1984. The organization of projections from the central nucleus of the amygdala to brainstem sites involved in central autonomic regulation: A combined retrograde transport-immunohistochemical study. *Brain Res* **303:** 337-357.

Waddell J, Morris RW, Bouton ME. 2006. Effects of bed nucleus of the stria terminalis lesions on conditioned anxiety: aversive conditioning with long-duration conditional stimuli and reinstatement of extinguished fear. *Behav Neurosci* **120:** 324-326.

Walker DL, Davis M. 1997. Double dissociation between the involvement of the bed nucleus of the stria terminalis and the central nucleus of the amygdala in startle increases produced by conditioned versus unconditioned fear. *J Neurosci* **17:** 9375-9383.

Walker DL, Miles LA, Davis M. 2009. Selective participation of the bed nucleus of the stria terminalis and CRF in sustained anxiety-like versus phasic fear-like responses. *Prog Neuropsychopharmacol Biol Psychiatry* **33:** 1291-308.

Wilensky AE, Schafe GE, Kristensen MP, LeDoux JE. 2006. Rethinking the fear circuit: the central nucleus of the amygdala is required for the acquisition, consolidation, and expression of Pavlovian fear conditioning. *J Neurosci* **26:** 12387-12396.

Yamaguchi T, Danjo T, Pastan I, Hikida T, Nakanishi S. 2013. Distinct roles of segregated transmission of the septo-habenular pathway in anxiety and fear. *Neuron* **78**:537-544.

CHAPTER III

High frequency oscillations are prominent in the extended amygdala

Previously, it was reported that various cortical and subcortical structures display high frequency local field potential (LFP) oscillations in the 110-160 Hz range (HFOs), distinct from sharp-wave ripples. In the present study, we characterize HFOs in the extended amygdala. Rats were implanted with tetrode bundles in the bed nucleus of the stria terminalis (BNST), central amygdala (CeA), as well as adjacent regions (pallidum, caudate-putamen, lateral septum). At all recorded sites, HFO power showed a systematic dependence on behavioral state: highest during quiet wakefulness, intermediate during paradoxical sleep, and lowest during active waking or slow-wave sleep. CO_2 asphyxiation as well as anesthesia with isoflurane or urethane abolished HFOs. HFOs stood out relative to all other fast frequency LFP components because they were highly coherent between distant sites of the extended amygdala, ipsi- and contralaterally. HFOs affected neuronal firing in two ways: firing rate could vary as a function of HFO power (rate modulation) or HFOs could entrain firing on a cycle-to-cycle basis (phase modulation). The incidence of phase-modulated neurons was about twice higher in BNST and CeA (20-40%) than in adjacent regions (≤8%). Among BNST and CeA neurons, many more were phase-modulated than rate-modulated, although about half the latter were also phase-modulated. Overall, these results indicate that HFOs entrain the activity of a high proportion of neurons in the extended amygdala. A major challenge for future studies will be to identify the mechanisms supporting the high coherence of HFOs within and across hemispheres.

Even in the absence of sensory stimulation, neuronal networks generate rhythmic population events, measurable in local field potentials (LFPs) as oscillations of various frequencies (Buzsaki, 2006). Rhythms of different frequencies predominate depending on the brain region and these oscillations vary markedly as a function of the subject's behavioral state. Understanding these oscillations is important because neuronal events underlying cognitive activity are embedded in these endogenous population rhythms.

Recently, a novel form of oscillatory activity (110-160 Hz) termed high frequency oscillations (HFOs) was observed in the neocortex, hippocampus (reviewed in Tort et al. 2013), and many subcortical structures (reviewed in Olszewski et al. 2013). While the HFO frequency band overlaps with that of sharp wave ripples (Buzsaki et al. 1992; Ylinen et al. 1995), the two oscillations are undoubtedly distinct because they predominate in different behavioral states. Indeed, HFOs were initially identified in studies of phase-amplitude coupling between oscillations of different frequencies, revealing a modulation of HFO amplitude as a function of theta phase (Tort et al. 2008). Subsequently, HFOs were demonstrated using power density analysis and observed in unfiltered LFPs (Scheffzuk et al. 2011; Scheffer-Teixeira et al. 2012), with a phase reversal between superficial and deep hippocampal layers (Tort et al. 2008).

Although little is known about the cellular mechanisms generating HFOs, the available evidence suggests that unlike gamma oscillations, HFOs are not dependent on rhythmic interactions between glutamatergic and GABAergic neurons (Fisahn et al. 1998; Whittington et al. 2000). Indeed, hippocampal HFOs

resist blockade of AMPA/kainate receptors, but are abolished by GABA-A receptor antagonists (Jackson et al. 2011). Moreover, in many subcortical structures (basal ganglia, septum, and thalamus), HFO amplitude increases markedly following systemic administration of NMDA receptor antagonists (Hunt et al. 2011; Hunt and Kasicki 2013). In the case of nucleus accumbens at least, HFOs are generated locally and/or in a nearby structure because they disappear or are largely reduced following local infusions of tetrodotoxin or muscimol (Olszewski et al. 2013). In contrast, TTX infusions in the frontal or parietal cortices as well as in the caudate nucleus had no effect on the power of HFOs recorded locally at these sites (Olszewski et al. 2013), suggesting that they are volume conducted from a distant source.

Although studying the relation between unit activity and HFOs might yield useful insights into the underlying network interactions, this question has received little attention so far. In part, this results from the difficulty of distinguishing genuine entrainment of unit firing by HFOs from spurious correlations resulting from spectral leakage of spike waveforms into LFPs (Scheffer-Teixeira et al. 2013). In the present study, we circumvent this confound by taking advantage of the high spatial coherence of HFOs. Because HFOs depend on interactions between GABAergic neurons (Jackson et al. 2011), we focused on structures of the extended amygdala, particularly the bed nucleus of the stria terminalis (BNST) and central amygdala, where GABAergic neurons prevail (Poulin et al. 2009; Swanson and Petrovich 1998).

MATERIALS AND METHODS

Procedures were approved by the Institutional Animal Care and Use Committee of Rutgers University, in compliance with the Guide for the Care and Use of Laboratory Animals (DHHS). Our subjects were male Lewis rats (310-360 g, Charles River Laboratories, Wilmington, MA) maintained on a 12 h light/dark cycle. They were housed individually with *ad libitum* access to food and water. Prior to the experiments, they were habituated to the animal facility and handling for one week.

Surgery

Eleven rats were anesthetized with a mixture of isoflurane and O_2, and administered atropine sulfate (0.05 mg/kg, i.m.) to aid breathing. In aseptic conditions, rats were mounted in a stereotaxic apparatus with nonpuncture ear bars. A local anaesthetic (bupivacaine, sc) was injected in the region of the scalp to be incised. Fifteen minutes later, the scalp was incised and a craniotomy was performed above the regions of interest. Then, movable bundles of four tetrodes (nichrome microwires, 20-µm inner diameter, impedance 100-300kΩ following gold plating) were stereotaxically aimed to the BNST and, in a subset of rats, CeA and immediately adjacent components of the extended amygdala (Heimer et al. 2008). Tetrode tip positions within a bundle were staggered to facilitate histological reconstructions. The reference electrode was a stainless steel screw anchored over the cerebellum. In two rats, we also compared HFOs referenced to the cerebellum vs. the bone overlying the olfactory bulbs. However, the same

results were obtained with the two references in terms of HFO power, coherence, and unit entrainment.

Data acquisition and analysis

Rats were allowed one week to recover from the surgery and then acclimated to handling for two additional days. In each rat, spontaneous neuronal activity was then recorded during prolonged (≥3 hours) daily recording sessions so that sufficient data could be obtained during different states of vigilance. Behavior was recorded by an overhead video-camera. During the recording sessions, rats were placed in a dimly lit (20 lux) standard plastic rat cage with bedding at the bottom. Electrodes were not moved during the experiments unless all units were lost overnight across all tetrodes within a bundle. In such rare cases (<5%), the tetrode bundle was lowered 60 μm and recordings resumed the following day.

Different behavioral states of vigilance were identified using a combination of spectral analyses of BNST LFPs and behavioral observations. Long epochs of spontaneous LFP activity were segmented in two-second windows and frequency distributions of LFP power in different frequency bands computed. Active waking could be distinguished from all other states because it was associated with a broadband increase in the power of high frequencies (200-240 Hz). This broadband increase at high frequencies likely reflects electromyographic activity. After eliminating active waking, we could easily distinguish slow-wave sleep from quiet waking and REM sleep because total

power at frequencies <20 Hz was distributed bimodally among the three states: epochs of high power at low frequencies corresponded to periods of slow-wave sleep. We then defined quiet waking as movement-free periods that followed active waking whereas REM sleep was defined as epochs that followed slow-wave sleep and were characterized by a high ratio of theta (6-10 Hz) to delta (1-5 Hz) power. These inferences were repeatedly confirmed by correlating LFP-based state scoring with off-line analyses of the rats' behavior, recorded on video. Invariably, as the broadband 200-240 Hz activity diminished and the rats transitioned from active to quiet waking, there was a sharp and sustained drop in movement. In contrast, analysis of behavior during electrophysiologically-identified REM sleep epochs revealed punctual movements (muscle twitches).

The signals were sampled at 40-kHz and stored on a hard drive. For spike extraction, the data was first high-passed filtered using a median-based filter and then thresholded to extract spikes. Next, we ran PCA on the spikes and the first three components were clustered using KlustaKwik (http://klustakwik.sourceforge.net/). Spike clusters were then refined manually using Klusters (Hazan et al. 2006). The reliability of cluster separation was verified by inspecting auto- and cross-correlograms. Units with unstable spike shapes during a given recording session were excluded from the analyses.

For LFP analyses, we first down-sampled the data to 1250 Hz with sinc interpolation. Analyses were performed in Matlab. Spectral and phase analyses were done using Chronux (http://chronux.org/) and the Circular Statistics Toolbox for Matlab (Berens 2009), respectively. For spectral LFP analyses, the magnitude

of each frequency in a given behavioral state was expressed as the deviation from the power law fit to the power spectrum of the data obtained during the entire recording period. When examining time-dependent changes in the spectral composition of LFPs, we used non-overlapping windows of 2 sec and multitaper spectral estimates with 5 tapers and a time-bandwidth product of three. Bandpassed LFP signals were obtained using forward and reverse filtering with a fifth order Butterworth filter over the frequency range indicated, and LFP phase and envelope were obtained using the Hilbert transform of the bandpassed signal.

For phase analyses of unit firing, the reference LFP was obtained using a microwire from a different tetrode than the one used to record the unit of interest and performed a Rayleigh test with a significance threshold of $p<0.01$. The lack of spike waveform in the reference LFP excludes the possibility that spectral leakage of the spike waveform is responsible for significant unit-HFO relationships. To assess whether high amplitude HFO spindles were associated with significant firing rate modulations, we first computed spike counts in windows of ± 1 s centered on HFO spindles of high amplitude (≥2 SD of averaged peak values). To assess significance, we performed a Kilmogorov-Smirnov test comparing the actual distribution of spike counts to a uniform distribution, for each cell independently. The significance threshold we used was $p \leq 0.01$. In addition to performing the K-S test, we excluded spurious positive results due to baseline modulations in firing rate using a binomial test comparing spike counts between the two 500 - 1000ms intervals flanking HFOs (with the

null hypothesis that total spike counts in these two intervals are equal). For unit analyses, we ignored neurons that fired less than 200 spikes in the epoch under consideration.

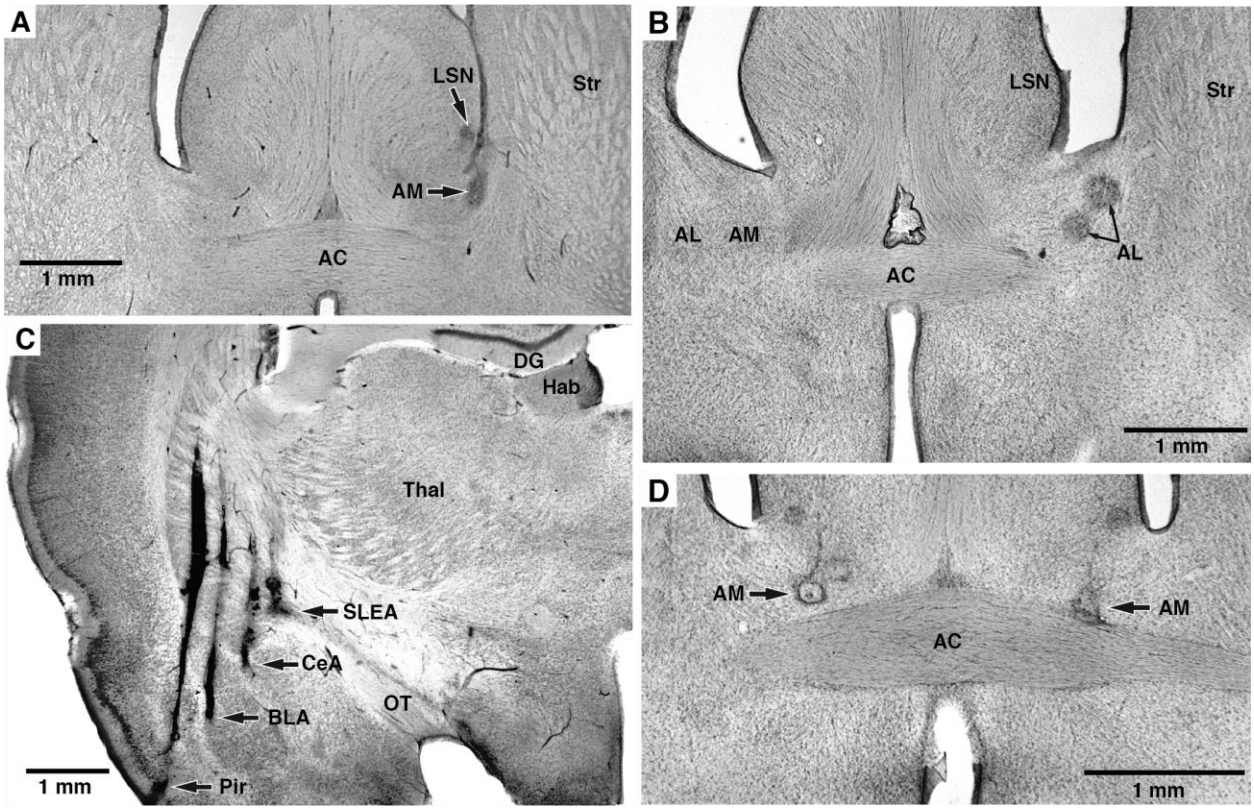

Figure 1. Histological identification of recording sites. (**A**-**D)** Coronal sections counterstained with cresyl violet. Recording sites are marked with small electrolytic lesions (arrows). (**A**) Electrolytic lesions in the lateral septal nucleus (LSN) and BNST-AM (AM). (**B**) Two recording sites in BNST-AL (AL). (**C**) Recording sites in the piriform (Pir) cortex, basolateral complex of the amygdala (BLA), central amygdala (CeA), and sublenticular extended amygdala (SLEA). Too few BLA and Pir recordings were obtained for meaningful analyses. Data obtained in CeA and SLEA were pooled since they are thought to constitute an anatomical entity. (**D**) Two recording sites in the left and right BNST-AM (AM). Other abbreviations: AC, anterior commissure; DBB, diagonal band of Broca; DG, dentate gyrus; Hab, habenula; OT, optic tract; Str, striatum; Thal, thalamus.

Histology

At the end of the experiments, the animals were deeply anesthetized and recording sites marked with small electrolytic lesions (20 µA between a tetrode channel and the animals' tail for 15 sec). One day later, the rats were perfused-

fixed through the heart, their brains extracted, cut on a vibrating microtome and the sections counterstained with cresyl violet, as shown in **figure 1**.

RESULTS

All rats included in this study (n=11) had tetrode bundles implanted in the anterior part of BNST, many bilaterally (n=6). BNST recording sites were subdivided in lateral (BNST-AL) and medial (BNST-AM) sites depending on whether the electrodes were positioned laterally or medially to the intra-BNST component of the stria terminalis. In a subset of rats (n = 4), we also aimed tetrode bundles to CeA. In some cases, tetrode bundles did not reach their intended targets because of tetrode bending. As a result, we also obtained data about HFOs in a number of additional structures including the lateral septum (5 rats), striatum (4 rats), and globus pallidus (2 rats). **Figure 1** shows examples of histologically identified recording sites.

Relation between HFO amplitudes and behavioral states of vigilance

To study the dependence of HFO amplitudes on the states of vigilance, we conducted LFP power analyses (**Fig. 2A1**) on prolonged (≥ 3 hours) epochs of spontaneous activity (**Fig. 2A2**) during which the rats cycled through different behavioral states multiple times. The magnitude of each frequency in a given 2 sec window (non-overlapping) was expressed as the deviation from the power law fit to the power spectrum of the data obtained during the entire recording period (**Fig. 2A1;** black, averaged data; red, fit). At all recording sites, we noticed

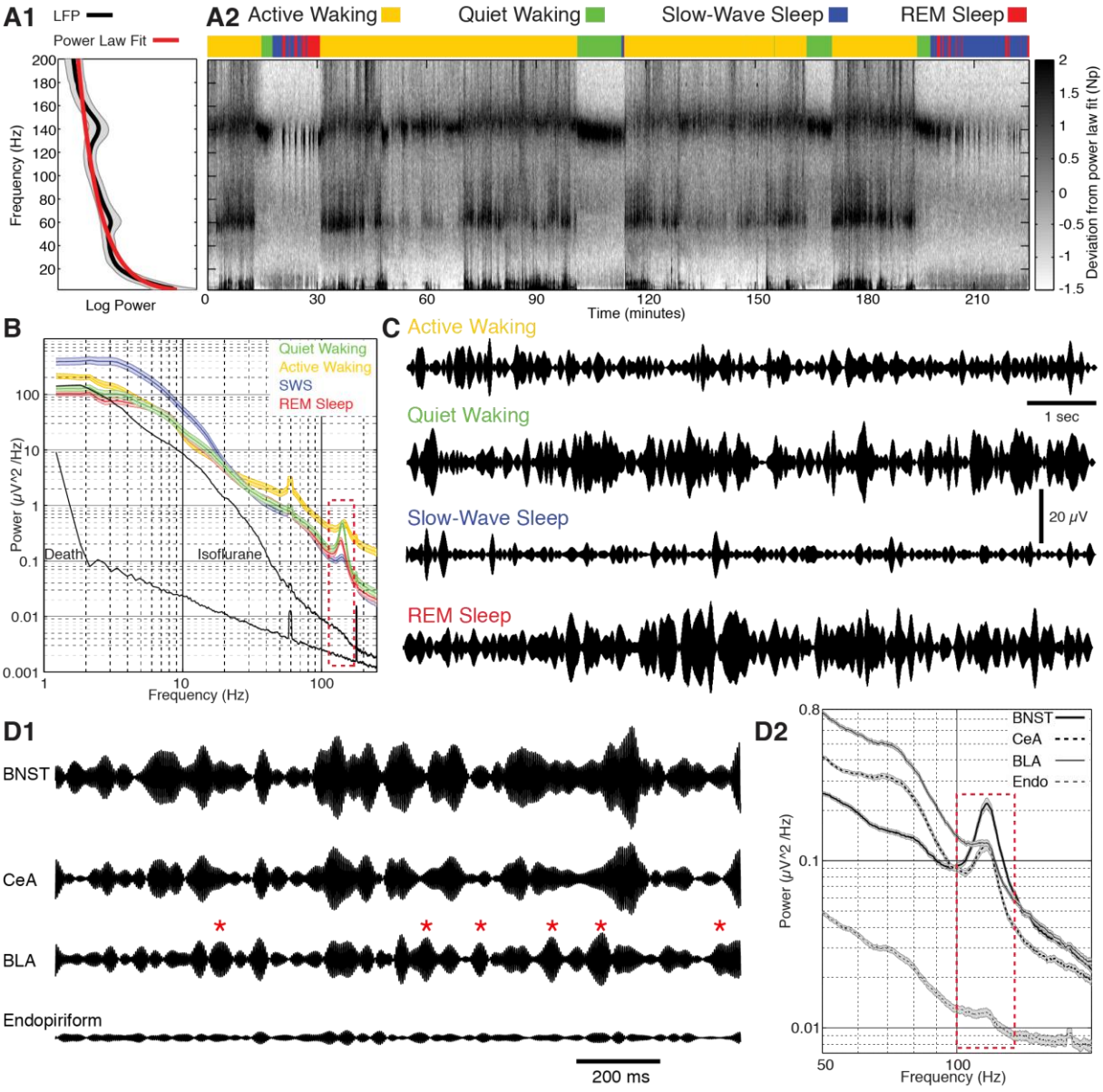

Figure 2. State-dependent changes in the spectral composition of LFPs recorded in BNST. (**A1**) Mean spectral power across frequencies for the entire session (black) is fit by a power law (red). (**A2**) Deviations from power law fit (gray scale) for different frequencies (y-axis) as a function of time (x-axis). The behavioral state of the rat is color coded (see legend at the top of the figure panel). (**B**) Average ± SEM power spectra in different behavioral states. A dashed red rectangle marks the HFO frequency band. For active waking, quiet waking, slow-wave sleep, and REM, the data shown is the average ± SEM of the power spectra of 32 BNST LFPs recorded in 7 rats. For death and anesthesia, we show the average of nine LFP recordings obtained from three rats. (**C**) Examples of LFPs recorded in BNST in different behavioral states (band-pass filtered 125-150 Hz). (**D1**) Simultaneously recorded LFPs in BNST, CeA, BLA, and endopiriform nucleus during quiet waking. LFPs were band-passed filtered at the HFO frequency (125-150 Hz). Note near complete lack of HFOs in endopiriform nucleus, and generally lower HFO amplitude in BLA relative to CeA and BNST. Red asterisks mark BLA HFO spindles that had no counterparts in CeA or BNST. (**D2**) Power spectra of the LFPs shown in D1. Dashed red rectangle marks the HFO frequency band and immediately adjacent regions. To compute these power spectra, a long epoch of quiet waking was segmented in 2 s windows and the data averaged across windows. Shading represents SEM.

consistent variations in HFO amplitudes depending on the rats' behavioral state.

Figure 2A2 and C illustrates this point using LFPs recorded in BNST-AM. Although there were marked moment-to-moment variations in HFO amplitudes, they were generally higher during quiet waking (green) and REM sleep (red). In contrast, HFO amplitudes were generally lower during SWS (blue) and active waking (yellow). This is also shown in **figure 2B** where we plot the average (line) ± SEM (shading) of the power spectra of 32 BNST LFPs recorded in 7 rats in active (yellow) and quiet (green) waking as well as in SWS (blue) and REM sleep (red). Note that for this analysis, HFO amplitude was defined as the difference between the power spectrum peak and the linear fit to flanking frequencies.

An ANOVA on HFO amplitudes revealed a main effect of behavioral state ($F=149$, $p<0.0001$). Bonferroni post-hoc t tests ($p<0.01$) revealed that the ranking of states by HFO power was quiet waking > REM > active waking ≈ SWS, with no significant difference between the latter two states. However, it should be stressed that active waking and SWS were not devoid of HFOs. Although HFO amplitudes were generally lower in these two states, high amplitude HFO spindles also occurred (**Fig. 2C**).

In a few rats, we also examined the impact of isoflurane (0.2% inhaled; n=3) or urethane (1.8 g/kg, ip; n=2) anesthesia on HFO amplitudes. In addition, to examine the possibility that HFOs constitute an electronic artifact independent of neuronal activity, we also recorded LFPs after CO_2 asphyxiation (n=2). As shown

in **figure 2B** (black lines), no HFO peak could be detected under anesthesia or after death.

Importantly, not all recording sites displayed HFOs. For instance, **figure 2D** illustrates examples of simultaneously recorded LFPs in the endopiriform nucleus and basolateral amygdala (BLA) as well as in BNST and CeA, all in the same hemisphere. HFOs were nearly absent from the endopiriform nucleus (**Fig. 2D1**) and of consistently lower amplitude in the BLA relative to those seen in BNST and CeA (**Fig. 2D1**). Moreover, whereas moment-to-moment variations HFO amplitudes in BNST and CeA generally coincided (see below), those seen in BLA showed much more independence (red asterisks mark BLA HFO spindles with no counterparts in BNST and CeA). The lower power of HFOs in the endopiriform nucleus and BLA relative to BNST and CeA is also documented in the power spectra depicted in **figure 2D2 (**t-tests, $p<0.0001$). Together, these results indicate that HFOs are not electronic artifacts.

HFO coherence within and across hemispheres

Previously, it was observed that LFP coherence decreases with distance and that this effect is more pronounced for high frequency components (Collins et al. 1999, 2001; Steriade et al. 1993, 1996). Although it was reported that the coherence of fast rhythms between distant cortical sites could be high during some stimulation paradigms (Desmedt and Tomberg 1994; Gray et al. 1989), this is generally not the case in spontaneous conditions (Bullock and McClune 1989; Murthy and Fetz 1992; Steriade et al. 1996).

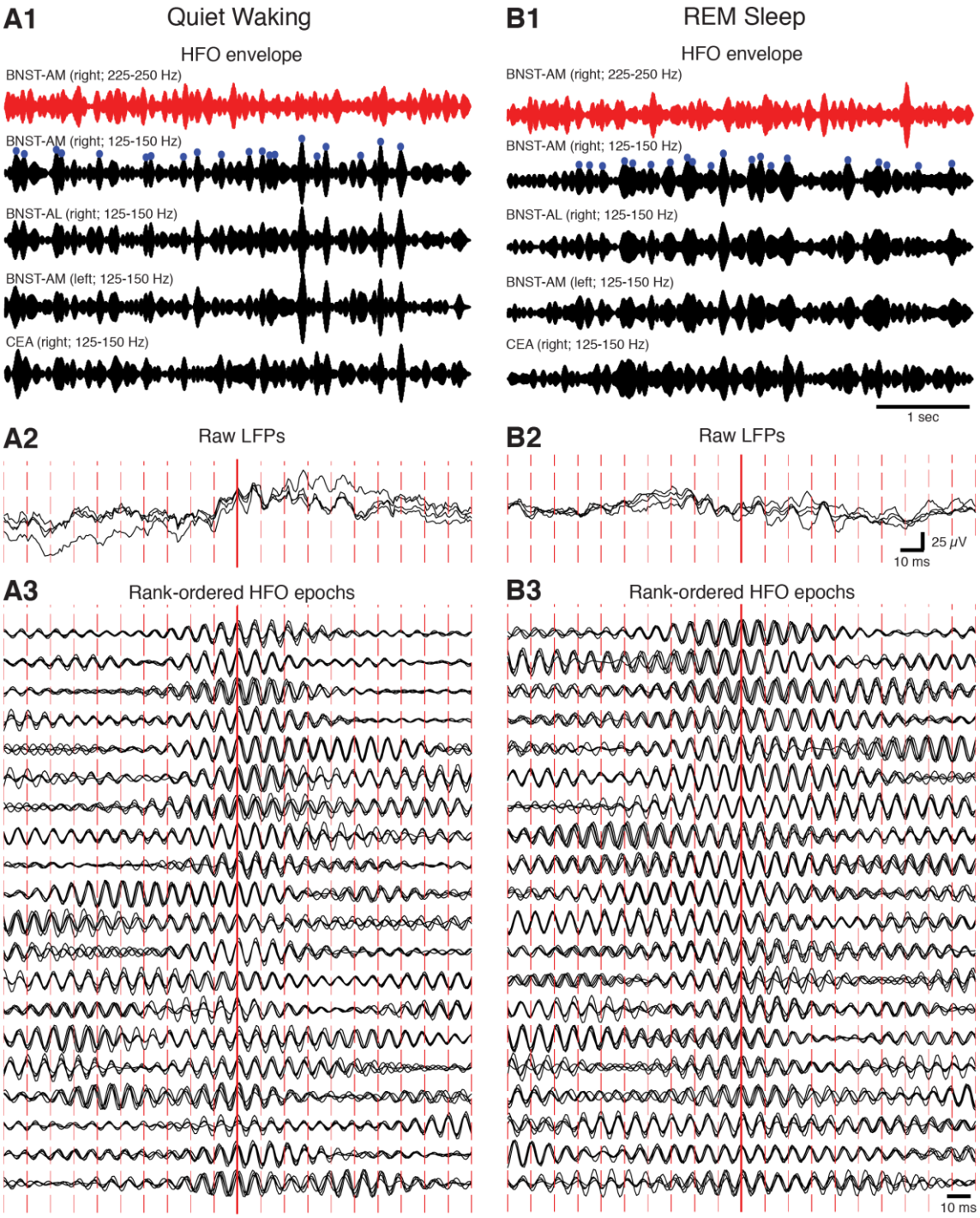

Figure 3. Synchrony of HFOs in BNST and the amygdala during different behavioral states. (**A**) Quiet Waking. (**B**) REM sleep. (**1**) Band-pass filtered LFPs from BNST and the central amygdala (red traces, 225-250 Hz; black traces, 125-150 Hz) shown with a slow time base. Blue circles mark the 20 largest HFO envelope peaks, which are depicted in panels 3 with an expanded time base. Note that high amplitude HFO spindles (black) were not associated with parallel increases in the power of the 225-250 Hz band (red). Thus, HFOs do not reflect a non-specific increase in the power of all high frequency components. To facilitate within-state comparisons, all signals are normalized by their standard deviation. (**2**) Raw LFPs with a fast time base. They correspond to the HFO epoch with the highest peak in panel 1. (**3**) Twenty HFO envelopes marked by blue circles in panels 1, rank-ordered by amplitude (highest to lowest from top to bottom). The signals in each row are normalized by the maximal value found across the four traces.

In contrast, spontaneous HFOs were highly coherent in the extended amygdala, within and across hemispheres. Indeed, in all rats, superimposition of LFPs recorded in the same or different hemispheres during waking or sleep states revealed that HFOs occurred nearly synchronously. For instance, **figure 3** shows band-passed filtered LFPs (black, 125-150Hz; red, 225-250 Hz) recorded in different sub-regions of the right BNST and CeA, as well as in the left BNST during quiet waking (**Fig. 3A**) and REM sleep (**Fig. 3B**). The twenty HFO spindles with the highest amplitude seen in the right BNST-AM (panels 1; blue circles) are shown with an expanded time-base in panels 3, superimposed on LFPs from the other ipsi- and contralateral recording sites. Note the remarkable cycle-to-cycle synchrony of high amplitude HFOs within and across hemispheres for quiet waking (**Fig. 3A**) and REM sleep (**Fig. 3B**). Similar results were obtained in active waking and SWS.

To further characterize this phenomenon, we compared the coherence of HFOs to that of other high frequency LFP components. In particular, in all cases of tetrodes in the CeA of one hemisphere and BNST bilaterally, we compared coherence between all available pairs of recording sites located in different parts of BNST ipsilaterally (24 pairs of recording sites in 6 rats), BNST bilaterally (36 pairs of recording sites in 6 rats), or between BNST and CeA ipsilaterally (16 pairs of recording sites in 4 rats) (**Fig. 4**). Because movement artifacts occurring during active waking yielded artificially high coherence values in all frequencies (yellow period in figure 4), we focused on behavioral states associated with immobility: quiet waking, SWS, and REM sleep.

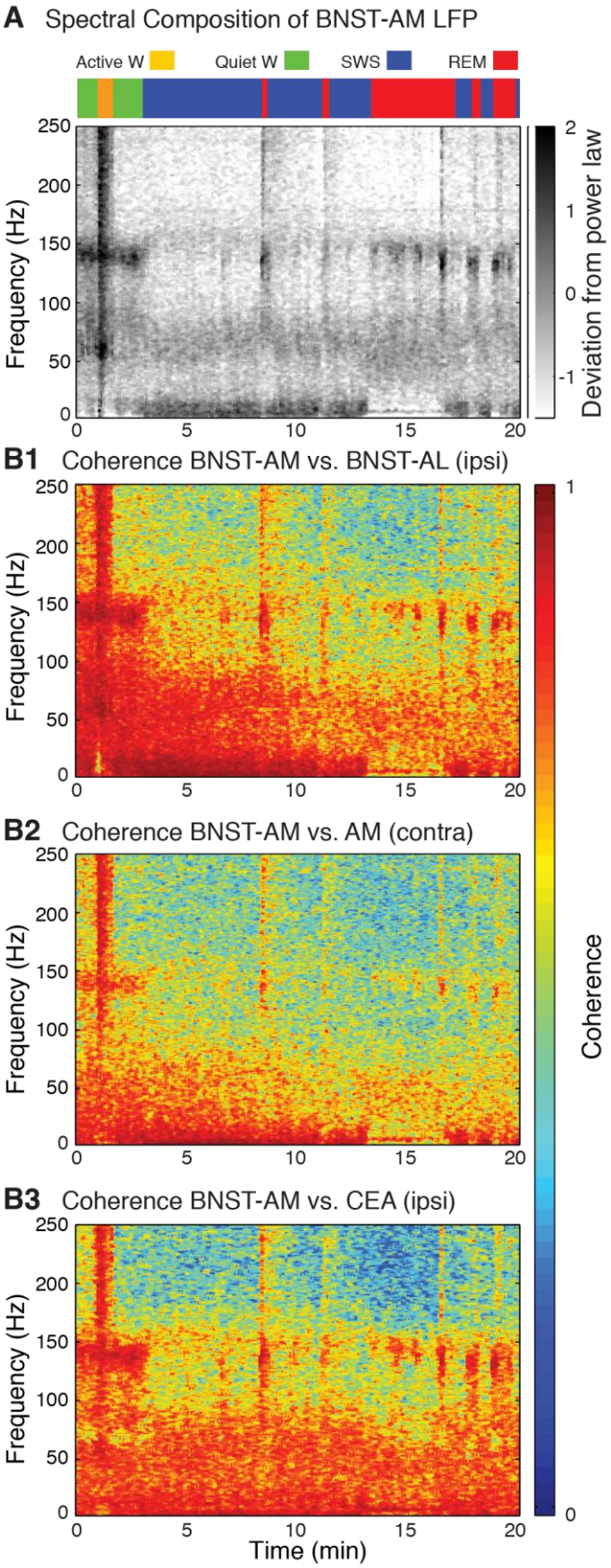

Figure 4. HFOs are highly coherent ipsilaterally but less so across hemispheres. (**A**) State-dependent changes in spectral composition of LFPs recorded in BNST-AM. (**B**) Time and frequency-dependent changes in coherence between LFPs recorded in BNST-AL and AM ipsilaterally (**B1**), BNST-AM in both hemispheres (**B2**) as well as in BNST-AM and CEA (**B3**).

An ANOVA on HFO coherence values revealed a significant dependence on recording configuration in the two behavioral states associated with high amplitude HFOs: quiet waking (**Fig. 5A**) and REM sleep (**Fig. 5B**; F's ≥ 37.8, p's < 0.0001). Bonferroni-corrected post-hoc t-tests revealed that ipsilateral intra-BNST HFO coherence was the highest (p<0.0001), as expected given the short distance between these recording sites (0.4-0.6 mm). Although distance between bilateral BNST recording sites was shorter (2-3 mm) than between ipsilateral BNST-CeA tetrode pairs (3.5-4.5 mm), HFO coherence across hemispheres was significantly lower (p < 0.0001). Of particular interest, for all recording configurations except cases where electrodes were within 0.6 mm of each other in BNST ipsilaterally, the coherence of HFOs was significantly higher than that of high (75-100 Hz) and low gamma (30-55 Hz, p's < 0.0001) as well as for the 100-125 Hz and 150-175 Hz frequency bands (p's < 0.0001). Overall, these results indicate that HFOs stand out, relative to all other fast LFP frequency components, for their remarkably high coherence.

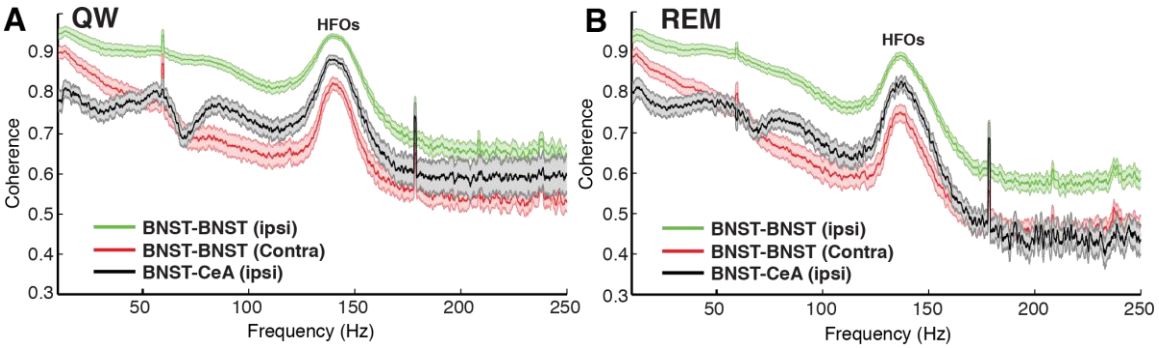

Figure 5. LFP coherence as a function of frequency. (**A**) Quiet waking (QW). (**B**) REM sleep. Group analyses of LFP coherence for three recording configurations depicted with different colors. **Green**: when the two electrodes were positioned in BNST of the same hemisphere. **Red:** when the two electrodes were positioned in BNST-AM of different hemispheres. **Black:** with one electrode in BNST-AM and the other in CeA ipsilaterally. Colored shading represents SEM.

Entrainment of unit firing by HFOs

A possible explanation for the high HFO coherence is volume conduction. Indeed, one could conceive of a situation where a densely interconnected group of neurons would generate open fields that are instantaneously conducted over large distances. This phenomenon would generate spurious LFP correlations, with no actual HFO-related firing or synaptic activity. However, if this were the case, one would not expect to find entrainment of unit activity by HFOs at many of the sites displaying them.

One problem when testing this prediction however is spectral leakage of spike waveforms into LFPs (Scheffer-Teixeira et al. 2013). Indeed, spike shapes can leak into several LFP bands, causing spurious unit-field correlations. To circumvent this difficulty, for all available units, we used spike-less reference LFPs (**Fig. 6A**, red; down-sampled to 1250 Hz) from a different tetrode than the one used to record the unit of interest (**Fig. 6A**, black; and performed Rayleigh tests (significance threshold of $p<0.01$). The lack of spike waveforms in the reference LFP excludes the possibility that spectral leakage of the spike shape into the LFP is responsible for significant unit-HFO relationships.

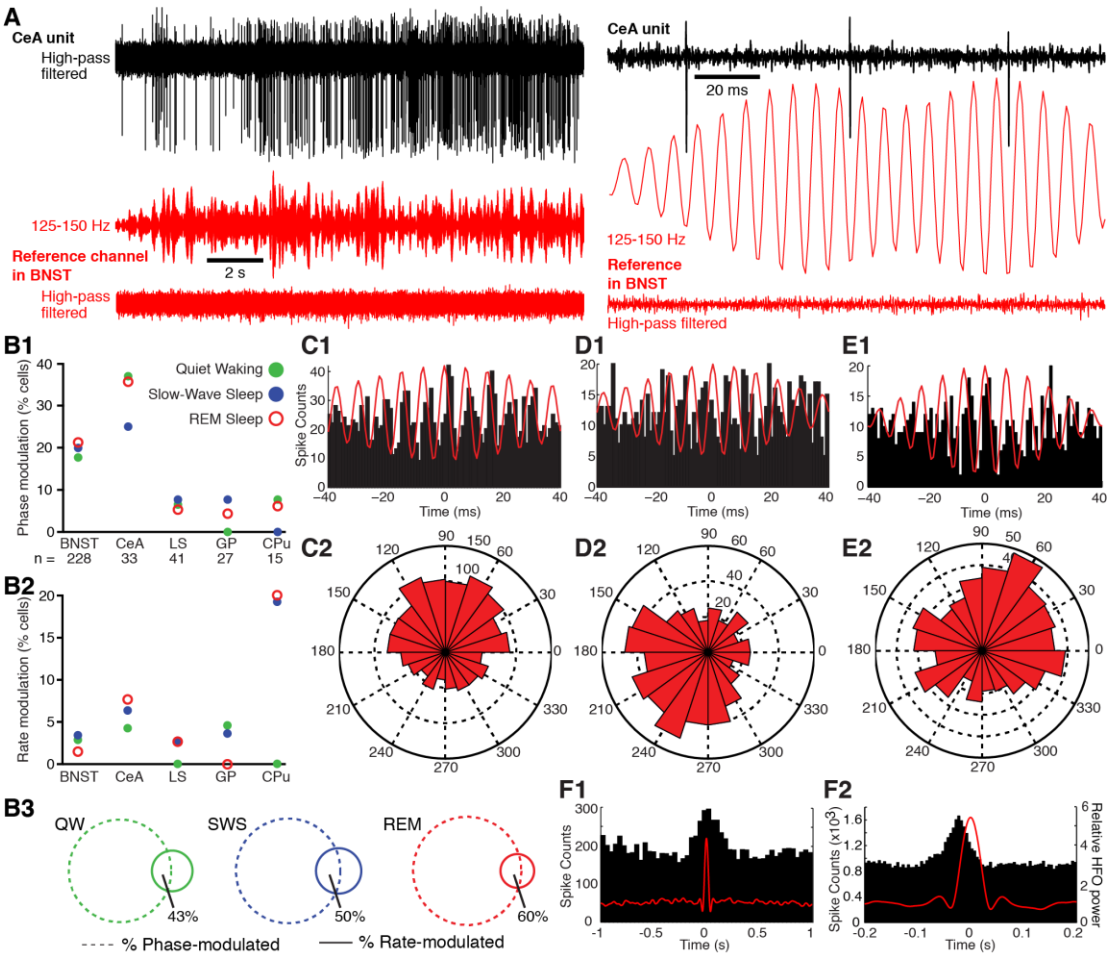

Figure 6. (**A**) Approach used to study entrainment of unit activity by HFOs. The band-passed (125-150 Hz) LFP recorded by a BNST reference channel (red) devoid of unit activity was used to assess the timing of unit activity in a different channel (CeA, black). From top to bottom: CeA unit activity (high-pass filtered), BNST reference signal band-pass filtered (125-150 Hz, middle) and same signal high-pass filtered (bottom), revealing lack of unit activity. Left, slow time base; right, expanded time base. Note that the gain on reference HFOs was doubled from left to right panel of A to facilitate inspection of HFO-spike phase relationships. (**B**) Incidence of units with significant phase- and rate-modulation by HFOs in different brain structures and behavioral states. (**B1**) Phase modulation. (**B2**) Rate modulation. (**B3**) Venn diagrams showing overlap between cells (BNST and CeA combined) with significant phase (dashed lines) and/or rate (continuous lines) modulation by HFOs in quiet waking (QW, left), slow-wave sleep (SWS, center) and REM sleep (right). Numbers adjacent to areas of overlap indicate proportion of rate-modulated units that are also phase-modulated. (**C-E**) Examples of units that were significantly phase-modulated by HFOs. (**C1, D1, E1**) Peri-HFO histogram of neuronal discharges. To compute these histograms, HFO spindles of high amplitude (top half of the overall distribution) were detected and centered on the positive cycle with the highest amplitude. Unit activity was then referenced to the corresponding HFO spindle. (**C2, D2, E2**) Rose plots of the cells shown in B1, C1, and D1, respectively. Unit in B was recorded in CeA during QW. Unit in C was recorded in BNST in REM sleep. Unit in D was recorded in BNST during QW. (**F**) Examples of cells recorded in BNST (**F1**) or CeA (**F2**) with significant firing rate modulation by HFOs. To construct these histograms, we computed spike counts (left y-axis; 20 ms bins) in windows (± 1 s, x-axis) centered on high amplitude HFO spindles (≥ 2 SD of averaged peak values). Right y-axis represents HFO power. To assess entrainment, we referenced unit activity to HFOs from a different tetrode than the one used to record the unit and performed a Rayleigh test with a significance threshold of $p<0.01$. To assess dependence of firing rate on HFO power, we computed spike counts in windows of ± 1 s centered on high amplitude HFO spindles (≥ 2 SD of averaged peak values). Then, to assess significance, we performed a Kilmogorov-Smirnov test comparing the actual distribution of spike counts to a uniform distribution, for each cell independently (significance threshold of $p \leq 0.01$). In addition, we excluded spurious positive results due to baseline modulations in firing rate using a binomial test comparing spike counts between the two 500 - 1000ms intervals flanking HFOs.

This analysis revealed that the incidence of units with significant HFO entrainment varied markedly depending on the recording sites (**Fig. 6B1**). Indeed, as many as 18-39% of BNST and CeA cells exhibited significant firing phase modulation by HFOs (**Fig. 6C,D**), indicating that HFOs are not volume conducted to the extended amygdala. In contrast, in the lateral septum, globus pallidus, and caudate-putamen, a significantly lower proportion of cells were entrained by HFOs (≤8%, chi-square test, p=0.016, units in BNST and CeA vs. all other sites). The higher incidence of phase modulated neurons in BNST and CeA relative to the other three recording sites was observed in all behavioral states (see colored symbols in **Fig. 6B1**). Although there were cell-to-cell variations in the preferred HFO firing phase of BNST and CeA neurons (compare **Fig. 6C-E**), most discharged preferentially during the negative phase of HFOs, irrespective of the behavioral state (**Fig. 7**).

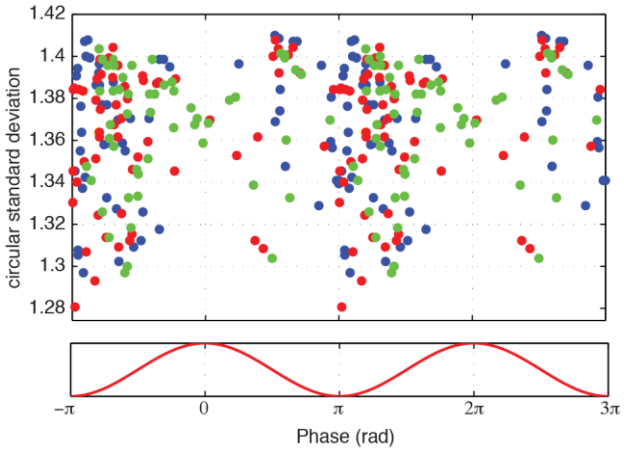

Figure 7. Preferred firing phase of significantly modulated BNST and CeA units. Colored symbols indicate behavioral state of epoch analyzed (red, REM; blue, SWS; green, quiet waking). Y-axis indicates depth of modulation. Data is replicated over two cycles for clarity.

It should be noted that a significant entrainment of spiking by HFOs does not imply that units fired at the HFO frequency, even transiently. In fact, the

majority of BNST and CeA cells with significant phase modulation had low firing rates, with 60, 68, and 79% of them firing below 5 Hz in quiet waking, REM sleep, and slow-wave sleep, respectively. However, the occasional spikes they generated tended to cluster at a consistent phase of the HFOs.

As mentioned above, relatively few neurons in the lateral septum, globus pallidus, and caudate-putamen showed a significant *firing phase* modulation by HFOs. Yet, a proportion displayed a significant *firing rate* modulation as a function of HFO power (**Fig. 6B2**). To assess this, we computed spike counts in windows of ± 1 s centered on high amplitude HFO spindles (≥2 SD of averaged peak values). Then, to assess significance, we performed a Kilmogorov-Smirnov test comparing the actual distribution of spike counts to a uniform distribution, for each cell independently (significance threshold of $p \leq 0.01$). In addition, we excluded spurious positive results due to baseline modulations in firing rate using a binomial test comparing spike counts between the two 500 – 1000 ms intervals flanking HFOs.

Using this approach, we observed that at all recording sites and in most behavioral states, a small proportion of neurons showed significant firing rate modulations in relation to HFOs (**Fig. 6B2**). As shown in the representative examples of **figure 6F**, the vast majority of these cells (≈90%) showed increases in firing rates in relation to HFOs with the remaining 10% showing either inhibitory or biphasic (excitation followed by inhibition) modulations. Importantly, the incidence of phase-modulated cells among BNST and CeA neurons was much higher (≥18%) than that of rate-modulated cells (≤7%; compare **Fig. 6B1**

and B2; note different y-axes) and only about half the latter were also phase-modulated (range 43-60%; **Fig. 6B3**). The highest incidence of rate-modulated cells was observed among striatal units in REM sleep and slow-wave sleep (**Fig. 6B2**), even though very few of these cells showed a significant phase modulation by HFOs (**Fig. 6B1**).

DISCUSSION

The present study was undertaken to characterize HFOs in structures of the extended amygdala, particularly, BNST, CeA, and immediately adjacent structures. We focused on the extended amygdala because work in other brain regions indicated that HFOs arise from interactions between GABAergic neurons (Jackson et al. 2011), the main cell type found in BNST and CeA (Poulin et al. 2009; Swanson and Petrovich 1998). Our experiments revealed that HFOs are prominent in the extended amygdala, they show systematic variations in amplitude as a function of behavioral states, they are coherent within and across hemispheres, and they entrain unit activity in a high proportion of neurons. The significance of these findings is considered below.

HFOs vary in a state-dependent manner and are highly coherent within and across hemispheres

In addition to the entrainment of extended amygdala neurons by HFOs (see below), several observations suggest that HFOs are not artifacts of our recording or filtering methods. First, periods of high-amplitude HFOs could be

observed in the raw LFPs throughout the sleep-waking cycle. Second, HFOs were abolished by common anesthetics (isoflurane and urethane) and could not be detected after CO_2 asphyxiation. Third, HFO amplitudes varied as a function of the animals' behavioral states. Indeed, they were significantly more pronounced during quiet wakefulness and REM sleep than during active waking or SWS.

An unusual property of HFOs relative to all other fast frequency LFP components was their high coherence. This is remarkable because LFP coherence generally decreases with distance and this reduction is particularly steep for high frequency components (Collins et al. 1999, 2001; Steriade et al. 1993, 1996). In contrast, HFO coherence was high within and between ipsilateral structures of the extended amygdala whereas that of other high frequency components was generally lower. Interestingly, for contralateral recording sites, HFO coherence although still very high, was significantly lower than between ipsilateral but more distant recording sites in the extended amygdala, again arguing against volume conduction.

HFOs are generated locally within the extended amygdala

Previously, HFOs were observed in a variety of cortical and subcortical structures (de Olszewski et al. 2013; Tort et al. 2013). In some cases, such as the hippocampus (Tort et al. 2013) and nucleus accumbens (Olszewski et al. 2013), HFOs appear to be generated locally. However in others, such as the caudate nucleus as well as the frontal and parietal cortices, local tetrodotoxin or

muscimol infusions did not affect HFO power (Olszewski et al. 2013), suggesting that they are volume conducted from a distant source.

Consistent with this, we found that the incidence of neurons whose firing were modulated by the phase of HFOs varied markedly depending on the recording sites. In all behavioral states, it was highest in the extended amygdala (BNST ≥ 18%; CeA ≥ 25%) and lowest in the lateral septum, globus pallidus, and caudate-putamen (≤ 8%). These findings support the view that the HFOs seen in the extended amygdala are not volume conducted from a distant source, but are generated locally. The scarcity of significantly entrained units in the globus pallidus and caudate-putamen is consistent with earlier findings suggesting that the HFOs seen in the caudate nucleus are not generated locally (Olszewski et al. 2013).

Origin of HFOs

It was reported that hippocampal HFOs resist blockade of AMPA/kainate receptors, but are abolished by GABA-A receptor antagonists (Jackson et al. 2011). Therefore, these results suggest that HFOs are not dependent on rhythmic interactions between glutamatergic and GABAergic neurons, in contrast with gamma oscillations (Fisahn et al. 1998; Whittington et al. 2000). Given their high frequency and independence from fast glutamatergic transmission, the high HFO coherence between distant recording sites raises a major explanatory challenge: what mechanisms could support the long-range synchronization of HFOs?

Unfortunately, the study of HFOs is just beginning and we are reduced to conjectures.

One possibility, put forward by Traub and colleagues (Traub et al. 2011), is that HFOs arise from electrical coupling between axons. Although computational modeling supports this possibility (for instance see Maex and De Schutter 2007; Traub et al. 2008), there is little if any electron microscopic evidence of gap junctions between axons in the hippocampus, amygdala, or BNST. A related possibility is that ephaptic coupling among unmyelinated axons is sufficient to synchronize the firing of many closely spaced axons. Ephaptic interactions are maximized when the extracellular conductance is low (Barr and Plonsey 1992), a condition met in bundles of tightly packed unmyelinated bundles of axons such as found in the olfactory nerve, stria terminalis, and anterior commissure (Lamantia and Rakic 1990; Blinder et al. 2003). A computational modeling study of the olfactory nerve provided support for this possibility (Bokil et al. 2001). Furthermore, actual demonstration of such ephaptic interactions was obtained in crab by Katz and Schmitt (1940, 1942). Of particular relevance to HFOs is the fact that ephaptic interactions can minimize differences in conduction velocity between neighboring axons with slightly different condition speeds (reviewed in Debanne et al. 2011). By synchronizing activity in bundles of unmyelinated axons, this effect might contribute to the high coherence of HFOs. However, this hypothetical model awaits experimental scrutiny.

ACKNOWLEDGEMENTS (GRANTS):

This work was supported by R01 grants MH-098738 and MH-083710 from NIMH.

DISCLOSURES:

The authors declare that they have no conflict of interest, financial or otherwise.

AUTHOR CONTRIBUTIONS:

Darrell Haufler carried out the electrophysiological experiments, analyzed most of the data, and contributed to the design of the experiments.

Denis Paré analyzed some of the data, wrote the manuscript and contributed to the design of the experiments.

REFERENCES

Barr RC, Plonsey R. Electrophysiological interaction through the interstitial space between adjacent unmyelinated parallel fibers. *Biophys J* 61:1164-75, 1992.

Berens P. CircStat: A Matlab Toolbox for Circular Statistics, *J Stat Software* 31 http://www.jstatsoft.org/, 2009.

Blinder KJ, Pumplin DW, Paul DL, Keller A. Intercellular interactions in the mammalian olfactory nerve. *J Comp Neurol* 466:230-9, 2003.

Bokil H, Laaris N, Blinder K, Ennis M, Keller A. Ephaptic interactions in the mammalian olfactory system. *J Neurosci* 21:RC173, 2001.

Bullock TH, McClune MC. Lateral coherence of the electrocorticogram: a measure of brain synchrony. *Electroencephalogr Clin Neurophysiol* 73: 479-498, 1989.

Buzsaki G. Rhythms of the brain. Oxford University Press, USA, 2006.

Buzsáki G, Horváth Z, Urioste R, Hetke J, Wise K. High-frequency network oscillation in the hippocampus. *Science* 256:1025-7, 1992.

Collins DR, Lang EJ, Paré D. Spontaneous activity of the perirhinal cortex in behaving cats. *Neuroscience* 89:1025-1039, 1999.

Collins DR, Pelletier JG, Paré D. Slow and fast (gamma) neuronal oscillations in the perirhinal cortex and lateral amygdala. *J Neurophysiol* 85:1661-1672, 2001.

Debanne D, Campanac E, Bialowas A, Carlier E, Alcaraz G. Axon physiology. *Physiol Rev* 91:555-602, 2011.

Desmedt JE and Tomberg C. Transient phase-locking of 40 Hz electrical oscillations in prefrontal and parietal human cortex reflects the process of conscious somatic perception. *Neurosci Lett* 168: 126-129, 1994.

Fisahn A, Pike FG, Buhl EH, Paulsen O. Cholinergic induction of network oscillations at 40 Hz in the hippocampus in vitro. *Nature* 9: 186-189, 1998.

Gray CM, Konig P, Engel AK, Singer W. Oscillatory responses in cat visual cortex exhibit inter-columnar synchronization which reflects global stimulus properties. *Nature* 338: 334-337, 1989.

Hazan L, Zugaro M, Buzsaki G. Klusters, NeuroScope, NDManager: a free software suite for neurophysiological data processing and visualization. *J Neurosci Methods* 155: 207-216, 2006.

Heimer L, Van Hoesen GW, Trimble M, Zahm DS. The anatomy of the basal forebrain. In: *Anatomy of Neuropsychiatry*. Amsterdam, Elsevier, 2008, Chap. 3, p. 27-67.

Hunt MJ, Falinska M, Łeski S, Wójcik DK, Kasicki S. Differential effects produced by ketamine on oscillatory activity recorded in the rat hippocampus, dorsal striatum and nucleus accumbens. *J Psychopharmacol* 25:808-21, 2011.

Hunt MJ, Kasicki S. A systematic review of the effects of NMDA receptor antagonists on oscillatory activity recorded in vivo. *J Psychopharmacol* 27:972-86, 2013.

Jackson J, Goutagny R, Williams S. Fast and slow γ rhythms are intrinsically and independently generated in the subiculum. *J Neurosci* 31:12104-17, 2011.

Katz B, Schmitt OH. Electric interaction between two adjacent nerve fibres. *J Physiol (London)* 97:471-88, 1940.

Katz B, Schmitt OH. A note on interaction between nerve fibers. *J Physiol (London)* 100:369-371, 1942.

Lamantia AS, Rakic P. Cytological and quantitative characteristics of four cerebral commissures in the rhesus monkey. *J Comp Neurol* 29:520-37, 1990.

Maex R, De Schutter E. Mechanism of spontaneous and self-sustained oscillations in networks connected through axo-axonal gap junctions. *Eur J Neurosci* 25:3347-58 2007.

Murthy VN, Fetz EE. Coherent 25-35 Hz oscillations in the sensorimotor cortex of awake behaving monkeys. *Proc Natl Acad Sci USA* 89: 5670-5674, 1992.

Olszewski M, Dolowa W, Matulewicz P, Kasicki S, Hunt MJ. NMDA receptor antagonist-enhanced high frequency oscillations: are they generated broadly or regionally specific? *Eur Neuropsychopharmacol* 23:1795-805, 2013.

Poulin JF, Arbour D, Laforest S, Drolet G. Neuroanatomical characterization of endogenous opioids in the bed nucleus of the stria terminalis. *Prog Neuropsychopharmacol Biol Psychiatry* 33:1356-65, 2009.

Scheffer-Teixeira R, Belchior H, Caixeta FV, Souza BC, Ribeiro S, Tort AB. Theta phase modulates multiple layer-specific oscillations in the CA1 region.

Cereb Cortex 22:2404-14, 2012.

Scheffer-Teixeira R, Belchior H, Leão RN, Ribeiro S, Tort AB. On high-frequency field oscillations (>100 Hz) and the spectral leakage of spiking activity. *J Neurosci* 33:1535-9, 2013.

Scheffzük C, Kukushka VI, Vyssotski AL, Draguhn A, Tort AB, Brankačk J. Selective coupling between theta phase and neocortical fast gamma oscillations during REM-sleep in mice. *PLoS One* 6:e28489, 2011.

Steriade M, Nuñez A, and Amzica F. A novel slow (<1 Hz) oscillation of neocortical neurons in vivo: depolarizing and hyperpolarizing components. *J Neurosci* 13: 3252-3265, 1993.

Steriade M, Amzica F, and Contreras D. Synchronization of fast (30-40 Hz) spontaneous cortical rhythms during brain activation. *J Neurosci* 16: 392-417, 1996.

Swanson LW, Petrovich GD. What is the amygdala? *Trends Neurosci* 21:323-31, 1998.

Tort AB, Kramer MA, Thorn C, Gibson DJ, Kubota Y, Graybiel AM, Kopell NJ. Dynamic cross-frequency couplings of local field potential oscillations in rat striatum and hippocampus during performance of a T-maze task. *Proc Natl Acad Sci USA* 105:20517-22, 2008.

Tort AB, Scheffer-Teixeira R, Souza BC, Draguhn A, Brankačk J. Theta-associated high-frequency oscillations (110-160Hz) in the hippocampus and neocortex. *Prog Neurobiol* 100:1-14, 2013.

Traub RD, Middleton SJ, Knöpfel T, Whittington MA. Model of very fast (> 75 Hz) network oscillations generated by electrical coupling between the proximal axons of cerebellar Purkinje cells. *Eur J Neurosci* 28:1603-16, 2008.

Traub RD, Cunningham, MO, Whittington MA. Chemical synaptic and gap junctional interactions between principal neurons: partners in epileptogenesis. *Neural Netw* 24:515-525, 2011.

Whittington MA, Traub RD, Kopell N, Ermentrout B, Buhl EH. Inhibition-based rhythms: experimental and mathematical observations on network dynamics. *Int J Psychophysiol* 38:315-36, 2000.

Ylinen A, Bragin A, Nádasdy Z, Jandó G, Szabó I, Sik A, Buzsáki G. Sharp wave-associated high-frequency oscillation (200 Hz) in the intact hippocampus: network and intracellular mechanisms. *J Neurosci* 15:30-46, 1995.

CHAPTER IV

De novo emergence of brain rhythms through nonlinear signal integration

In the fields of electronics and signal processing, *frequency mixing* refers to the combining of oscillations in the presence of a non-linearity, resulting in the emergence of novel spectral components. This effect has found widespread practical application to technologies such as radio (Fessenden, 1902; Poole, 2015) and sound synthesis (Roads and Strawn, 1985). Despite its simplicity, this mechanism has been largely ignored in neuroscience. Here test for frequency mixing in the cross-frequency interactions of local field potentials (LFPs) recorded from multiple sites in the extended amygdala and neighboring structures. By identifying dependences in the phases across sets of frequencies, we show that the LFP exhibits hallmark characteristics of convergent oscillatory signals undergoing frequency mixing. Specifically, we find oscillatory activity at the frequency sum and difference (*emergent* components) of two putative input signals, as well as at double these frequencies (*harmonic* components), and at the input frequencies themselves (*root* components). Critically, the identity and expression of the root, emergent, and harmonic rhythms change in a state- and region-specific manner and emergent rhythms entrain neuronal activity. Thus, considering non-linear interference effects disambiguates the origin of multiple concurrent oscillatory processes and their relationship to neuronal activity. These findings are of general importance for interpreting cross-frequency interactions, relating the spiking activity of single neurons to LFPs, and inferring signal propagation and integration throughout the brain.

Even when bombarded with random inputs, neural networks assume oscillatory states (Reyes, 2003; Bartos et al., 2007) that arise from the interplay between the intrinsic properties of neurons (Llinas, 1988; Whittington and Traub, 2003) and the architecture of the network in which they are embedded (Steriade and Llinas, 1988). Supporting the idea that these rhythms fulfill critical signaling functions, neural oscillations are well conserved across mammalian species (Buzsaki et al., 2013) and in some cases, phyla (Kay, 2015). Indeed, oscillations provide an energy efficient way to coordinate interactions within and between networks by creating alternating periods of increased and decreased neuronal excitability. As a result, oscillations allow for the selective routing of information and the flexible formation of cell assemblies based on phase (Buzsaki and Draguhn, 2004; Fries, 2015; Sejnowski and Paulsen, 2006).

Oscillations range widely in frequency (~0.1-300 Hz) with lower frequency rhythms recruiting larger networks than faster rhythms (Steriade et al. 1993; Konig et al., 1995) and the power of the faster oscillations changing as a function of the phase of the slower ones (Bragin et al., 1995; Steriade and Amzica, 1996). Although the amplitude of oscillations generally decreases as their frequency increases (Nunez, 1981), in specific networks and functional contexts some rhythms deviate from this global trend and become more salient (Gray et al., 1989; Singer, 1999). Depending on the brain region and behavioral state, oscillations of distinct frequencies predominate, but many can coexist and interact in the same or different networks (Buzsaki and Draguhn, 2004). At any given moment, local field potentials (LFPs) exhibit a continuously evolving

mixture of oscillatory components, which are thought to reflect interactions between different local circuit elements with different oscillatory propensities.

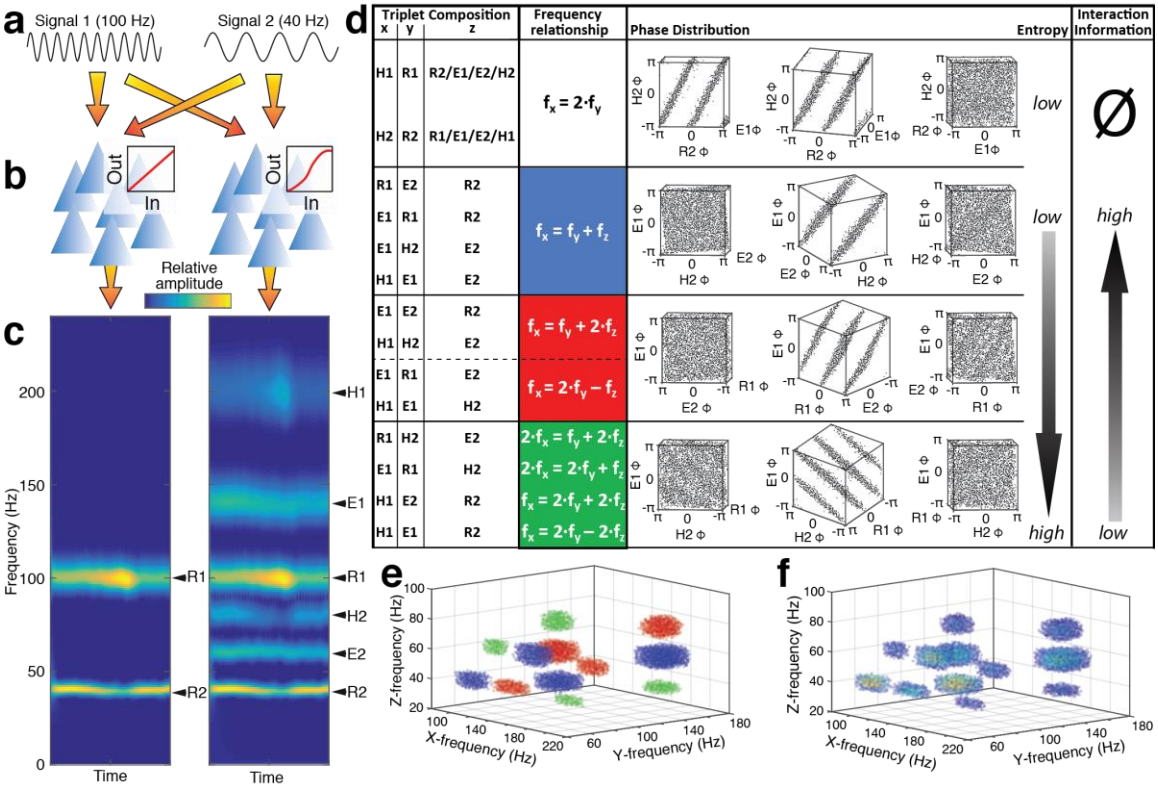

Figure 1. Mixing model of frequency generation. a, Two oscillatory inputs are integrated by a simulated neuronal network with a linear (**b**, left) or non-linear (**b**, right) transfer function. In the linear case (**c**, left), the network expresses only activities at the frequency of the two original signals (Root 1 – R1; Root – R2). In the non-linear case (**c**, right), the network expresses additional oscillatory components at the sum of (Emergent 1 – E1), difference between (Emergent 2 – E2), and double of the input signals (Harmonic 1 – H1; Harmonic 2 – H2). The left and right plots each show 2 seconds of simulated data. **d,** Different combinations of three output signals (x, y, z, left three columns) entertain different frequency (fourth column) and phase relationships (fifth column), resulting in different magnitudes of phase entropy (sixth column) and phase interaction information (seventh column). Color-coding in third column of **d** matches that of the clusters in **e**. The fifth column of **d** shows graphs plotting the phase of three of these oscillations against each other, as seen from three different perspectives. **e**, Frequency triplets with large phase interaction information, color coded by their composition and magnitude of interaction information, as defined in the fourth column of **d** **(**blue, highest; red, intermediate; green, lowest. **f**, Phase interaction information between different frequencies (warmer colors indicating higher values). In the noisy and constantly fluctuating conditions of the brain, the blue clusters are the most likely to be detected.

At present, mechanisms that govern cross-frequency interactions are poorly understood. Here we take a unique approach to this problem. It can be shown through elementary trigonometry that when oscillatory signals are added in the presence of a nonlinearity, new signals are formed at the sums and differences of original signal frequencies, a phenomenon called *frequency mixing* (**Fig. 1a-c**). Assuming that neuronal networks integrate multiple narrow band oscillations, and considering that non-linearities are ubiquitous in the nervous system (Moutard et al., 2015), frequency mixing should readily occur and particular relationships between oscillations would be predicted. Below, we first describe frequency mixing in the context of a very basic model of neuronal network integration and then describe a novel method for detecting it in the brain.

Consider two sinusoidal signals of the form:

$$S_k(t) = A_k \sin\left(2\pi f_k(t + t_{k)}\right) \quad (1)$$

where f_k represents the frequency of the signal in Hz, and t_k determines the signal phase at time 0. We employ a second order polynomial to represent the activation function of the network for input *s*:

$$F(s) = B + Cs + Ds^2 \quad (2)$$

Note that this can be viewed as the first three terms of the Maclaurin Series approximating an arbitrary nonlinear function around 0. In applying sinusoidal input to this activation function, we set constant *B* so that the resulting output oscillates around 0, and so we omit it in the equations that follow. *C* defines a

linear amplification factor and *D* determines the magnitude of the non-linearity. If we apply eq. 3 to a compound input consisting of sinusoids S_1 and S_2 we get:

$$F(S_1 + S_2) = CS_1 + CS_2 + DS_1{}^2 + DS_2{}^2 + 2DS_1S_2 \quad (3)$$

Replacing the signals in eq. 3 by their full sinusoidal representation and applying the product-to-sum trigonometric identity yields a sum of six sinusoids characterized in **Table 1** below.

	AMPLITUDE	FREQUENCY	UNWRAPPED PHASE
ROOT COMPONENTS (R1, R2)	CA_1	f_1	$2\pi f_1(t + t_1)$
	CA_2	f_2	$2\pi f_2(t + t_2)$
HARMONIC COMPONENTS (H1, H2)	$\frac{DA_1}{2}$	$2f_1$	$2 \cdot 2\pi f_1(t + t_1)$
	$\frac{DA_2}{2}$	$2f_2$	$2 \cdot 2\pi f_2(t + t_2)$
EMERGENT COMPONENTS (E1, E2)	DA_1A_2	$f_1 - f_2$	$2\pi f_1(t + t_1) - 2\pi f_2(t + t_2)$
	DA_1A_2	$f_1 + f_2$	$2\pi f_1(t + t_1) + 2\pi f_2(t + t_2)$

Table 1. Amplitude, frequency, and phase of output signals predicted by frequency mixing. Parameters of sinusoids resulting from the interaction of S_1 and S_2 described in equation 3, representing the faster and slower input signals, respectively. The harmonic and emergent components are cosine functions whereas the root components are sine waves.

This model makes specific predictions regarding the frequency, amplitude and phase of the oscillations resulting from the interaction between the two original oscillations. We first describe these predictions and then explain how we exploited them to determine whether frequency mixing influences cross-

frequency relationships in neuronal networks. Under the model presented, six components are expected to result from the two input signals. *Root* components occur at the input signal frequencies themselves. *Harmonic* components, (H1, H2), exhibit frequency double that of the root components, while *emergent* components oscillate at the sum of (E1), or difference between (E2), the root component frequencies (**Fig. 1d; Table 1**). As to their amplitude, harmonic components are expected to vary proportionally to the root signal's amplitude whereas emergent components are expected to vary proportionally to the amplitudes of both root components (**Table 1**). Last, the phases of the harmonic and emergent components bare a special relationship to the phases of the root signals. Insights into these relationships can be gained by comparing 3D distributions that plot the phase of three output components against one another for simulated LFP data that expresses mixing (**Fig. 1d**, fifth column). For all triplet combinations that include a root and its harmonic (**Fig. 1d**, top row), knowing the phase of one of the two decreases uncertainty regarding the phase of the other, with no further information provided by the phase of a third output signal. In contrast, plots relating the phase of frequency triplets that include an emergent component but not a root and its harmonic (**Fig. 1d**, rows 2-4) exhibit a three-way phase relationship. In these cases, no combination of two frequencies is sufficient to describe the phase relationships that exist in the plot because the distribution is concentrated on a plane with an oblique orientation to all three axes.

Overall, these considerations suggest that if frequency mixing influences cross-frequency relationships in neuronal networks, particular triplets of oscillatory components should hold a predictive three-way phase relationship to each other. One approach to detect such relationships would be to compute phase entropy for different frequency triplets (**Fig. 1d**, sixth column). For interacting frequency triplets, entropy would be lower because the phase relationships between them is are random. However, phase entropy is expected to be similarly low for frequency triplets that hold a two-way (**Fig. 1d**, top row) or three-way relationship (**Fig. 1d**, rows 2-4) and these are important to distinguish: The former can be due to simple waveform asymmetry or pairwise cross-frequency interactions while the latter cannot. To detect relationships that strictly depend on three-way phase relationships, we computed the *interaction information* of signal phases (pII; **Fig. 1d**, right-most column), a measure used in several scientific disciplines to quantify multi-way dependencies between three or more variables (McGill 1954; Jakulin and Bratko 2004).

Interaction information quantifies the amount of information expressed by a set of attributes, in this case about the phase of three different frequencies, which is not present in any subsets. In contrast with phase entropy, pII can distinguish between two- and three-way phase dependencies. Therefore, pII will be negligible for frequency triplets including a root, its harmonic and any other frequency **(Fig. 1d**, top row) since only the first two frequencies hold a predictive relationship to each other, independently of the third. In contrast, pII will be non-zero for frequency triplets that exhibit a three-way predictive relationship (**Fig. 1d**,

rows 2-4). Different sets of components exhibit distinct phase distributions (**Fig. 1d**, rows 2 to 4), with the spacing between high-density regions decreasing from the blue to red to green groups. As the spacing decreases and the number of bands increases, the pII will decrease because of the associated increase in phase uncertainty across the specific three-way interaction under consideration.

Armed with these predictions, we first tested the usefulness of pII estimates on simulated data expressing mixing, where two noisy oscillatory signals are combined through a non-linear function (**Fig. 1b,c**, right). This is meant as a simple model of afferent signals integrated by a local network, as indicated by the figure. The signals varied randomly in amplitude (± 16.7%) and had a mean frequency of 40 and 100 Hz with SDs of 1.0 and 1.5 Hz, respectively. The phases of the resulting oscillations were determined by applying wavelet analysis and pII was computed for across all possible combinations of three frequencies in the range of 2 to 220 Hz, in intervals of 2 Hz. Frequency triplets with pII values that exceeded the 95th percentile are either colored based on phase distribution of their centroids as per **figure 1d** (fourth column; **Fig. 1e**) or based on pII values (**Fig. 1f**; warmer colors indicate higher pII values). Consistent with the model's predictions, blue-type clusters had the highest pII centroid values and occurred at frequencies satisfying the relationship $x = y + z$ (**Fig. 1e,f; Supplementary Fig. 1**).

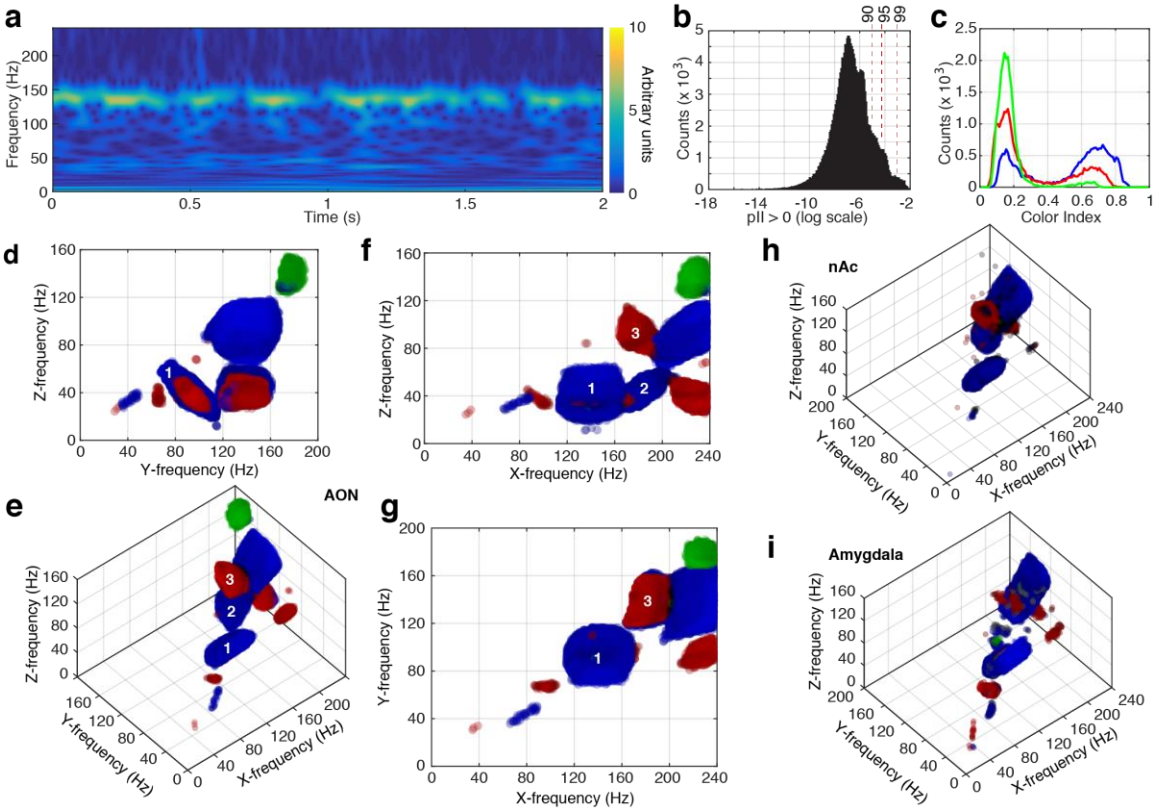

<u>Figure 2</u>. Applying the mixing model to LFPs recorded in the AON under MK-801. **a**, Spectrogram. **b**, Frequency distribution of pII values (x-axis: natural logarithmic scale). Red dashed vertical lines mark the 90, 95, and 99 percentile pII values. **c**, Frequency distributions of color index (see Methods). **d-g**, Interacting frequency triplets color coded by the frequency relation they satisfy (see Fig. 1d) on 2D (**d-f**) and 3D (**g**) graphs. Similar data is provided for LFPs recorded in nAc (**h**) and the amygdala (**i**).

In contrast with the stable signals used in our simulations, neurons receive changing input patterns. Given the predictions of **Figure 1d**, even in these more complex conditions, the mixing principle is expected to have a clear signature: frequency triplets with the highest pII values should cluster along the diagonal of plots relating the highest frequency (x) against the sum of the two lower frequencies (y, z).

To test whether the mixing principle is operative in the brain, we obtained LFP and unit recordings from many cortical and subcortical structures in eleven rats (**Supplementary Table 1**). The data was segmented by behavioral state

including active waking (AW), quiet waking (QW), slow-wave sleep (SWS) and in conditions of partial N-methyl-D-aspartate receptor (NMDAR) blockade (MK-801, 0.1 mg/kg, i.p.). The latter state, which is considered a model of schizophrenia (Gonzalez-Burgos and Lewis, 2012), is particularly favorable to test the mixing model because it is associated with a stereotyped pattern of LFP activity, including prominent high-frequency oscillations (HFOs) in the 130-150 Hz range (**Fig. 2a**).

We first consider the case of the anterior olfactory nucleus (AON) under MK-801 (**Fig. 2a-g**). Recording sites in the extended amygdala and adjacent structures yielded similar results (**Fig. 2h,i; Supplementary Figs. 2-4**). To determine whether interacting frequency triplets corresponded to the frequency relations predicted by the mixing model (**Fig. 1d**), phase plots of frequency triplets with high pII values (>90 percentile; **Fig. 2b**) were analyzed with 3D analogues of Fast Fourier Transforms (FFTs) to assign each frequency triplet to the blue, red, or green grouping (**Fig. 2c;** see Methods). The position of the frequency triplets with high pII values is shown in 2D (**Fig. 2d,f,g**) and 3D (**Fig. 2e**) graphs.

As predicted by the mixing model, blue-type phase distributions were most frequently observed followed by red and green (**Fig. 2c**), and the highest pII values (**Fig. 2d-g**, blue) characterized frequency triplets near the plane defined by $x = y+z$ in the space of frequencies (**Fig. 2f**).

In further support of the mixing model, and suggesting the identities of specific frequency components, several clusters exhibited an elongated ellipsoid

form with distinct orientations with respect to the frequency axes. The most parsimonious interpretation is as follows: cluster 1, with (X,Y,Z) coordinates at ~ (140, 100, 40) Hz is comprised of the high root, low emergent, and low root components respectively. In this state characterized by pronounced 140Hz activity in the LFP, the 140 Hz root signal is relatively fixed in frequency, whereas the lower root at 40 Hz is more variable. The oblique orientation of this cluster, showing negative correlation between the Y and Z components (**Fig. 2d**), is therefore due to the low emergent signal on the Y axis decreasing in frequency as a consequence of the low root increasing in frequency towards the higher root signal and thereby decreasing the difference between them. Consistent with this, cluster 2 (**Fig. 2f,e)**, located at ~(180, 140, 40) and consisting of the high emergent, high root, and low root components, shows a positive correlation between the high emergent component and low root. This is expected as the sum of the two root signals increases as the low root increases. Finally, cluster 3, located at ~ (180, 140, 100), consists of the high emergent, high root, and low emergent. Its phase distribution matches the red-group as predicted, and it is oriented such that the lower emergent component decreases in frequency as the high emergent increases (**Fig. 2f,e**), which would be expected when the lower root increases in frequency.

The state induced by partial NMDAR blockade is unusual for its stability and stereotypy, raising the question of whether the mixing principle is expressed in other behavioral states. To address this question, we obtained LFP recordings from different structures and in different behavioral states. To test whether the

interacting frequencies conform to the model's predictions, we extracted the centroid of clusters with the highest pII values (blue clusters) and plotted their frequencies on x vs. y+z plots (**Fig. 3a-d**). These analyses confirmed the general applicability of the mixing principle. That is, in a variety of structures and behavioral states, frequency triplets with the highest pII values lay on the main diagonal (x=y+z; **Fig. 3a-d**). The probability that such distributions could have been obtained by chance was p<10^-5.

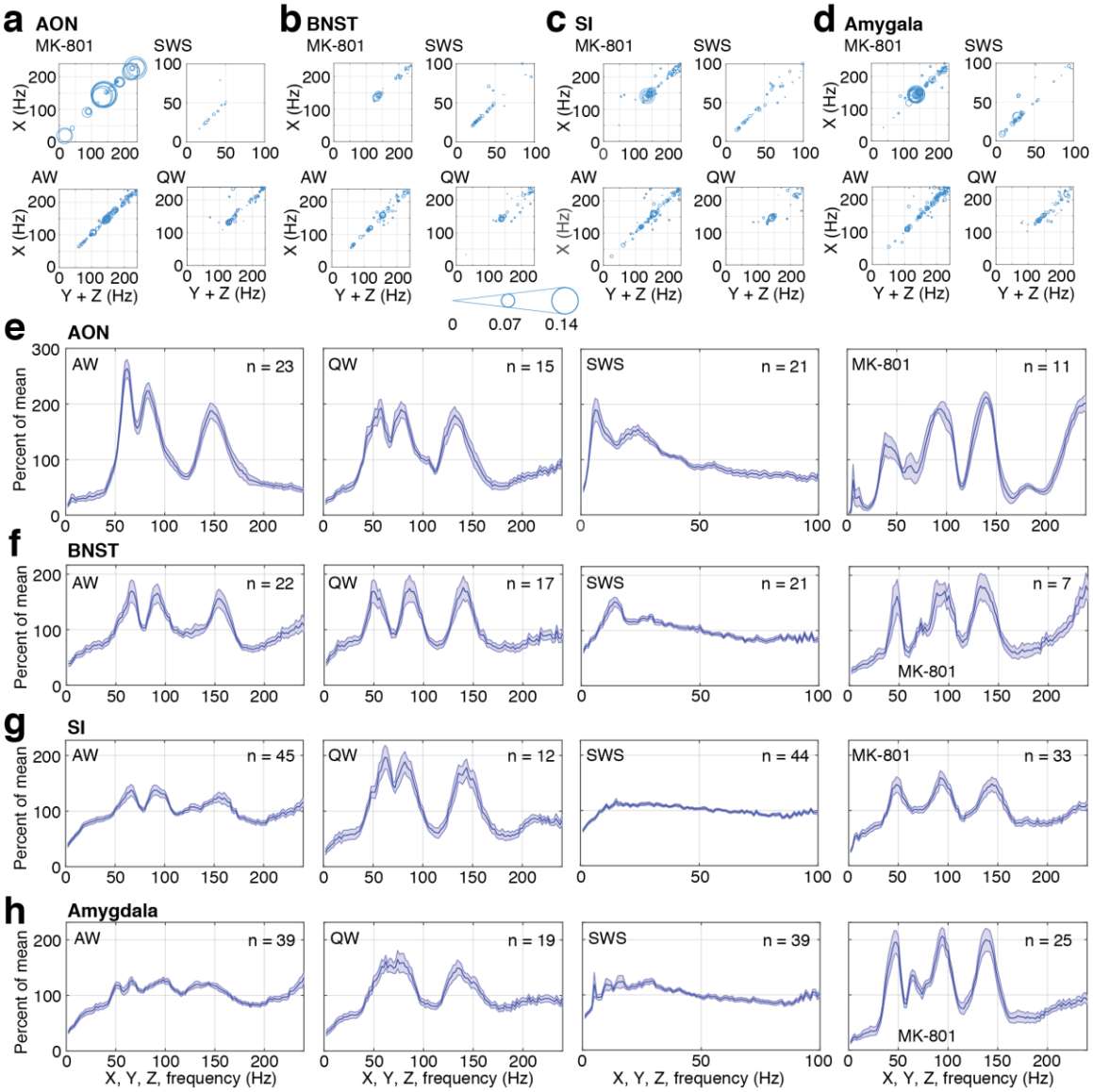

Figure 3. Region- and state-dependent variations in pII values and interacting frequencies. **a-d**, x vs. y + z frequency plots for the structures and behavioral states indicated. The diameters of the circles is proportional to the magnitude of the pII values (scaling at bottom of **b**). In all cases shown in **a-d**, the probability that the centroid locations would satisfy the x = y + z relation by chance is p < 10^-5. **e-h**, pII amplitudes of triplets with an x, y, or z frequency including a given value, expressed relative to all pII values, for the structures and behavioral states indicated. The n values refer to total recording sites over all recordings used.

Importantly, we observed marked region and state-dependent differences in the magnitude of pII values (indicated by the diameters of the circles in **Fig. 3a-d**) and in the identity of the interacting frequencies (**Fig. 3e-h; Supplementary Figs. 5-6**). With respect to regional variations, LFPs obtained

from the extended amygdala and adjacent structures (**Fig. 3, Supplementary Fig. 5**) generally displayed higher pII values than at cortical sites (**Supplementary Fig. 6**). With respect to state-dependence, in all recorded regions, interacting frequencies were lower and more variable in SWS than in QW, AW, and MK-801 (note different frequency axis range for SWS vs. other states in **Fig. 3e-h**). In the latter three states, most subcortical regions had three dominant frequencies, with the highest one in the 130-170 Hz range, and the lower two frequencies adding up to the highest one (**Fig. 3e-h; Supplementary Fig. 5**). In cortical regions, a similar situation was usually observed under MK-801 but not in other states (**Supplementary Fig. 6**). Although the centroid positions match prediction, there are multiple possible identities for the x, y, and z components of each centroid. A complete picture of local signal dynamics thus requires further study.

While these results suggest that the mixing principle is expressed in the brain, the question remains as to whether it has a significant impact on LFP power. In order to address this question, mixing has to be assessed on a moment-to-moment basis. However, because pII is a property of the phase *distribution* for particular frequency triplets, pII cannot be determined directly for individual LFP samples. Instead, using a frequency triplet with high pII, we sorted samples based on whether they occurred at the expected (preferred) regions of the phase distribution (overexpressed during high mixing) or in non-preferred regions (low mixing; **Supplementary Fig. 7**). We use the cluster corresponding to the high emergent and two root frequencies for the AON recording analyzed in

Fig. 2, for which pII values are high (cluster 2, **Fig. 2d,e**). This allows examination of the low emergent component without its explicit use the sorting process. We computed the ratio of LFP power in conditions of high vs. low mixing (**Fig. 4a,b**). Using the frequency triplet at the center of the cluster to determine mixing (**Fig. 4a,b,** black), power at the low emergent frequency was increased by nearly 30% in conditions of high mixing (bootstrap resampling, $p<0.001$).

When nearby frequency triplets were used to identify mixing, with the low root and high emergent frequencies both shifted down (**Fig. 4a-b**, blue) or up (**Fig. 4a-b**, red), LFP power in high mixing conditions increased less than with the preferred frequencies (bootstrap resampling, p's <0.001). Moreover, the shift in the frequency of maximum increase of the low emergent component was *opposite* that of the selecting frequencies, supporting our assessment of component identities and demonstrating their interdependence (bootstrap resampling, p's <0.001).

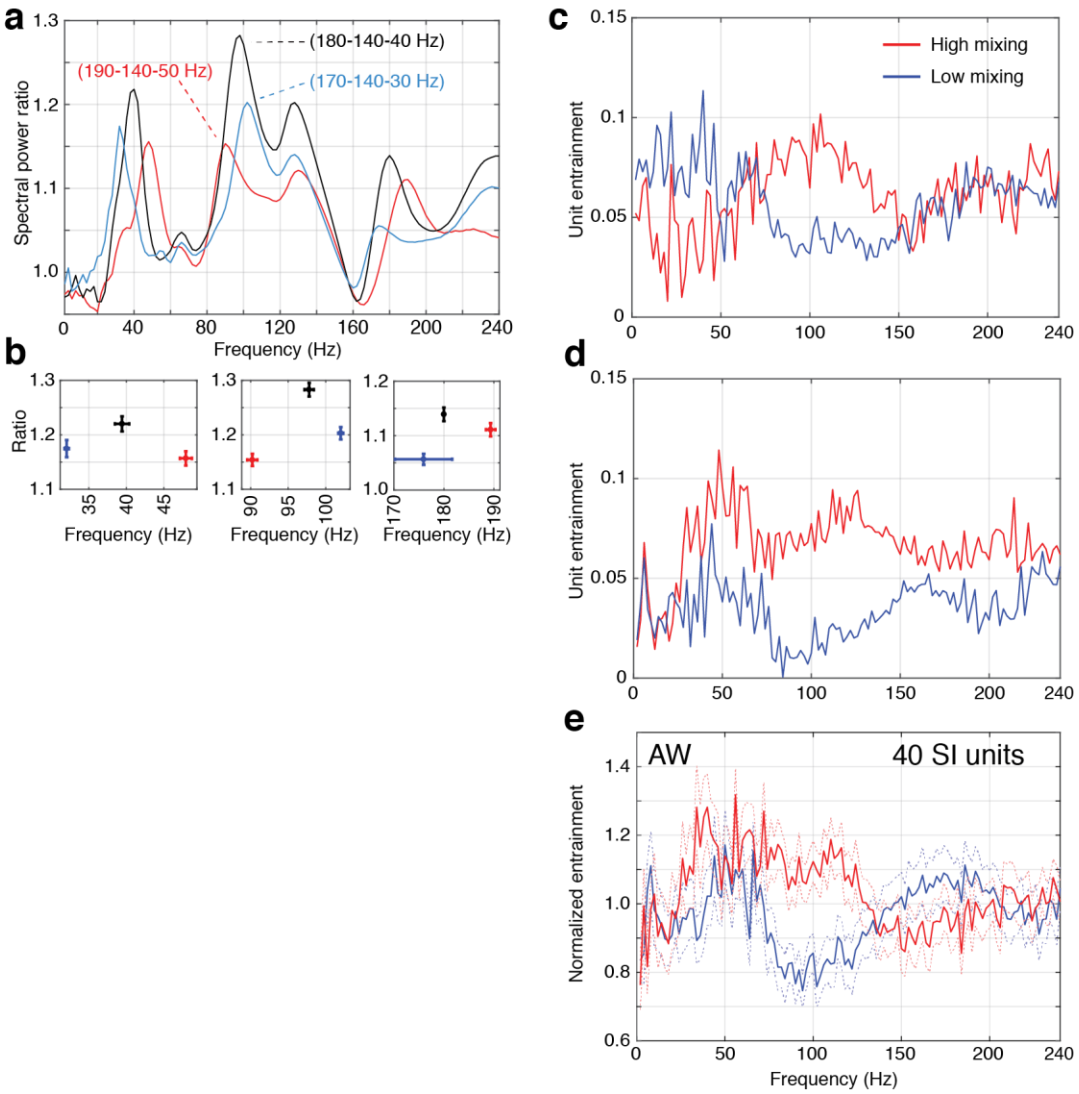

Figure 4. Impact of mixing on LFP power and unit entrainment. **a**, Ratio of spectral power in conditions of high vs. low mixing. LFP samples were sorted into high and low mixing groups as described in supplementary figure 6. Black lines show the power ratio with the preferred interacting frequencies at 40, 140, and 180 Hz, or neighboring non-preferred frequencies belonging to the same high pII cluster (cluster 2 of Fig. 2e,f) that were shifted down (blue; 30, 140, 170) or up (red; 50, 140, 190). **b**, Mean ± SD of the frequency and spectral power ratio of the peaks centered around 40 Hz, 100 Hz, and 180 Hz. With the preferred selecting frequencies, power at the low emergent frequency was increased by nearly 30%. When using non-preferred interacting frequencies that were shifted down (blue) or up (red), LFP power in high mixing conditions increased less and it was maximal at a frequency shifted in the opposite direction to that of the selecting frequencies. **c-d,** Unit entrainment (y-axis) as a function of frequency (x-axis) of example fast-spiking SI cells in conditions of low (blue) and high (red) mixing during active waking (AW). **e**, Normalized entrainment (mean ± SEM) of 40 SI fast-spiking unit during active waking.

To rule out the possibility that the higher power of the low emergent frequency observed in conditions of high mixing was due to changes in the power of the selecting frequencies themselves, we repeated this analysis after matching

the two mixing conditions for the power of the three selecting frequencies individually or the sum of their power. Even after matching for the power of selecting frequencies, the low emergent frequency was still significantly increased in high mixing conditions (bootstrap resampling, $p<0.001$).

Since mixing alters LFP power, it should also affect unit activity. To test this prediction, we compared unit entrainment in conditions of high and low mixing after matching LFP power and ensuring uniform distribution of phases at each frequency (see Methods). Because these controls limit the amount of data available for the comparison, we restricted our attention to fast-spiking SI neurons recorded during AW, when these cells spontaneously fire at high rates (23.1±7.5 Hz; mean ± SD). The entrainment of SI units by the low emergent frequency was significantly increased in conditions of high mixing, assuming a value nearer the mean entrainment by the low and high root frequencies, consistent with prediction from the LFP power analysis (**Fig. 4c-d**, individual examples; **4e**, average ± SD, n=40; single-tailed paired t-test, $p<0.0075$).

We have used the theory of frequency mixing to explore cross-frequency interactions in brain oscillations. While this theory is not new, its application to the brain results in non-trivial predictions about the relationship between different oscillatory activities. Furthermore, it provides a framework for resolving a complex spectral composition into a simpler picture where oscillatory inputs may be distinguished from their downstream effects. While many of the model's predictions were supported by the data, some deviations were noted. In particular, for non-drug states, often only a couple well-defined clusters could be

observed, while in the drug state we would typically see portions of additional, unexpected clusters that extended beyond the boundaries of our analysis.

The detection of frequency mixing in the brain is hampered by the richness and heterogeneity of neuronal activity. In different brain states, neural networks likely express different types of frequency. Such complexity reduces the likelihood that mixing can be detected with pII. Indeed, in our analyses, the clearest results were obtained when rats were administered an NMDAR antagonist, inducing a highly stereotyped and pathological brain state. Another potential complication is that even in a homogeneous brain state, the input frequencies may be such that some of the root, harmonic, and emergent components overlap, making them harder to characterize using our approaches. For example, if the interacting input signals input happen to be 40 and 120 Hz, the harmonic of the 40 Hz signal and lower emergent component would coincide at 80 Hz. The prevalence of this type of interference increases dramatically in neuronal networks that receive additional input signals. Finally, given that neural activity often feeds back on itself, harmonic and emergent activities might become root signals themselves, resulting in high-order interactions and phase-shifts that will be more pronounced for higher frequencies.

References

Reyes, A. D. Synchrony-dependent propagation of firing rate in iteratively constructed networks in vitro. ***Nat. Neurosci****.* **6**, 593-599 (2003).

Bartos, M., Vida, I. & Jonas, P. Synaptic mechanisms of synchronized gamma oscillations in inhibitory interneuron networks. *Nat. Rev. Neurosci.* **8**, 45-56 (2007).

Llinás, R. R. The intrinsic electrophysiological properties of mammalian neurons: insights into central nervous system function. *Science* **242**, 1654-1664 (1988).

Whittington, M. A. & Traub, R. D. Interneuron diversity series: inhibitory interneurons and network oscillations in vitro. *Trends Neurosci.* **26**, 676-682 (2003).

Steriade, M. & Llinás, R. R. The functional states of the thalamus and the associated neuronal interplay. *Physiol. Rev.* **68**, 649-742 (1988).

Buzsáki, G., Logothetis, N. & Singer, W. Scaling brain size, keeping timing: evolutionary preservation of brain rhythms. *Neuron* **80**, 751-764 (2013).

Kay, L. M. Olfactory system oscillations across phyla. *Curr. Opin. Neurobiol.* **31**, 141-147 (2015).

Buzsáki, G. & Draguhn, A. Neuronal oscillations in cortical networks. *Science* **304**, 1926-1929 (2004).

Fries, P. Rhythms for Cognition: Communication through Coherence. *Neuron* **88**, 220-235 (2015).

Sejnowski, T. J. & Paulsen, O. Network oscillations: emerging computational principles. *J. Neurosci.* **26**, 1673-1676 (2006).

Steriade, M., Nuñez, A. & Amzica, F. A novel slow (< 1 Hz) oscillation of neocortical neurons in vivo: depolarizing and hyperpolarizing components. *J. Neurosci.* **13**, 3252-3265 (1993).

König, P., Engel, A. K. & Singer, W. Relation between oscillatory activity and long-range synchronization in cat visual cortex. *Proc. Natl. Acad. Sci. USA* **92**, 290-294 (1995).

Bragin, A. et al. Gamma (40-100 Hz) oscillation in the hippocampus of the behaving rat. *J. Neurosci.* **15**, 47-60 (1995).

Steriade, M., Amzica, F. & Contreras, D. Synchronization of fast (30-40 Hz) spontaneous cortical rhythms during brain activation. *J. Neurosci.* **16**, 392-417 (1996).
Nunez, P.L. Electric Fields of the Brain. Oxford: Oxford University Press; 1981.
Gray, C. M., König, P., Engel, A. K. & Singer, W. Oscillatory responses in cat visual cortex exhibit inter-columnar synchronization which reflects global stimulus properties. *Nature* **338**, 334-337 (1989).

Singer, W. Neuronal synchrony: a versatile code for the definition of relations? *Neuron* **24**, 49-65, 111-125 (1999).
Moutard, C., Dehaene, S. & Malach, R. Spontaneous Fluctuations and Non-linear Ignitions: Two Dynamic Faces of Cortical Recurrent Loops. *Neuron* **88**, 194-206 (2015).

Gonzalez-Burgos, G. & Lewis, D.A. NMDA receptor hypofunction, parvalbumin-positive neurons, and cortical gamma oscillations in schizophrenia. *Schizophr. Bull.* **38**, 950-7 (2012).

Javitt, D. C. & Zukin, S. R. Recent advances in the phencyclidine model of schizophrenia. *Am. J. Psychiatry* **148**, 1301-1308 (1991).

Uhlhaas, P. J. & Mishara, A. L. Perceptual anomalies in schizophrenia: integrating phenomenology and cognitive neuroscience. *Schizophr. Bull.* **33**, 142-156 (2007).

Hunt, M. J. & Kasicki, S. A systematic review of the effects of NMDA receptor antagonists on oscillatory activity recorded in vivo. *J. Psychopharmacol.* **27**, 972-986 (2013).

Goda, S. A., Piasecka, J., Olszewski, M., Kasicki, S. & Hunt, M. J. Serotonergic hallucinogens differentially modify gamma and high frequency oscillations in the rat nucleus accumbens. *Psychopharmacology (Berl)* **228**, 271-282 (2013).

Hunt, M. J, Olszewski, M., Piasecka, J., Whittington, M. A. & Kasicki, S. Effects of NMDA receptor antagonists and antipsychotics on high frequency oscillationsrecorded in the nucleus accumbens of freely moving mice. *Psychopharmacology (Berl)* **232**, 4525-4535 (2015).

Mori, K., Manabe, H. , Narikiyo, K. & Onisawa, N. Olfactory consciousness and gamma oscillation couplings across the olfactory cortex, and orbitofrontal cortex. *Front. Psychol.* **4**, 743 (2013).

Methods

Mathematical Model. The artificial LFP data used in **Figure 1** was generated in three steps. First, time-series of instantaneous-frequencies were generated for each input signal. Second, the instantaneous-frequency time-series were used as arguments to a cosine function and multiplied point-wise by a time-varying amplitude. Third, the input signals were added and passed through a linear or non-linear transfer function. The instantaneous-frequency time-series were constructed by generating a random-walk process and fitting this by a low order polynomial which was subtracted from it. The residual was added to the mean frequency value (40 or 100 Hz). We used a time increment of 0.8 ms, and at each step added a uniformly distributed random frequency value of between [-1/30 - 1/30] Hz to generate the random walk. The process was integrated for a total of 300 seconds, and fit with a 10th order polynomial. The transfer function consisted of a linear coefficient of 0.5 in the case of the linear model, or linear and quadratic terms of 0.5 and -0.2 respectively in the case of the nonlinear model. Note that higher-order terms in the description of the non-linear transfer function would result in the addition of higher emergent and harmonic component. However, because of the higher number of bands in three-way phase plots, the pII would become smaller and harder to detect.

Computation of the pII group-index. To quantify the degree to which a phase-triplet distribution resembled each of those predicted for the different frequency relationships (**Fig. 1d**), we characterized the distribution using a 3D discrete Fourier transform (*fftn* in MATLAB). Note that because the phase distributions were periodic in each of the X, Y, and Z coordinates, they were well-suited to characterization in the Fourier domain. The data was first binned using a 32-by-32-by-32 mesh, normalized by the total count, and then passed to *fftn*. The relative periodicity of the phase distribution of each of the three dimensions is reflected in the relative frequency indices for which the Fourier transform is large: 1:1:1 for the blue group, 1:2:1 for the red group, and 1:2:2 for the green group. The "color index" for each of the blue, red, and green groups is defined as the maximum Fourier component with indices in the ratio characteristic of the group, divided by the sum of these values for all three groups.

Animals and electrode implantation. Procedures were approved by the Institutional Animal Care and Use Committee of Rutgers University in compliance with the *Guide for the Care and Use of Laboratory Animals* (National Institutes of Health). Our subjects were male Lewis rats (n=7) and Sprague-Dawley rats (n=5) (310–360 g; Charles River Laboratories, Wilmington, MA) maintained on a 12:12-h light-dark cycle and housed individually with ad libitum access to food and water. After habituation to the animal facility and handling for 1 wk, rats were anesthetized with a mixture of isoflurane and O_2 and then administered atropine sulfate (0.05 mg/kg im) to aid breathing. In aseptic conditions, rats were mounted

in a stereotaxic apparatus with nonpuncture ear bars. A local anesthetic (subcutaneous bupivacaine) was injected in the region of the scalp to be incised. Fifteen minutes later, the scalp was incised, and a craniotomy was performed above the regions of interest. Then, movable bundles of tetrodes or fixed microwires (nichrome, 20-μm inner diameter, impedance 100–300 kΩ following gold plating) were stereotaxically aimed to the BLA, CeA, SI, BNST, nAC and AON. Tetrode tip positions within a bundle were staggered to facilitate histological reconstructions. The reference electrode was a stainless steel screw anchored over the cerebellum. Rats were allowed 1 wk to recover from the surgery and then acclimated to handling for 2 additional days.

Data acquisition. In each rat, spontaneous neuronal activity was then recorded during prolonged (≥3 h) daily recording sessions so that sufficient data could be obtained during different states of vigilance and under the influence of MK-801. Behavior was recorded by an overhead video camera. During the recording sessions, rats were placed in a dimly lit (20 lx), standard plastic rat cage with bedding at the bottom. Electrodes were not moved during the experiments unless all units were lost overnight across all tetrodes. In such rare cases (<5%), the tetrode bundle was lowered 60 μm, and recordings resumed the following day. Signals were sampled at 40 kHz and stored on a hard drive. Different behavioral states of vigilance were identified using a combination of spectral LFP analyses and behavioral observations, as previously described (Haufler and Paré, 2014). Between 1 and 3 recordings are analyzed for each rat.

Histology. At the end of the experiments, the animals were deeply anesthetized, and recording sites were marked with small electrolytic lesions (20 μA between a tetrode channel and the animals' tail for 15 s). One day later, the rats were perfused-fixed through the heart, their brains extracted and cut on a vibrating microtome, and the sections counterstained with cresyl violet.

Spike extraction and clustering. For spike extraction, the data were first high-pass filtered using a median-based filter and then thresholded to extract spikes. Next, we ran principal component analysis on the spikes, and the first three components were clustered using KlustaKwik (http://klustakwik.sourceforge.net). Spike clusters were then refined manually using Klusters (Hazan et al., 2006). The reliability of cluster separation was verified by inspecting auto- and cross-correlograms. Units with unstable spike shapes during a given recording session were excluded from the analyses.

Processing of LFPs and units. The data was first downsampled to 1,250 Hz with sinc interpolation. Analyses were performed in MATLAB. Spectral analyses was done using Chronux (http://chronux.org) or with wavelet analysis using functions developed in-house. The mean resultant vector used to quantify phase entrainment of units was computed with the Circular Statistics Toolbox for MATLAB (Berens, 2009).

Calculation of phase entropy and interaction information. To identify frequencies with putative fundamental-emergent component interactions, we binned the distribution of phase triplets for three frequencies selected from the set of independent components. Binning is performed over the range of -π to π at bin step of π/4. Each edge of the 3D space of phase triplets is thus divided into 8 segments, and the total volume consists of 512 bins (8^3). Because of the issues associated with direct computation of the Shannon entropy directly from the histogram, we do this using the BUB estimator (Paninski, 2003). To specifically identify frequency triplets where all 3 phases are related but no pair is related (for example, a fundamental-fundamental-emergent component triplet), we compute the 3-way *phase interaction information* (pII, Jakulin and Bratko, 2004). For three variables X, Y, and Z (here the phases of activity at three frequencies), the pII is computed from the entropy of various phase distributions as follows:

$$\mathrm{pII}(X; Y; Z) = -[H(X) + H(Y) + H(Z)] + [H(X,Y) + H(X,Z) + H(Y,Z)] - H(X,Y,Z)$$

Intuitively this the information gained by considering the set of three phases together above the information inherent in each pair of phases. This quantity is also estimated using the BUB estimator by expressing the interaction information in terms of entropies. Because pII estimates are affected by sampling density as well as the width and edge position of phase bins, we examined the impact of

these factors on simulated data and optimized them such that our analyses could distinguish small effect sizes from random variations in pII (**Supplementary Figs. 2-5**). Last, because the autocorrelation structure of LFPs can lead to artificially inflated pII values, sampling density was lowered accordingly.

Statistics. For evaluating the significance of the scatterplots in Figure 3, we consider the null hypothesis that the frequency indices of the pII cluster centroids occur where they do relative to the plane X = Y + Z, where X, Y, and Z are frequencies such that X > Y > Z. We first construct a distribution of the distances from this plane for all such X, Y, and Z frequencies. For active waking, quiet waking, and the drug states, we consider the frequency range 2 to 240 Hz in 2 Hz intervals, and for slow-wave sleep we consider the range 1 to 100 Hz in 1 Hz intervals. We use the proportion of frequency indices within a given distance from the predicted relationship as the probability of successful outcome in a binomial test, and evaluate the likelihood of the observed data given this model. Centroids must be within 10 Hz of the predicted relationship for active waking, quiet waking, and drug conditions, and 5 Hz for slow wave sleep. Because the centroids of larger clusters may be precluded from approaching the boundaries of the space of possible frequencies, there may be a small bias for these values to lie closer to the predicted relationship even under the null hypothesis. To control for this we exclude possible X, Y, Z coordinates near the boundary in constructing the distribution and success probability for the null model (within 10

Hz of the boundary for non-sleep, and within 5 Hz for slow-wave sleep). We also verify that all significant results hold true when the frequency indices of the maximum value within a cluster are used instead of the cluster centroid.

To compute the significance of the relative peak locations in the spectral power ratio in Figure 4, we perform bootstrap resampling on spectral power estimates within the high and low mixing groups. We draw 1000 pairs of bootstrap samples for each of the two groups and compute the spectral ratio for pairs. The p-values associated with a particular ordering of peak locations are computed from the proportion of samples in which it is observed.

REFERENCES FOR METHODS

Haufler, D. & Paré, D. High-frequency oscillations are prominent in the extended amygdala. *J. Neurophysiol.* **112**, 110-119 (2014).

Hazan, L., Zugaro, M. & Buzsáki G. Klusters, NeuroScope, NDManager: a free software suite for neurophysiological data processing and visualization. *J Neurosci. Methods* **155**, 207–216 (2006).

Berens, P. CircStat: A MATLAB Toolbox for Circular Statistics. *J. Stat. Softw.* 31 (2009)

McGill, W.J. Multivariate information transmission. *Psychometrika* **19**, 97-116 (1954).

Jakulin, A. & Bratko, I. Quantifying and Visualizing Attribute Interactions: An Approach Based on Entropy. *Entropy* **48**, 1–30 (2004).

Paninski, L. Estimation of Entropy and Mutual Information. *Neural Comput.* **15**, 1191-1253 (2003).

Extended Data, Figures, and Tables

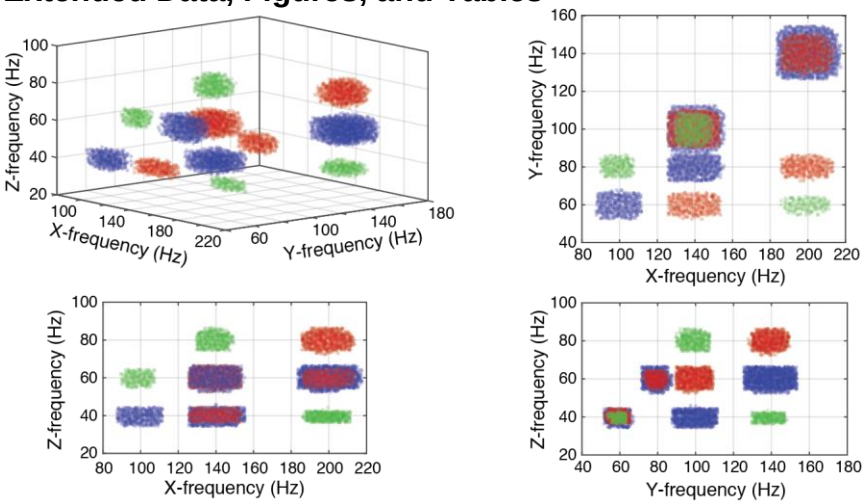

Supplementary figure 1. Frequency triplets with different levels of phase interaction information. A network model integrated two oscillatory signals with a non-linear function in low noise conditions. The signals had a mean frequency of 40 and 100 Hz with SDs of 1.0 and 1.5, respectively. The phases of the resulting oscillations were determined by applying the wavelet transform method and phase interaction information was computed for all possible combination of three frequencies. Frequency triplets with interaction information values that exceeded the 95th percentile are color coded as per **figure 1d** (fourth column): blue, highest; red, intermediate; green, lowest. The clusters are depicted using a 3D plot as well as three different two-dimensional perspectives. In the noisy and constantly fluctuating conditions of the brain, the blue clusters are the most likely to be detected.

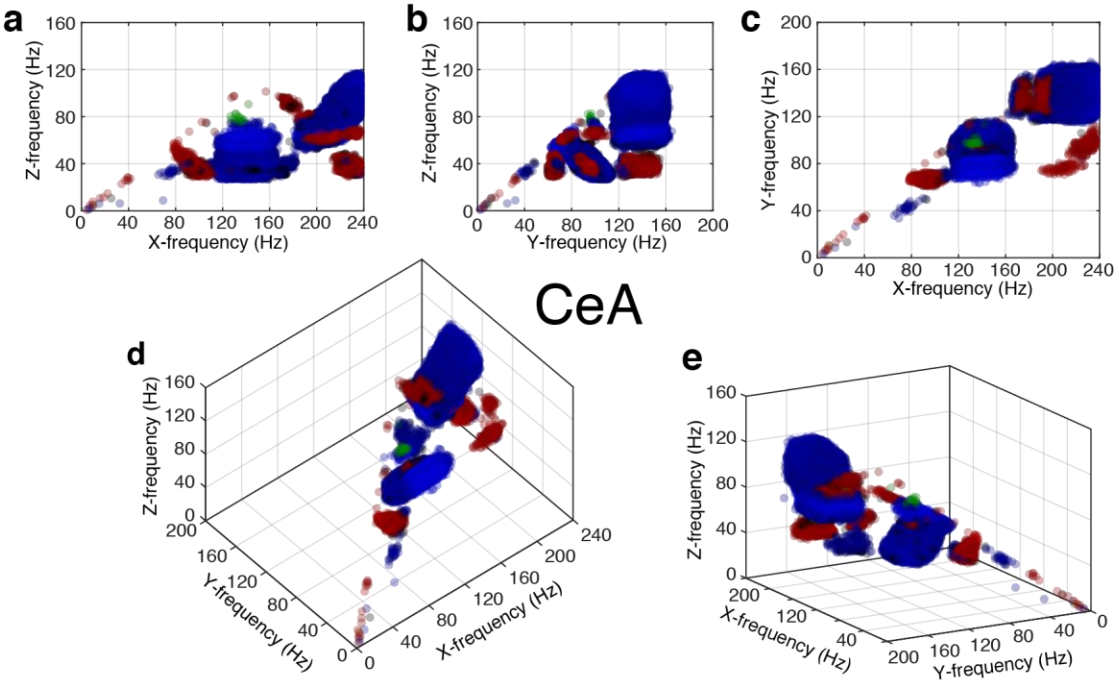

Supplementary figure 2. Identification of interacting frequencies in LFPs recorded from the amygdala. Interacting frequency triplets color-coded by the frequency relation they satisfy (see Fig. 1d) on 2D (**a-c**) and 3D (**d,e**) graphs.

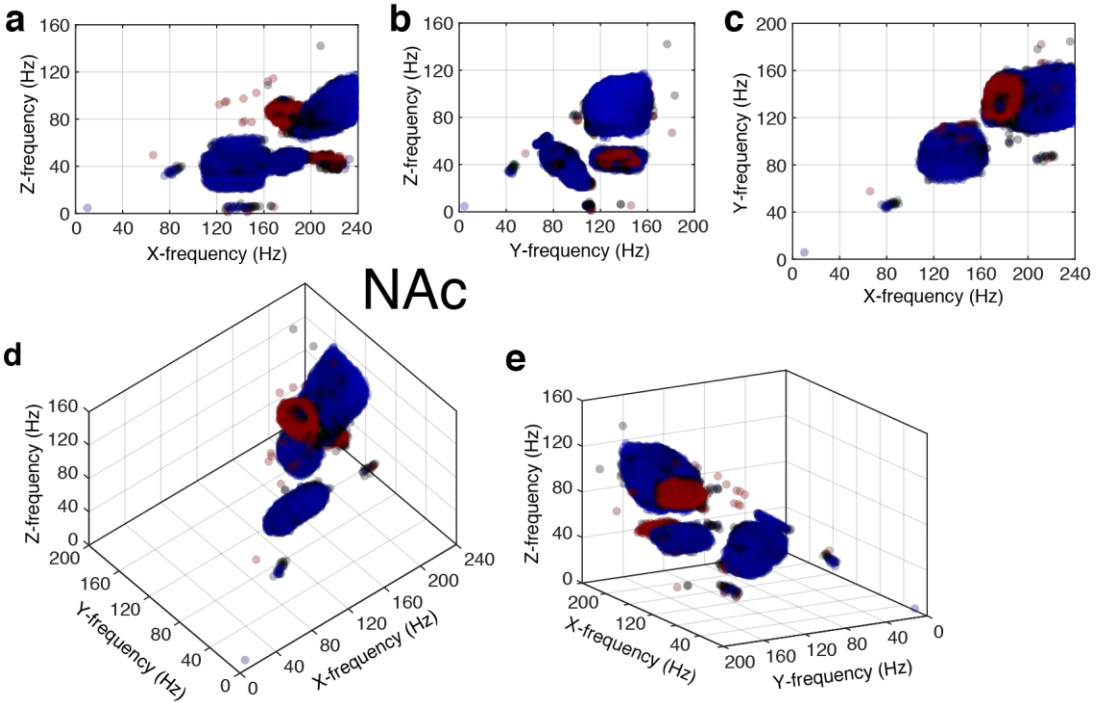

Supplementary figure 3. Identification of interacting frequencies in LFPs recorded from nucleus accumbens. Interacting frequency triplets color-coded by the frequency relation they satisfy (see Fig. 1d) on 2D (**a-c**) and 3D (**d,e**) graphs.

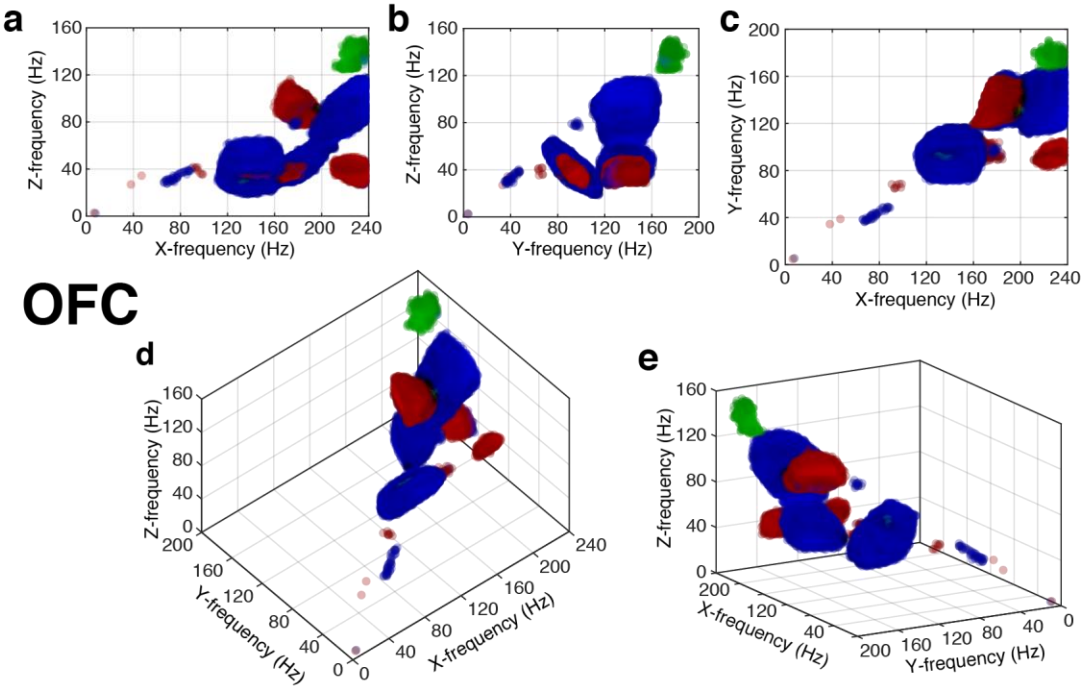

Supplementary figure 4. Identification of interacting frequencies in LFPs recorded from the orbitofrontal cortex. Interacting frequency triplets color-coded by the frequency relation they satisfy (see Fig. 1d) on 2D (**a-c**) and 3D (**d,e**) graphs.

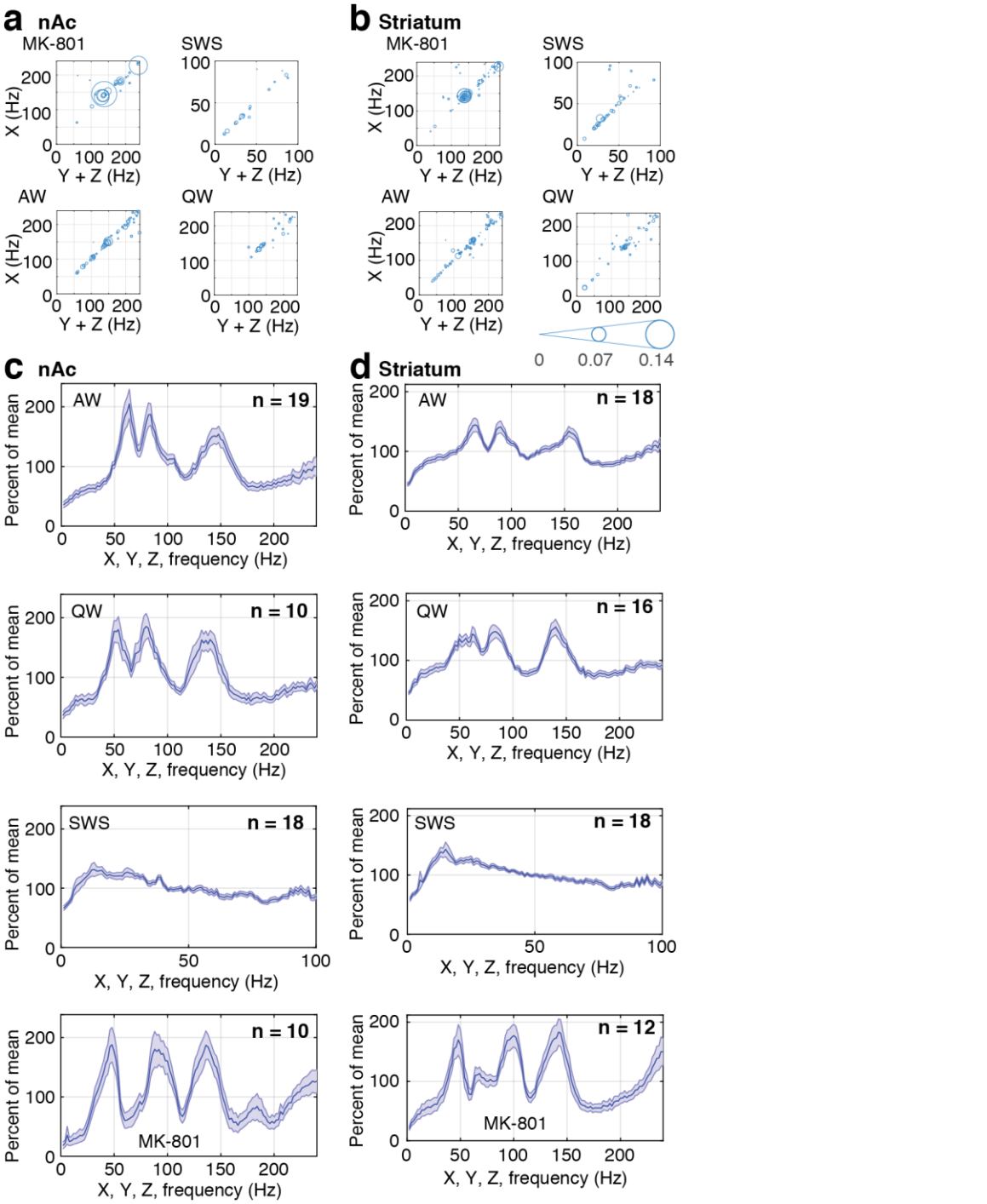

Supplementary figure 5. Region- and state-dependent variations in pII values and interacting frequencies in nAc and striatum. **a,b**, x vs. y + z frequency plots for the structures and behavioral states indicated. The diameters of the circles is proportional to the magnitude of the pII values (scale bar at bottom of **b**). In all cases shown in **a** and **b**, the probability that the centroid locations would satisfy the x = y + z relation by chance is p < 10^-5. **c,d**, pII amplitudes of triplets with an x, y, or z frequency including a given value, expressed relative to all pII values, for the structures and behavioral states indicated.

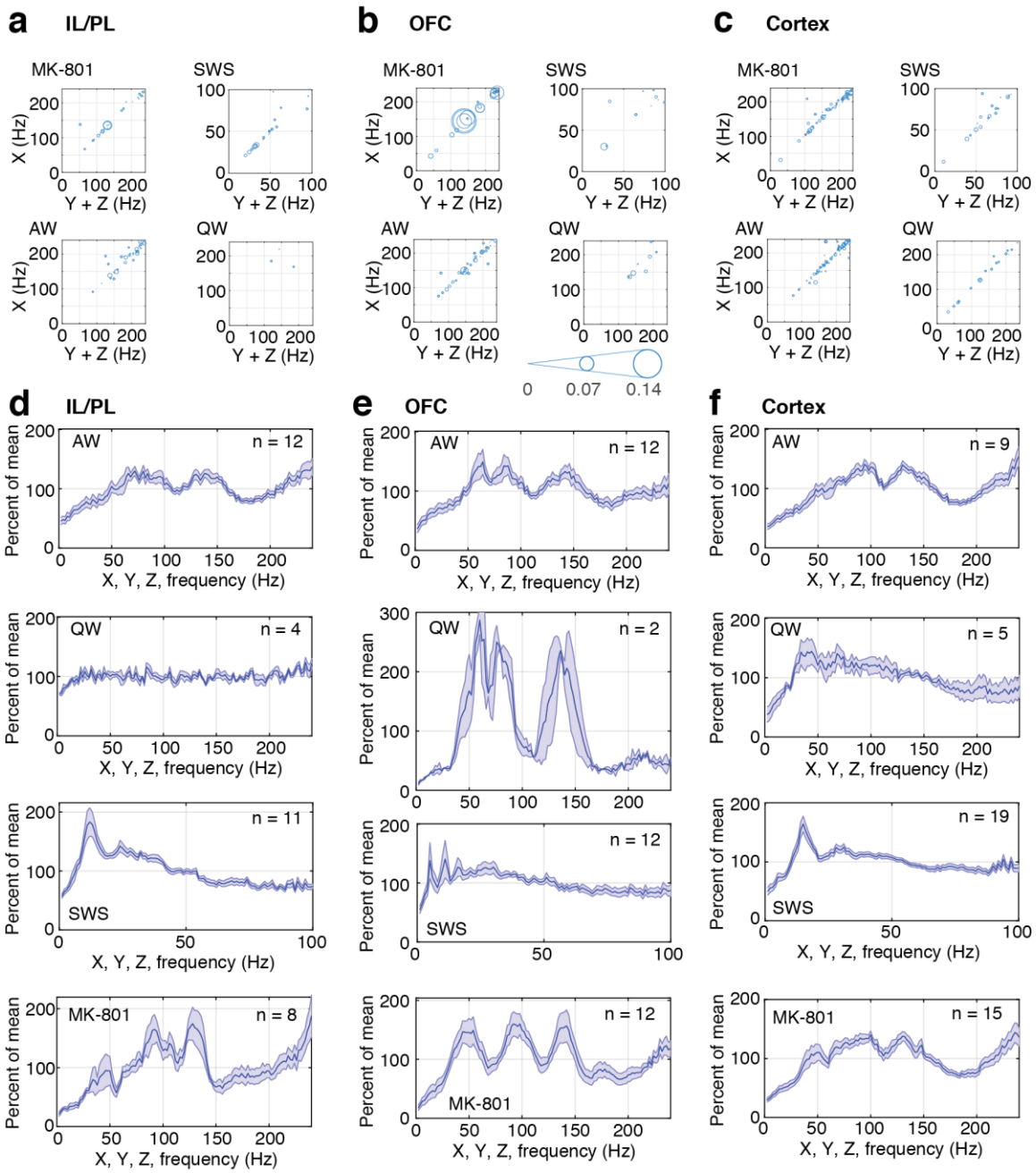

Supplementary figure 6. Region- and state-dependent variations in pII values and interacting frequencies in various cortical areas. **a-c**, x vs. y + z frequency plots for the structures and behavioral states indicated. The diameters of the circles is proportional to the magnitude of the pII values (scale bar at bottom of **b**). In all cases shown in **a-c**, the probability that the centroid locations would satisfy the x = y + z relation by chance is p < 10^-5 with the exception of IL-PL QW (p=0.08), OFC SWS (p=0.0013), and OFC QW (p=0.0004). **d-f**, pII amplitudes of triplets with an x, y, or z frequency including a given value, expressed relative to all pII values, for the structures and behavioral states indicated.

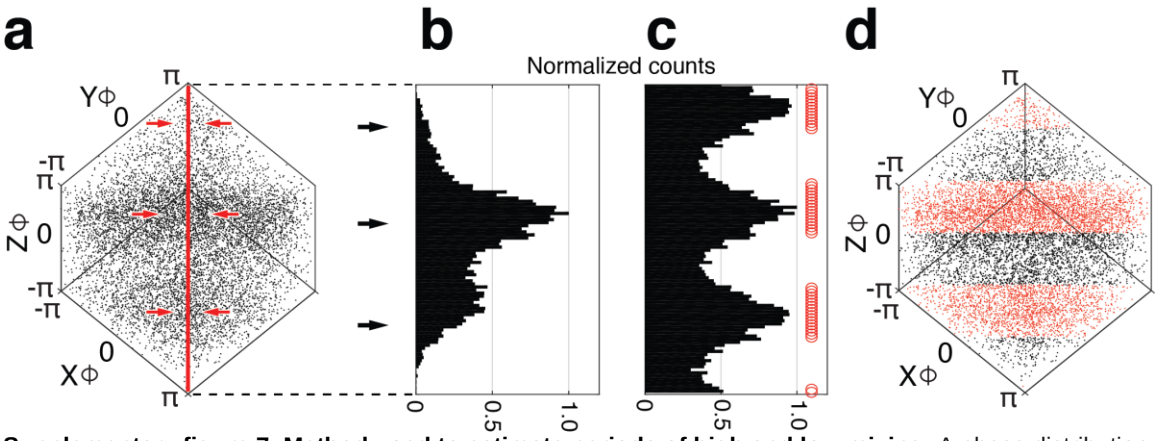

Supplementary figure 7. Method used to estimate periods of high and low mixing. A phase distribution characteristic of a blue-group pII cluster is shown in a. For frequencies x, y, and z where x > y > z, the density of the distribution varies along the diagonal shown in red. Because phase is a circular quantity, the data is "wrapped", such that opposing faces of the cube in a are continuous with one another. A simple projection of the data onto the diagonal (b) is thus misleading in estimating density. Panel c shows a corrected estimate of density where the full distribution is first shifted such that the bin is centered within the cube before projecting the data. The preferred phase relationships, where mixing of frequencies is presumably higher, are denoted by shown by the circles in c and by red data points in d.

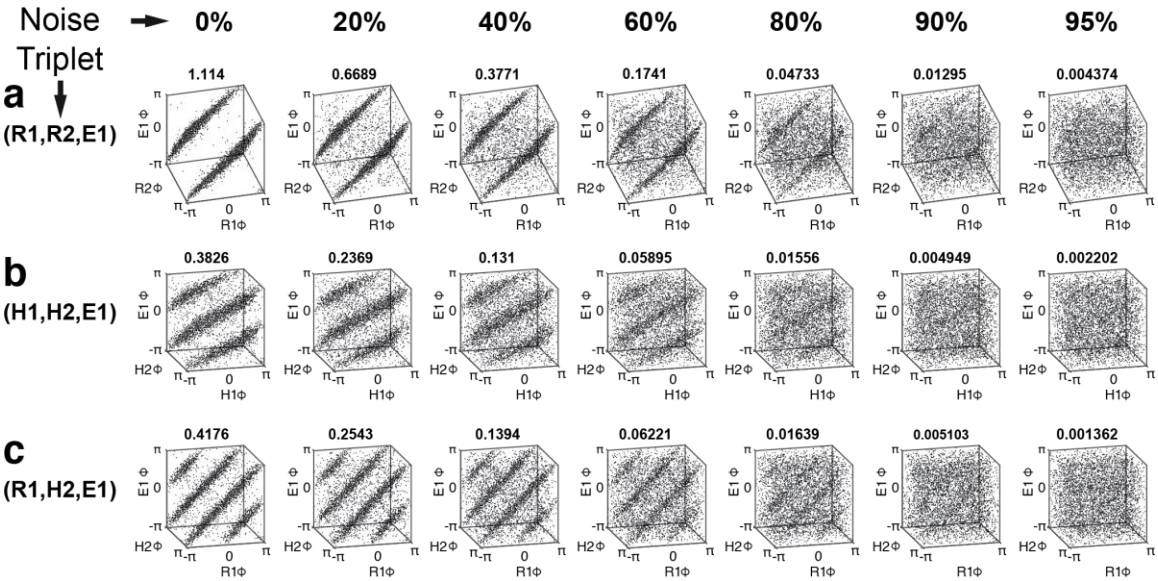

Supplementary figure 8. Impact of noise on three-way phase relationships between oscillations of three different frequencies. Two oscillatory signals were integrated by a simulated network model with a nonlinear transfer function, leading to the expression of the original oscillations (root – R1 or R2), as well as emergent (E1 or E2) and harmonic (H1 or H2) frequencies. The graphs plot the phase of three of these oscillations against each other. Each row in **a-c** plots different triplet of oscillations, as indicated on the left. The phase of the oscillations was determined using the wavelet transform method on the simulated data. Phases were sampled 5000 times. From left to right, a gradually increasing proportion of the 5000 samples was assigned a random position in the phase plots, as indicated by the percentages at the top of the figure. The bold numbers above each graph indicate the value of the phase interaction information. Expectedly, as noise increases, phase interaction information decreases. Interaction information estimates were computed using an array of 8 by 8 by 8 phase bins. Note that the three frequency triplet examples in **a-c** fall in the color-coded classes defined in **Fig. 1d.**

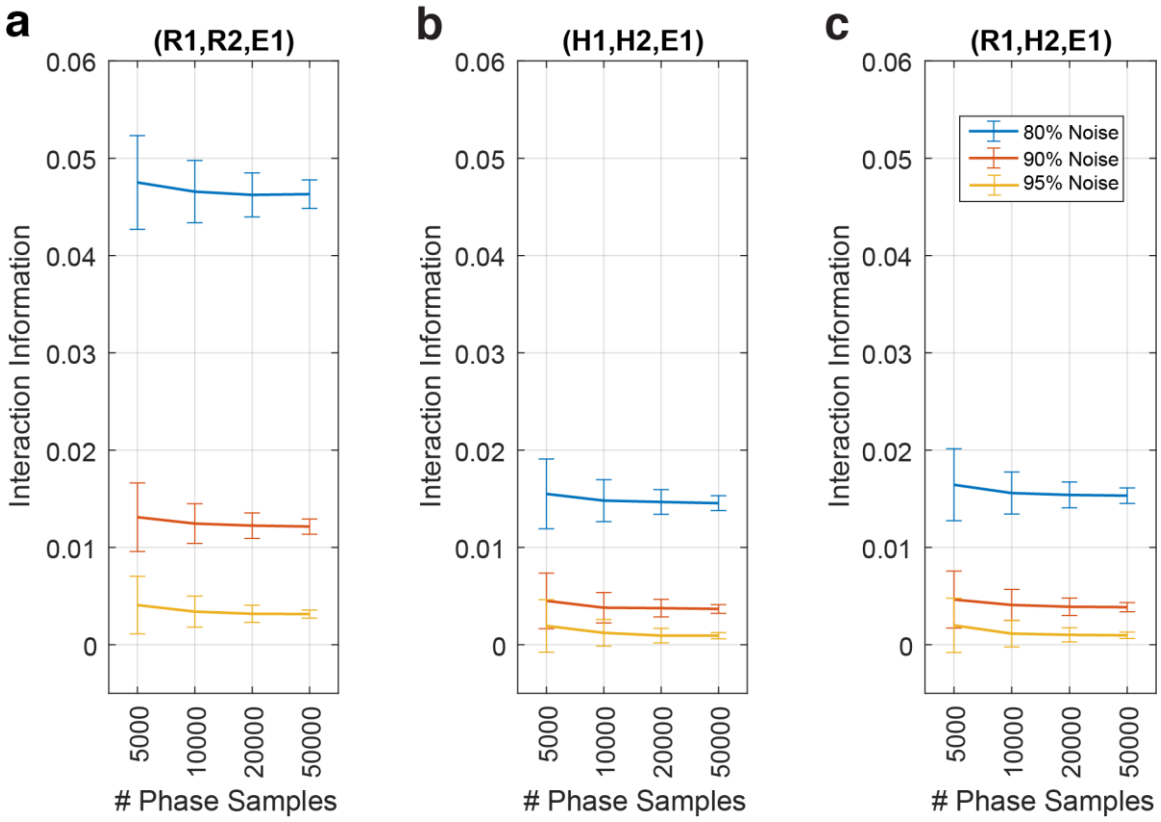

Supplementary figure 9. Impact of sampling on the detection of phase relationships between oscillations of three different frequencies. a-c, Same simulated data and frequency triplets as in supplementary figure 2. Phase interaction information (y-axis) as a function of number of samples (x-axis) for three different noise levels (blue, 80%; red, 90%; yellow, 95%). For each condition, the same simulated data was sampled 1000 times, randomly shifting the bin edges along the three axes to control for the influence of their exact position. Values are averages ± SD.

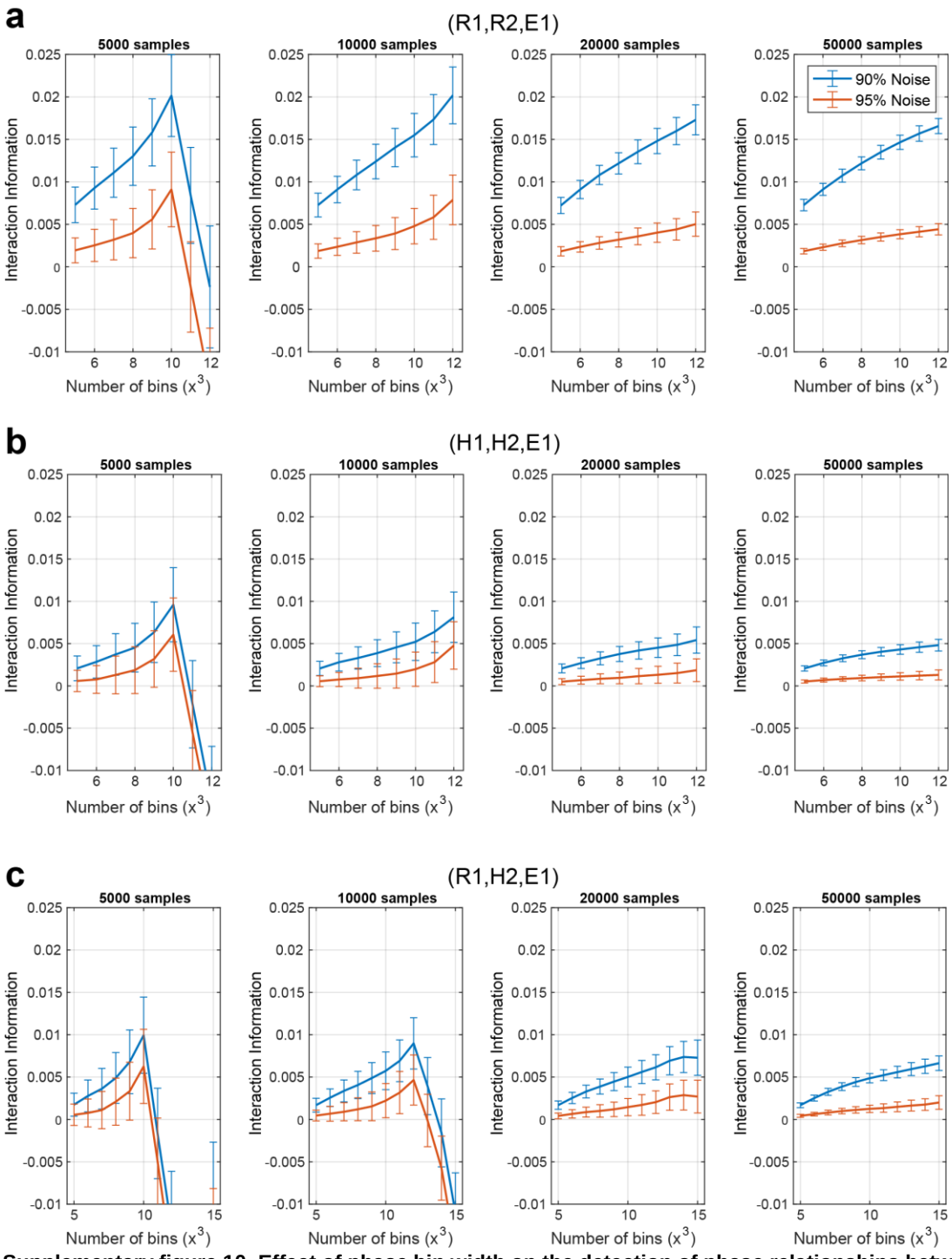

<u>Supplementary figure 10</u>. Effect of phase bin width on the detection of phase relationships between oscillations of three different frequencies. a-c, Same simulated data and frequency triplets as in supplementary figures 2-3. Phase interaction information (y-axis; averages ± SD) for two noise levels (blue, 90%; red, 95%) and different number of samples (from left to right, 5000 to 50,000) as a function of binning density (x-axis; number of bins along each axis the three-way phase plots). For each condition, the same simulated data was sampled 1000 times, randomly shifting the bin edges along the three axes to control for the influence of their exact position.

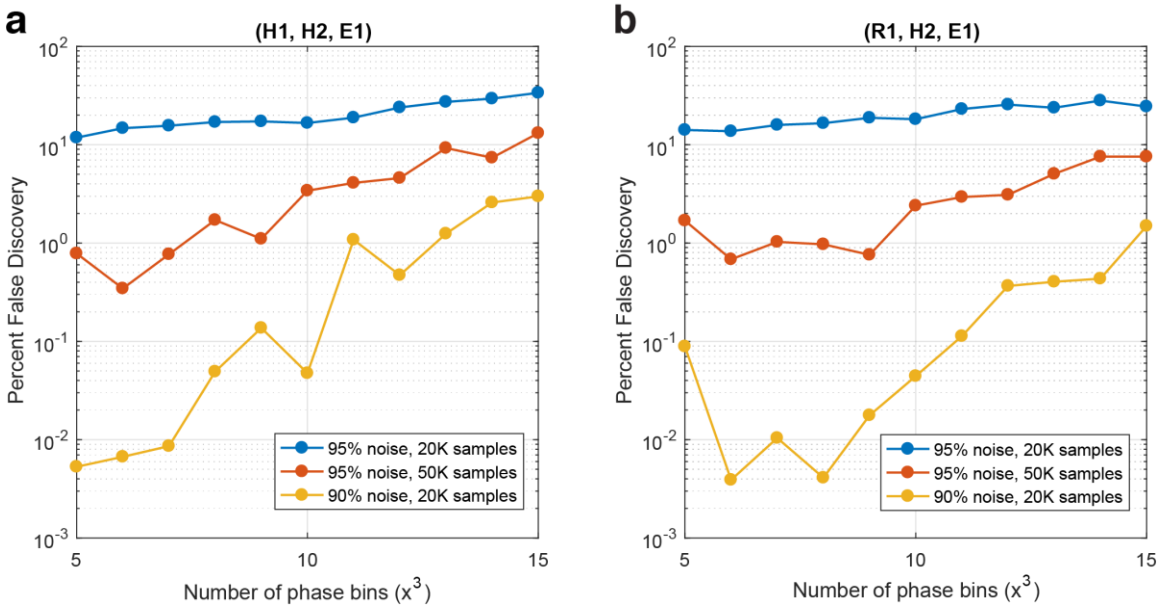

Supplementary figure 11. Influence of binning on false discovery rates of phase relationships between oscillations of three different frequencies. Same simulated data for two of the frequency triplets (**a,b**) shown in supplementary figures 2-4. The data was sampled 1000 times using different phase bin widths and noise levels (yellow, 90%; red and blue, 95%). Each interaction information estimate was compared to 10,000 distributions of totally random phase data. Graphs plot the average proportion of random distributions (y-axis) where the phase interaction information exceeded that seen in the actual data as a function of phase bin density (x-axis, number of bins). For each condition, bin edges were randomly shifted along the three axes to control for the influence of their exact position.

Region	Sites
Amygdala	19
SI	25
BNST	9
nAc	15
Striatum	15
AON	14
OFC	5
IL/PL	12
Neocortex	9

Supplementary table 1. Recording site number by region

CHAPTER V

General Discussion

5.1. ROLE OF BNST IN THE GENESIS OF CONDITIONED FEAR

5.1.1 A model of BNST-CeA interactions during fear and anxiety

Because BNST lesions impair contextual fear but not cued fear whereas cued fear is blocked by CeA lesions, Walker, Miles, and Davis (2009) suggested that the amygdala and BNST play complementary roles in fear and anxiety. They suggested that BNST generates sustained anxiety-like responses to diffuse environmental threats whereas CeA mediates brief defensive behaviors in response to imminent danger (Walker et al., 2009). This model proved extremely influential and galvanized interest in the field.

To account for the differing functions of BNST and CeA, Walker, Miles, and Davis hypothesized that the basal amygdala nuclei would, in parallel, convey threat signals to BNST and CeM. In turn, neurons in CeM would be activated rapidly, recruiting brainstem fear networks. To explain the delayed activation of BNST with respect to CeM, they proposed that the recruitment of BNST would not only depend on BM and BL inputs, but also on CRF afferents arising in CeL. As a result, BNST would be activated slowly and remain so for a longer period of time, explaining the selective involvement of BNST in anxiety.

5.1.2 Relation between the model's predictions and BNST activity during conditioned fear.

5.1.2.1 Short-latency responses of BNST neurons to discrete cues. In my first data chapter, I tested some of the model's predictions by recording BNST-AL and AM neurons in rats subjected to a differential auditory fear conditioning

paradigm. During habituation, I found that very few BNST neurons were responsive to the CS. However, after fear conditioning, 20% of BNST-AL neurons developed inhibitory responses to the CS. In BNST-AM, 26% of neurons developed excitatory responses to the CS. The behavior of BNST-AM and AL neurons during contextual fear paralleled their CS responsiveness, raising the possibility that they exert opposite influences on fear output networks.

In many ways, the results of these experiments do not match the predictions of the Walker et al. model. A first discrepancy is found in the timing of BNST activation by the CSs. Walker et al. predicted that BNST activation would be delayed compared to CeA's but this is not what I observed. The latency of BNST responses to CSs was short and comparable to that reported in prior studies on the activity of CeA neurons during the presentation of aversive CSs (Ciocchi et al., 2010; Duvarci et al., 2011). Moreover, the proportion of CS responsive BNST neurons I observed is similar to that reported in prior studies on CeA neurons (Ciocchi et al., 2010; Duvarci et al., 2011). In support of my findings, similar results have subsequently been obtained in mice (Jennings et al., 2013).

Since BNST-AL neurons project to CeA (Sun and Cassell, 1993; Dong et al., 2001b; Gungor et al., 2016) and considering their short-latency responses to aversive CSs, one would expect BNST lesions to alter cued fear. While this reasoning does not fit with the early finding that BNST lesions do not alter cued fear more recent data indicates that this common view might be incorrect. For instance, it was found that muscimol infusions in BNST increases fear-

potentiated startle (Meloni et al., 2006). Also, it was reported that BNST lesions enhance the stimulus specificity of cued fear (Duvarci et al., 2009). More evidence that BNST neurons regulate behavioral responses to discrete cues is found in the addiction literature. BNST is shown to regulate many aspects of addiction, such as the dysphoria that follows drug consumption (Wenzel et al., 2011, 2014), the stress produced by drug withdrawal, and the relapse to drug-seeking (Erb and Stewart, 1999; Aston-Jones and Harris, 2004; Koob, 2009). The latter phenomenon is particularly relevant to the present discussion. In these experiments, rats are trained to self-administer drugs in response to a short CS by pressing a lever. When lever pressing no longer causes drug administration, this behavior is extinguished. However, re-introduction of the cue leads to a resurgence of the drug-seeking behavior, an effect blocked by BNST inactivation (Buffalari and See, 2010). Finally, human functional imaging studies that compared BNST activity elicited by stimulus contingencies associated with immediate threats vs. unpredictable perils also reached the conclusion that BNST is similarly activated during fear and anxiety (reviewed in Shackman and Fox, 2016).

5.1.2.2 Heterogeneous responses of BNST neurons to discrete cues. The Walker et al. model implies that BNST neurons act uniformly to generate anxiety but not fear. Opposite to this, I found that BNST-AL and BNST-AM display the same opposite profiles of activity during cued and contextual fear. First, during cued fear conditioning, BNST-AL neurons acquired *inhibitory* responses to the CS (Off-cells). Two days later, during the recall test, the proportion of Off-cells

remained high but an additional subset of cells developed positive responses to the CS (On-cells). In contrast, the CS responsiveness of BNST-AM neurons did not change during training. However, during the recall test two days later, we observed a large increase in the incidence of cells with *excitatory* responses to the CS. Importantly, BNST-AL and AM neurons also displayed an opposite activity profile in relation to contextual fear. Indeed, when rats were exposed to the training context the day after fear conditioning, a third of BNST-AM neurons fired at significantly *higher* rates during freezing than movement. Few BNST-AM cells showed the opposite behavior. By contrast, in BNST-AL, neurons with *lower* firing rates during freezing prevailed, consistent with the pattern of CS responsiveness described above.

These findings point to regional differences in the activity of BNST-AL and AM in relation to learned fear, raising the possibility that they exert opposite influences on fear output networks. Several factors likely underlie these differences, including regionally heterogeneous amygdala projections to BNST as well as the intrinsic BNST network. Indeed, the amygdala sends strong but neurochemically diverse projections to BNST: GABAergic/peptidergic inputs from CeA and glutamatergic inputs from BLA (Krettek and Price 1978b; Dong et al. 2001a; McDonald, 2003). Importantly, CeA contributes stronger projections to BNST-AL than AM (Dong et al. 2001a). Conversely, a major component of BNST-AL, the oval nucleus, is largely devoid of BLA inputs (Dong et al. 2001a). In addition, a recent in vitro study on the intrinsic connections of BNST reported that BNST-AL neurons receive inhibitory inputs from other BNST neurons

(Turesson et al. 2013). Thus, CS-related BLA inputs might excite BNST cells that send GABAergic projections to neurons of the oval nucleus, causing a feedforward inhibition. This inhibition of BNST-AL neurons might be reinforced by CeA inputs, which are much stronger to BNST-AL than AM (Dong et al. 2001a).

Consistent with the above, there is a correspondence between the CS responsiveness of neurons in the lateral (CeL) and medial (CeM) sectors of CeA and BNST. In particular, most CS responsive CeM neurons exhibit positive responses to the CS (Ciocchi et al. 2010; Duvarci et al. 2011), as in BNST-AM. In contrast, as in BNST-AL, CeL responses to the CS are heterogeneous, with different CeL neurons exhibiting inhibitory or excitatory responses (Ciocchi et al. 2010; Duvarci et al. 2011). Perhaps not coincidentally, the incidence of CeL Off-cells does not increase during training, but after a consolidation period (Duvarci et al. 2011). In parallel, an inflation of CS-evoked responses develops in BLA (Amano et al. 2011). At present, the cellular interactions leading to these time-dependent changes in CS responsiveness remain unclear. However, given the strong interconnections existing between BLA, CeA, and BNST neurons, a causal relation is likely. Also, considering the dramatic impact of medial prefrontal lesions on the expression of learned fear (Sierra-Mercado et al. 2011) and the preferential innervation of BNST-AM by prelimbic afferents (reviewed in McDonald 1999), it is probable that prefrontal inputs also play a role.

5.1.2.3 Preferential BNST contribution to contextual fear**.** The impetus for the present study was to determine why BNST lesion and inactivation interfere with contextual but not cued fear given that BNST and CeA contribute similar

projections to brainstem fear effector neurons. We found that BNST-AM and AL neurons show a similar differential activity profile in relation to cued and contextual fear. These findings raise the following possibilities. First, it is conceivable that neurons in a different BNST sector, not explored in the present study, show a different activity profile in relation to the two forms of fear. Second, it is possible that earlier inactivation or lesion studies inadvertently affected a structure adjacent to BNST, which is involved in contextual fear. Consistent with this possibility, recent findings implicate components of the septal region in the regulation of fear and anxiety (Yamaguchi et al. 2013). Additional experiments will be required to settle this question.

5.1.3 Conclusions

Together, my findings suggest that the role of BNST is not limited to anxiety but that it also regulates responses to discrete threats. Moreover, they imply that reciprocal inhibitory interactions between BNST and CeA likely modulate the specificity and intensity of aversive responses. In addition, my findings add to the rapidly growing body of data indicating that BNST is a heterogeneous structure comprised of several functionally distinct cell groups and regions. A critical challenge for future studies will be to determine how different BNST regions and cell types interact with each other and the amygdala.

5.2 *DE NOVO* EMERGENCE OF BRAIN RHYTHMS THROUGH NONLINEAR SIGNAL INTEGRATION

In Chapter IV, we utilize the theory of frequency mixing to explore the relationship between neural oscillations of different frequencies. In our model, input signals are added and passed through a nonlinear function representing activation of the network. The non-linearity introduces an output term that involves the product of the two signals, which, through basic trigonometry, can be re-expressed as a sum of sinusoids including components at the sum and differences of the original frequencies.

5.2.1 Frequency mixing in other domains

The theory of frequency mixing has been well developed, aimed mainly at applications in electronics and signal processing. The principle was originally articulated as part of a patent by the Canadian inventor Reginald Fessenden, which was filed in 1901 for early radio technology. In the context of signal transmission technology, transforming signals to higher or lower frequencies (or *heterodyning*) can make them more suitable for encoding and transmission by electronic components (see Poole, 2015).

Another domain where frequency mixing is utilized is computer music synthesis. The technique of waveshaping involves creating sounds of a particular timbre by passing sinusoidal tones or signals through a nonlinear function (known in this field as a transfer function rather than activation function). In the frequency domain this transforms the input, a pure tone with spectrum consisting of a single delta function, to one that is more complex with power at integer-

multiples of the fundamental frequency. It was recognized that further interesting effects could be achieved by passing complex, multi-component signals through the nonlinearity (see Roads and Strawn, 1985). In this case the resulting signal also includes cross-terms, or what we call emergent components, that depend on the multiple input components and their relative spacing in the frequency domain.

5.2.2 Frequency mixing *in vivo*

We outlined the predictions expected in the LFP as a consequence of frequency mixing and proposed the use of an information-theoretic measure to test for them. Even in the absence of a priori knowledge of the input activities involved, frequency mixing provides a framework for resolving a complicated set of spectral components into a simpler picture, where these inputs may be identified and distinguished from their downstream effects.

5.2.2.1 Evidence for mixing To test for frequency mixing, I characterized the LFP using *interaction information*, that measures organization existing across multiple variables that is not present in their lower dimensional projections. Specifically, I apply this measure to phases of the time-frequency transformation of the LFP, obtained from wavelet analysis, for sets of three distinct frequencies. For pairs of input signals with frequencies known in advance, frequency mixing makes specific predictions about how particular sets of three frequencies should be related in phase and amplitude. Even when initial input signals are not known in advance, there remain several testable predictions of frequency mixing, about how the pII magnitude should be distributed across the 3D space defined by

triplets of frequency.

Through our analysis, we observe localized clusters of high pII in frequency space, with phase distributions of frequencies in these clusters showing patterns characteristic of the distinct categories we outline. For the most readily observed type, we find that centroids of these clusters consistently exhibit an expected relationship: that the largest frequency index of its position be equal to the sum of the other two indices. This holds true across different behavioral states and locations.

The most compelling evidence for frequency mixing comes from rats administered the NMDAR antagonist MK-801 and exhibiting a stereotyped LFP and behavior. In this state, several well-defined pII clusters are apparent, and show consistent expression across animals and locations. Many clusters are of an ellipsoid shape, with peculiar oblique orientations with respect to the axes. This seeming complexity is resolved through a simple model involving frequency mixing of two components, and allowing the lower input to vary in frequency while the higher input remains fixed. Several of the components resulting from mixing are expected to covary with the low input signal, with either a positive or negative correlation. For example, as the lower input signal increases in frequency, its harmonic and the high emergent component also increase, while the lower emergent component decreases (because the difference between input signals is reduced). Cluster orientation can then be seen to depend on the specific three output components that comprise it.

5.2.2.2 HFOs and mixing A tantalizing possibility suggested by frequency mixing was that HFOs represent an emergent component arising through the mixing of two lower frequency gamma oscillations. Indeed, as HFOs are prominent in structures comprised primarily of GABAergic neurons, and inhibitory cells can generate fast oscillations through reciprocal connections (Bartos et al., 2007), this seemed quite plausible. In our analysis of the state induced by MK-801, HFOs are strongly expressed, and interactions are seen with the 40 Hz and 100 Hz rhythms as quantified through the pII of this frequency triplet. Considering this relationship in isolation, the three oscillations may represent different combinations of output components of frequency mixing. The 40 Hz and 100 Hz signals may indeed be root signals at the input frequencies, with HFOs, at the sum of the two input frequencies, being their higher emergent signal. Alternatively, the 40 Hz and 140 Hz signals may represent root signals, and 100 Hz, at their difference, may be a lower emergent. Determining component identity must be done with consideration of additional information from other sets of frequency components. As discussed above, the bulk of the evidence favors the later: 40 Hz and 140 Hz signals acting as inputs in the mixing. Therefore, our analysis does not account for the generation of HFOs, but does describe their relationship to other frequencies.

5.2.3 Limitations and conclusion

Our analysis has many limitations. Neural activity in healthy behaving brains is extremely rich and heterogeneous. While each of several brain states

may express frequency mixing of different varieties, when these are superimposed the structure present in each of them will be diminished (as measured through interaction information). Indeed, in our analysis, the clearest results were obtained when rats were administered an NMDAR antagonist, creating a highly stereotyped but pathological brain state. Another potential issue is that even in a homogeneous brain state where mixing is occurring, the input frequencies may be such that some of the root, harmonic, and emergent components will overlap, making them harder to characterize using our approach. In the example we give in Figure 4.1, choosing inputs at 40 and 100 Hz yields an output with regularly spaced components at 40(R2), 60(E2), 80(H2), 100(R1), 140(E1), and 200(H1) hertz. If, for example, the input signals were chosen to be 40 and 120 Hz instead, the harmonic of the 40 Hz signal and lower emergent component would both coincide at 80 Hz. The likelihood of this type of interference occurring increases rapidly as additional input signals are included.

Two final aspects of our simplified framework should be noted. First, there are no temporal dynamics represented in the input-output transformation of our model. In reality, action potentials propagate with finite velocity and particular classes of neurons have distinct membrane time constants that are essential to their function. Second, local neuronal activity feeds back on itself. Indeed, it has been recognized that finite propagation times together with recurrent dynamics allows for a computational richness that isn't otherwise possible (Izhikevich, 2006). In the context of our frequency mixing model, recurrence means that harmonic and emergent activities themselves act as inputs and can become root

signals in higher-order interactions and temporal delays would result in phase-shifts that would be more pronounced for higher frequencies. Clearly these complexities warrant explicit study and would be well suited to computational simulations.

With these limitations in mind and despite the simplifying assumptions underlying the analysis we have presented, we believe the quote by George E. P. Box--"All models are wrong, but some are useful"--holds true, often more so for models that offer transparency and a unique perspective at the expense of opaque realism.

VI. FULL LIST OF REFERENCES

Adhikari A, Lerner TN, Finkelstein J, Pak S, Jennings JH, Davidson TJ, Ferenczi E, Gunaydin LA, Mirzabekov JJ, Ye L, Kim S, Lei A, Deisseroth K (2015) Basomedial amygdala mediates top-down control of anxiety and fear. Nature 527:179–185.

Adrian ED (1950) The electrical activity of the mammalian olfactory bulb. Electroencephalogr Clin Neurophysiol 2:377–388.

Alheid GF, Heimer L (1988) New perspectives in basal forebrain organization of special relevance for neuropsychiatric disorders: The striatopallidal, amygdaloid, and corticopetal components of substantia innominata. Neuroscience 27:1–39.

Amano T, Duvarci S, Popa D, Pare D (2011) The fear circuit revisited: contributions of the basal amygdala nuclei to conditioned fear. J Neurosci 31:15481–15489.

Aston-Jones G, Harris GC (2004) Brain substrates for increased drug seeking during protracted withdrawal. Neuropharmacology 47:167–179.

Barr RC, Plonsey R (1992) Electrophysiological interaction through the interstitial space between adjacent unmyelinated parallel fibers. Biophys J 61:1164–1175.

Barthó P, Hirase H, Monconduit L, Zugaro M, Harris KD, Buzsáki G (2004) Characterization of neocortical principal cells and interneurons by network interactions and extracellular features. J Neurophysiol 92:600–608.

Bartos M, Vida I, Jonas P (2007) Synaptic mechanisms of synchronized gamma oscillations in inhibitory interneuron networks. Nat Rev Neurosci 8:45–56.

Bauer EP, Paz R, Pare D (2007) Gamma Oscillations Coordinate Amygdalo-Rhinal Interactions during Learning. J Neurosci 27:9369–9379.

Berke JD (2009) Fast oscillations in cortical-striatal networks switch frequency following rewarding events and stimulant drugs. Eur J Neurosci 30:848–859.

Bienkowski MS, Rinaman L (2013) Common and distinct neural inputs to the medial central nucleus of the amygdala and anterior ventrolateral bed nucleus of stria terminalis in rats. Brain Struct Funct 218:187–208.

Blanchard DC, Blanchard RJ (1972) Innate and Conditioned Reactions to Threat in Rats with Amygdaloid Lesions. J Comp Physiol Psychol 81:281–290.

Blinder KJ, Pumplin DW, Paul DL, Keller A (2003) Intercellular interactions in the mammalian olfactory nerve. J Comp Neurol 466:230–239.

Bokil H, Laaris N, Blinder K, Ennis M, Keller A (2001) Ephaptic interactions in the mammalian olfactory system. J Neurosci 21:RC173.

Box GEP, Hunter JS, Hunter WG. (2005). *Statistics for experimenters: Design, innovation, and discovery* (2nd ed.). Hoboken, N.J.: Wiley-Interscience.

Bragin A, Jandó G, Nádasdy Z, Hetke J, Wise K, Buzsáki G (1995) Gamma (40-100 Hz) oscillation in the hippocampus of the behaving rat. J Neurosci 15:47–60.

Buffalari DM, See RE (2011) Inactivation of the bed nucleus of the stria terminalis in an animal model of relapse: Effects on conditioned cue-induced reinstatement and its enhancement by yohimbine. Psychopharmacology (Berl) 213:19–27.

Bullock TH, McClune MC (1989) Lateral coherence of the electrocorticogram: a new measure of brain synchrony. Electroencephalogr Clin Neurophysiol 73:479–498.

Buzsaki G (2006) Rhythms of the Brain.

Buzsáki G (2002) Theta oscillations in the hippocampus. Neuron 33:325–340.

Buzsáki G, Draguhn A (2004) Neuronal oscillations in cortical networks. Science 304:1926–1929.

Buzsáki G, Horváth Z, Urioste R, Hetke J, Wise K (1992) High-frequency network oscillation in the hippocampus. Science 256:1025–1027.

Buzsáki G, Lai-Wo S. L, Vanderwolf CH (1983) Cellular bases of hippocampal EEG in the behaving rat. Brain Res Rev 6:139–171.

Buzsáki G, Logothetis N, Singer W (2013) Scaling brain size, keeping timing: Evolutionary preservation of brain rhythms. Neuron 80:751–764.

Campeau S, Falls WA, Cullinan WE, Helmreich DL, Davis M, Watson SJ (1997) Elicitation and reduction of fear: Behavioural and neuroendocrine indices and brain induction of the immediate-early gene c-fos. Neuroscience 78:1087–1104.

Campeau S, Davis M (1995) Involvement of the Central Nucleus and Basolateral Complex of the Amygdala in Fear Conditioning Measured With Fear- Potentiated Startle in Rats Trained Concurrently With Auditory and Visual Conditioned-Stimuli. J Neurosci 15:2301–2311.

Chrobak JJ, Buzsáki G (1998) Gamma oscillations in the entorhinal cortex of the freely behaving rat. J Neurosci 18:388–398.

Chrobak JJ, Buzsáki G (1996) High-frequency oscillations in the output networks of the hippocampal-entorhinal axis of the freely behaving rat. J Neurosci 16:3056–3066.

Ciocchi S, Herry C, Grenier F, Wolff SBE, Letzkus JJ, Vlachos I, Ehrlich I, Sprengel R, Deisseroth K, Stadler MB, Muller C, Luthi A (2010) Encoding of conditioned fear in central amygdala inhibitory circuits. Nature 468:277–282.

Colgin LL, Denninger T, Fyhn M, Hafting T, Bonnevie T, Jensen O, Moser M-B, Moser EI (2009) Frequency of gamma oscillations routes flow of information in the hippocampus. Nature 462:353–357.

Collins DR, Pelletier JG, Paré D (2001) Slow and fast (gamma) neuronal oscillations in the perirhinal cortex and lateral amygdala. J Neurophysiol 85:1661–1672.

Collins DR, Lang EJ, Paré D (1999) Spontaneous activity of the perirhinal cortex in behaving cats. Neuroscience 89:1025–1039.

Cullinan WE, Herman JP, Watson SJ (1993) Ventral subicular interaction with the hypothalamic paraventricular nucleus: Evidence for a relay in the bed nucleus of the stria terminalis. J Comp Neurol 332:1–20.

Dabrowska J, Hazra R, Guo JD, DeWitt S, Rainnie DG (2013) Central CRF neurons are not created equal: Phenotypic differences in CRF-containing neurons of the rat paraventricular hypothalamus and the bed nucleus of the stria terminalis. Front Neurosci.

Daniel SE, Rainnie DG (2015) Stress Modulation of Opposing Circuits in the Bed Nucleus of the Stria Terminalis. Neuropsychopharmacology 41:1–23.

Day HE, Curran EJ, Watson SJ, Akil H (1999) Distinct neurochemical populations in the rat central nucleus of the amygdala and bed nucleus of the stria terminalis: evidence for their selective activation by interleukin-1beta. J Comp Neurol 413:113–128.

De Olmos JS, Heimer L (1999) The concepts of the ventral striatopallidal system and extended amygdala. In: Annals of the New York Academy of Sciences, pp 1–32.

De Olmos JS, Heimer L (1999) The concepts of the ventral striatopallidal system and extended amygdala. In: Annals of the New York Academy of Sciences, pp 1–32.

Debanne D, Campanac E, Bialowas A, Carlier E, Alcaraz G (2011) Axon physiology. Physiol Rev 91:555–602.

Dempsey EW, Morison RS (1942) The reproduction of rhythmically recurrent cortical potentials after localized thalamic stimulation. Am J Physiol. 135:293–300.

Desmedt JE, Tomberg C (1994) Transient phase-locking of 40 Hz electrical oscillations in prefrontal and parietal human cortex reflects the process of conscious somatic perception. Neurosci Lett 168:126–129.

Desmedt JE, Tomberg C (1994) Transient phase-locking of 40 Hz electrical oscillations in prefrontal and parietal human cortex reflects the process of conscious somatic perception. Neurosci Lett 168:126–129.

Dobolyi A, Irwin S, Makara G, Usdin TB, Palkovits M (2005) Calcitonin gene-related peptide-containing pathways in the rat forebrain. J Comp Neurol 489:92–119.

Dong HW, Petrovich GD, Swanson LW (2000) Organization of projections from the juxtacapsular nucleus of the BST: A PHAL study in the rat. Brain Res 859:1–14.

Dong HW, Petrovich GD, Swanson LW (2001a) Topography of projections from amygdala to bed nuclei of the stria terminalis. Brain Res Rev 38:192–246.

Dong HW, Petrovich GD, Watts AG, Swanson LW (2001b) Basic organization of projections from the oval and fusiform nuclei of the bed nuclei of the stria terminalis in adult rat brain. J Comp Neurol 436:430–455.

Dong HW, Swanson LW (2006a) Projections from bed nuclei of the stria terminalis, magnocellular nucleus: Implications for cerebral hemisphere regulation of micturition, defecation, and penile erection. J Comp Neurol 494:108–141.

Dong HW, Swanson LW (2006b) Projections from bed nuclei of the stria terminalis, dorsomedial nucleus: Implications for cerebral hemisphere integration of neuroendocrine, autonomic, and drinking responses. J Comp Neurol 494:75–107.

Dong HW, Swanson LW (2006c) Projections from bed nuclei of the stria terminalis, anteromedial area: Cerebral hemisphere integration of neuroendocrine, autonomic, and behavioral aspects of energy balance. J Comp Neurol 494:142–178.

Dong HW, Swanson LW (2003) Projections from the rhomboid nucleus of the bed nuclei of the stria terminalis: Implications for cerebral hemisphere regulation of ingestive behaviors. J Comp Neurol 463:434–472.

Dong HW, Swanson LW (2004) Organization of Axonal Projections from the Anterolateral Area of the Bed Nuclei of the Stria Terminalis. J Comp Neurol 468:277–298.

Dunn JD (1987) Plasma corticosterone responses to electrical stimulation of the bed nucleus of the stria terminalis. Brain Res 407:327–331.

Duvarci S, Popa D, Pare D (2011) Central amygdala activity during fear conditioning. J Neurosci 31:289–294.

Duvarci S, Bauer EP, Paré D (2009) The bed nucleus of the stria terminalis mediates inter-individual variations in anxiety and fear. J Neurosci 29:10357–10361.

Erb S, Stewart J (1999) A role for the bed nucleus of the stria terminalis, but not the amygdala, in the effects of corticotropin-releasing factor on stress-induced reinstatement of cocaine seeking. J Neurosci 19:RC35.

Esclapez M, Tillakaratne NJ, Kaufman DL, Tobin a J, Houser CR (1994) Comparative localization of two forms of glutamic acid decarboxylase and their mRNAs in rat brain supports the concept of functional differences between the forms. J Neurosci 14:1834–1855.

Fanselow MS, Kim JJ (1994) Acquisition of contextual Pavlovian fear conditioning is blocked by application of an NMDA receptor antagonist D,L-2-amino-5-phosphonovaleric acid to the basolateral amygdala. Behav Neurosci 108:210–212.

Fellous JM, Sejnowski TJ (2000) Cholinergic induction of oscillations in the hippocampal slice in the slow (0.5-2 Hz), theta (5-12 Hz), and gamma (35-70 Hz) bands. Hippocampus 10:187–197.

Fendt M, Endres T, Apfelbach R (2003) Temporary inactivation of the bed nucleus of the stria terminalis but not of the amygdala blocks freezing induced by trimethylthiazoline, a component of fox feces. J Neurosci 23:23–28.

Fessenden R (1902) U.S. Patent 706, 740, “Wireless Signaling” (heterodyne principle).

Fisahn A (2004) Distinct Roles for the Kainate Receptor Subunits GluR5 and GluR6 in Kainate-Induced Hippocampal Gamma Oscillations. J Neurosci 24:9658–9668.

Fisahn A, Pike FG, Buhl EH, Paulsen O (1998) Cholinergic induction of network oscillations at 40 Hz in the hippocampus in vitro. Nature 394:186–189.

Fries P (2015) Rhythms for Cognition: Communication through Coherence. Neuron 88:220–235.

Fu L-Y, van den Pol AN (2008) Agouti-related peptide and MC3/4 receptor agonists both inhibit excitatory hypothalamic ventromedial nucleus neurons. J Neurosci 28:5433–5449.

Gewirtz JC, McNish KA, Davis M (1998) Lesions of the bed nucleus of the stria terminalis block sensitization of the acoustic startle reflex produced by repeated stress, but not fear-potentiated startle. Prog Neuropsychopharmacol Biol Psychiatry 22:625–48.

Gloor P (1960) Amygdala. In: Handbook of Physiology (Field J, ed), pp 1395–1420. Washington, DC.

Goda SA, Piasecka J, Olszewski M, Kasicki S, Hunt MJ (2013) Serotonergic hallucinogens differentially modify gamma and high frequency oscillations in the rat nucleus accumbens. Psychopharmacology (Berl) 228:271–282.

Gonzalez-Burgos G, Lewis DA (2012) NMDA receptor hypofunction, parvalbumin-positive neurons, and cortical gamma oscillations in schizophrenia. Schizophr Bull 38:950–957.

Goosens KA, Maren S (2001) Contextual and auditory fear conditioning are mediated by the lateral, basal, and central amygdaloid nuclei in rats. Learn Mem 8:148–155.

Gray CM, König P, Engel AK, Singer W (1989) Oscillatory responses in cat visual cortex exhibit inter-columnar synchronization which reflects global stimulus properties. Nature 338:334–337.

Gray TS, Magnuson DJ (1992) Peptide immunoreactive neurons in the amygdala and the bed nucleus of the stria terminalis project to the midbrain central gray in the rat. Peptides 13:451–460.

Gray TS, Magnuson DJ (1987) Neuropeptide neuronal efferents from the bed nucleus of the stria terminalis and central amygdaloid nucleus to the dorsal vagal complex in the rat. J Comp Neurol 262:365–374.

Gross CT, Canteras NS (2012) The many paths to fear. Nat Rev Neurosci 13:651–658.

Gungor NZ, Paré D (2014) CGRP inhibits neurons of the bed nucleus of the stria terminalis: implications for the regulation of fear and anxiety. J Neurosci 34:60–65.

Gungor NZ, Paré D (2016) Functional Heterogeneity in the Bed Nucleus of the Stria Terminalis. J Neurosci 36:8038–8049.

Gungor NZ, Yamamoto R, Paré D (2015) Optogenetic study of the projections from the bed nucleus of the stria terminalis to the central amygdala. J Neurophysiol 114:2903–2911.

Gustafson EL, Greengard P (1990) Localization of DARPP-32 immunoreactive neurons in the bed nucleus of the stria terminalis and central nucleus of the amygdala: co-distribution with axons containing tyrosine hydroxylase, vasoactive intestinal polypeptide, and calcitonin gene-related peptide. Exp brain Res 79:447–458.

Hammack SE, Mania I, Rainnie DG (2007) Differential expression of intrinsic membrane currents in defined cell types of the anterolateral bed nucleus of the stria terminalis. J Neurophysiol 98:638–656.

Hammack SE, Todd TP, Kocho-Schellenberg M, Bouton ME (2015) Role of the Bed Nucleus of the Stria Terminalis in the Acquisition of Contextual Fear at Long or Short Context-Shock Intervals. Behav Neurosci 129:673–678.

Hazan L, Zugaro M, Buzsáki G (2006) Klusters, NeuroScope, NDManager: A free software suite for neurophysiological data processing and visualization. J Neurosci Methods 155:207–216.

Hazan L, Zugaro M, Buzsáki G (2006) Klusters, NeuroScope, NDManager: A free software suite for neurophysiological data processing and visualization. J Neurosci Methods 155:207–216.

Hazra R, Guo J-D, Ryan SJ, Jasnow AM, Dabrowska J, Rainnie DG (2011) A transcriptomic analysis of type I-III neurons in the bed nucleus of the stria terminalis. Mol Cell Neurosci 46:699–709.

Headley DB, Paré D (2013) In sync: gamma oscillations and emotional memory. Front Behav Neurosci 7:170.

Heimer L, Van Hoesen G, Trimble M, Zahm D (n.d.) The anatomy of the basal forebrain. In: Anatomy of Neuropsychiatry., pp 2008.

Heisenberg W (1958) Physics and Philosophy The Revolution in Modern Science. Book:206.

Henke PG (1984) The bed nucleus of the stria terminalis and immobilization-stress. Behav Brain Res 11:35–45.

Hitchcock JM, Davis M (1987) Fear-potentiated startle using an auditory conditioned stimulus: Effect of lesions of the amygdala. Physiol Behav 39:403–408.

Holstege G, Meiners L, Tan K (1985) Projections of the bed nucleus of the stria terminalis to the mesencephalon, pons, and medulla oblongata in the cat. Exp Brain Res 58:379–391.

Hopkins DA, Holstege G (1978) Amygdaloid projections to the mesencephalon, pons and medulla oblongata in the cat. Exp Brain Res 32:529–547.

Hubbard JI, Llinás R, Quastel DMJ (1969) Electrophysiological Analysis of Synaptic Transmission. London: Edward Arnold Ltd; Extracellular field potentials in the central nervous system; pp. 265–293.

Hunt MJ, Olszewski M, Piasecka J, Whittington MA, Kasicki S (2015) Effects of NMDA receptor antagonists and antipsychotics on high frequency oscillations recorded in the nucleus accumbens of freely moving mice. Psychopharmacology (Berl) 232:4525–4535.

Hunt MJ, Falinska M, Łeski S, Wójcik DK, Kasicki S (2011) Differential effects produced by ketamine on oscillatory activity recorded in the rat hippocampus, dorsal striatum and nucleus accumbens. J Psychopharmacol 25:808–821.

Hunt MJ, Kasicki S (2013) A systematic review of the effects of NMDA receptor antagonists on oscillatory activity recorded in vivo. J Psychopharmacol 27:972–986.

Ide S, Hara T, Ohno A, Tamano R, Koseki K, Naka T, Maruyama C, Kaneda K, Yoshioka M, Minami M (2013) Opposing roles of corticotropin-releasing factor and neuropeptide Y within the dorsolateral bed nucleus of the stria terminalis in the negative affective component of pain in rats. J Neurosci 33:5881–5894.

Izhikevich EM (2006) Polychronization: computation with spikes. Neural Comput 18:245–282.

Jackson J, Goutagny R, Williams S (2011) Fast and slow gamma rhythms are intrinsically and independently generated in the subiculum. J Neurosci 31:12104–12117.

Javitt DC, Zukin SR (1991) Recent advances in the phencyclidine model of schizophrenia. Am J Psychiatry 148:1301–1308.

Jennings JH, Sparta DR, Stamatakis AM, Ung RL, Pleil KE, Kash TL, Stuber GD (2013) Distinct extended amygdala circuits for divergent motivational states. Nature 496:224–228.

Jimenez S a, Maren S (2009) Nuclear disconnection within the amygdala reveals a direct pathway to fear. Learn Mem 16:766–768.

Ju G, Swanson LW (1989a) Studies on the cellular architecture of the bed nuclei of the stria terminalis in the rat: I. Cytoarchitecture. J Comp Neurol 280:587–602.

Ju G, Swanson LW, Simerly RB (1989b) Studies on the cellular architecture of the bed nuclei of the stria terminalis in the rat: II. Chemoarchitecture. J Comp Neurol 280:603–621.

Kash TL, Nobis WP, Matthews RT, Winder DG (2008) Dopamine enhances fast excitatory synaptic transmission in the extended amygdala by a CRF-R1-dependent process. J Neurosci 28:13856–13865.

Katz B (1942) A note on interaction between nerve fibres. J Physiol 100:369–371.

Katz B, Schmitt OH (1940) Electric interaction between two adjacent nerve fibres. J Physiol 97:471–488.

Kay LM (2015) Olfactory system oscillations across phyla. Curr Opin Neurobiol 31:141–147.

Kellicut M, Schwartzbaum J (1963) Formation of a conditioned emotional response (CER) following lesions of the amygdaloid complex in rats. Psychol Rev 12:351–358.

Kim M, Campeau S, Falls WA, Davis M (1993) Infusion of the non-NMDA receptor antagonist CNQX into the amygdala blocks the expression of fear-potentiated startle. Behav Neural Biol 59:5–8.

Kim S-Y, Adhikari A, Lee SY, Marshel JH, Kim CK, Mallory CS, Lo M, Pak S, Mattis J, Lim BK, Malenka RC, Warden MR, Neve R, Tye KM, Deisseroth K (2013) Diverging neural pathways assemble a behavioural state from separable features in anxiety. Nature 496:219–223.

Klüver H, Bucy PC (1939) PRELIMINARY ANALYSIS OF FUNCTIONS OF THE TEMPORAL LOBES IN MONKEYS. Arch Neurol Psychiatry 42:979–1000.

König P, Engel a K, Singer W (1995) Relation between oscillatory activity and long-range synchronization in cat visual cortex. Proc Natl Acad Sci U S A 92:290–294.

Koo JW, Han J-S, Kim JJ (2004) Selective neurotoxic lesions of basolateral and central nuclei of the amygdala produce differential effects on fear conditioning. J Neurosci 24:7654–7662.

Koob GF (2009) Brain stress systems in the amygdala and addiction. Brain Res 1293:61-75.

Krettek JE, Price JL (1978a) Amygdaloid projections to subcortical structures within the basal forebrain and brainstem in the rat and cat. J Comp Neurol 178:225–253.

Krettek JE, Price JL (1978b) A description of the amygdaloid complex in the rat and cat with observations on intra-amygdaloid axonal connections. J Comp Neurol 178:255–279.

Kudo T, Uchigashima M, Miyazaki T, Konno K, Yamasaki M, Yanagawa Y, Minami M, Watanabe M (2012) Three types of neurochemical projection from the bed nucleus of the stria terminalis to the ventral tegmental area in adult mice. J Neurosci 32:18035–18046.

Lamantia A -S, Rakic P (1990) Cytological and quantitative characteristics of four cerebral commissures in the rhesus monkey. J Comp Neurol 291:520–537.

Laurent G (2002) Olfactory network dynamics and the coding of multidimensional signals. Nat Rev Neurosci 3:884–895.

LeDoux JE (1995) Emotion: clues from the brain. Annu Rev Psychol 46:209–235.

LeDoux JE (1993) Emotional memory: in search of systems and synapses. Ann N Y Acad Sci 702:149–157.

LeDoux JE, Iwata J, Cicchetti P, Reis DJ (1988) Different projections of the central amygdaloid nucleus mediate autonomic and behavioral correlates of conditioned fear. J Neurosci 8:2517–2529.

Lee H, Kim D-W, Remedios R, Anthony TE, Chang A, Madisen L, Zeng H, Anderson DJ (2014) Scalable control of mounting and attack by Esr1+ neurons in the ventromedial hypothalamus. Nature 509:627–632.

Llinás RR (1988) The intrinsic electrophysiological properties of mammalian neurons: insights into central nervous system function. Science 242:1654–1664.

Maex R, De Schutter E (2007) Mechanism of spontaneous and self-sustained oscillations in networks connected through axo-axonal gap junctions. Eur J Neurosci 25:3347–3358.

Markram H, Toledo-Rodriguez M, Wang Y, Gupta A, Silberberg G, Wu C (2004) Interneurons of the neocortical inhibitory system. Nat Rev Neurosci 5:793–807.

McDonald AJ (2006) Is There an Amygdala and How Far Does It Extend? Ann N Y Acad Sci 985:1–21.

McDonald AJ (2003) Is there an amygdala and how far does it extend? An anatomical perspective. Ann N Y Acad Sci 985:1–21.

McDonald AJ, Shammah-Lagnado SJ, Shi C, Davis M (1999) Cortical afferents to the extended amygdala. In: Annals of the New York Academy of Sciences, pp 309–338.

Meloni EG, Jackson A, Gerety LP, Cohen BM, Carlezon WA (2006) Role of the bed nucleus of the stria terminalis (BST) in the expression of conditioned fear. In: Annals of the New York Academy of Sciences, pp 538–541.

Moga MM, Saper CB, Gray TS (1989) Bed nucleus of the stria terminalis: cytoarchitecture, immunohistochemistry, and projection to the parabrachial nucleus in the rat. J Comp Neurol 283:315–332.

Mori K, Manabe H, Narikiyo K, Onisawa N (2013) Olfactory consciousness and gamma oscillation couplings across the olfactory bulb, olfactory cortex, and orbitofrontal cortex. Front Psychol 4:743.

Murthy VN, Fetz EE (1992) Coherent 25- to 35-Hz oscillations in the sensorimotor cortex of awake behaving monkeys. Proc Natl Acad Sci U S A 89:5670–5674.

Nagano Y, Kaneda K, Maruyama C, Ide S, Kato F, Minami M (2015) Corticotropin-releasing factor enhances inhibitory synaptic transmission to type III neurons in the bed nucleus of the stria terminalis. Neurosci Lett 600:56–61.

Nobis WP, Kash TL, Silberman Y, Winder DG (2011) Adrenergic receptors enhance excitatory transmission in the bed nucleus of the stria terminalis through a corticotrophin-releasing factor receptor dependent and cocaine-regulated mechanism. Biol Psychiatry 69:1083–1090.

Nunez PL, Srinivasan R (2006). Electric Fields of the Brain. Oxford University Press. doi:10.1093/acprof:oso/9780195050387.001.0001.

Olszewski M, Dolowa W, Matulewicz P, Kasicki S, Hunt MJ (2013) NMDA receptor antagonist-enhanced high frequency oscillations: Are they generated broadly or regionally specific? Eur Neuropsychopharmacol 23:1795–1805.

Pape H-C, Paré D (2010) Plastic synaptic networks of the amygdala for the acquisition, expression, and extinction of conditioned fear. Physiol Rev 90:419–463.

Paré D, Smith Y, Paré JF (1995) Intra-amygdaloid projections of the basolateral and basomedial nuclei in the cat: Phaseolus vulgaris-leucoagglutinin anterograde tracing at the light and electron microscopic level. Neuroscience 69:567–583.

Paré D, Gaudreau H (1996) Projection cells and interneurons of the lateral and basolateral amygdala: distinct firing patterns and differential relation to theta and delta rhythms in conscious cats. J Neurosci 16:3334–3350.

Petrovich GD, Risold PY, Swanson LW (1996) Organization of projections from the basomedial nucleus of the amygdala: A PHAL study in the rat. J Comp Neurol 374:387–420.

Petsche H, Stumpf C, Gogolak G (1962) The significance of the rabbit's septum as a relay station between the midbrain and the hippocampus I. The control of hippocampus arousal activity by the septum cells. Electroencephalogr Clin Neurophysiol 14:202–211.

Phelix CF, Paull WK (1990) Demonstration of distinct corticotropin releasing factor--containing neuron populations in the bed nucleus of the stria terminalis. A light and electron microscopic immunocytochemical study in the rat. Histochemistry 94:345–364.

Pitts MW, Todorovic C, Blank T, Takahashi LK (2009) The central nucleus of the amygdala and corticotropin-releasing factor: insights into contextual fear memory. J Neurosci 29:7379–7388.

Pleil KE, Rinker JA, Lowery-Gionta EG, Mazzone CM, McCall NM, Kendra AM, Olson DP, Lowell BB, Grant KA, Thiele TE, Kash TL (2015) NPY signaling inhibits extended amygdala CRF neurons to suppress binge alcohol drinking. Nat Neurosci 18:545–552.

Polston EK, Gu G, Simerly RB (2004) Neurons in the principal nucleus of the bed nuclei of the stria terminalis provide a sexually dimorphic gabaergic input to the anteroventral periventricular nucleus of the hypothalamus. Neuroscience 123:793–803.

Poole I (2015) A Guide to Superheterodyne Radio Technology. Surrey, UK.: Adrio Communications Ltd.

Popescu AT, Popa D, Paré D (2009) Coherent gamma oscillations couple the amygdala and striatum during learning. Nat Neurosci 12:801–807.

Potter E, Sutton S, Donaldson C, Chen R, Perrin M, Lewis K, Sawchenko PE, Vale W (1994) Distribution of corticotropin-releasing factor receptor mRNA expression in the rat brain and pituitary. Proc Natl Acad Sci U S A 91:8777–8781.

Poulin J-F, Arbour D, Laforest S, Drolet G (2009) Neuroanatomical characterization of endogenous opioids in the bed nucleus of the stria terminalis. Prog Neuropsychopharmacol Biol Psychiatry 33:1356–1365.

Poulin J-F, Arbour D, Laforest S, Drolet G (2009) Neuroanatomical characterization of endogenous opioids in the bed nucleus of the stria terminalis. Prog Neuropsychopharmacol Biol Psychiatry 33:1356–1365.

Reyes AD (2003) Synchrony-dependent propagation of firing rate in iteratively constructed networks in vitro. Nat Neurosci 6:593–599.

Reynolds SM, Zahm DS (2005) Specificity in the projections of prefrontal and insular cortex to ventral striatopallidum and the extended amygdala. J Neurosci 25:11757–11767.

Roads C, Strawn J (1985) Foundations of Computer Music. Cambridge, Massachusetts: The MIT Press.

Rodríguez-Sierra OE, Turesson HK, Pare D (2013) Contrasting distribution of physiological cell types in different regions of the bed nucleus of the stria terminalis. J Neurophysiol 110:2037–2049.

Russchen FT (1982) Amygdalopetal projections in the cat. I. Cortical afferent connections. A study with retrograde and anterograde tracing techniques. J Comp Neurol 206:159–179.

Sah P, Faber ESL, Lopez De Armentia M, Power J (2003) The amygdaloid complex: anatomy and physiology. Physiol Rev 83:803–834.

Sahuque LL, Kullberg EF, Mcgeehan AJ, Kinder JR, Hicks MP, Blanton MG, Janak PH, Olive MF (2006) Anxiogenic and aversive effects of corticotropin-releasing factor (CRF) in the bed nucleus of the stria terminalis in the rat: Role of CRF receptor subtypes. Psychopharmacology (Berl) 186:122–132.

Sakanaka M, Shibasaki T, Lederis K (1987) Corticotropin releasing factor-like immunoreactivity in the rat brain as revealed by a modified cobalt-glucose oxidase-diaminobenzidine method. J Comp Neurol 260:256–298.

Saper CB, Loewy AD (1980) Efferent connections of the parabrachial nucleus in the rat. Brain Res 197:291–317.

Savander V, Go CG, LeDoux JE, Pitkanen A (1995) Intrinsic connections of the rat amygdaloid complex: projections originating in the basal nucleus. J Comp Neurol 361:345–368.

Scheffer-Teixeira R, Belchior H, Caixeta F V., Souza BC, Ribeiro S, Tort ABL (2012) Theta phase modulates multiple layer-specific oscillations in the CA1 region. Cereb Cortex 22:2404–2414.

Scheffer-Teixeira R, Belchior H, Leão RN, Ribeiro S, Tort ABL (2013) On high-frequency field oscillations (>100 Hz) and the spectral leakage of spiking activity. J Neurosci 33:1535–1539.

Scheffzük C, Kukushka VI, Vyssotski AL, Draguhn A, Tort ABL, Brankačk J (2011) Selective coupling between theta phase and neocortical fast gamma oscillations during REM-sleep in mice. PLoS One 6.

Schwaber JS, Kapp BS, Higgins GA, Rapp PR (1982) Amygdaloid and basal forebrain direct connections with the nucleus of the solitary tract and the dorsal motor nucleus. J Neurosci 2:1424–1438.

Sejnowski TJ, Paulsen O (2006) Network oscillations: emerging computational principles. J Neurosci 26:1673–1676.

Shackman AJ, Fox AS (2016) Contributions of the Central Extended Amygdala to Fear and Anxiety. J Neurosci 36:8050–8063.

Sierra-Mercado D, Padilla-Coreano N, Quirk GJ (2011) Dissociable roles of prelimbic and infralimbic cortices, ventral hippocampus, and basolateral amygdala in the expression and extinction of conditioned fear. Neuropsychopharmacology 36:529–538.

Silberman Y, Matthews RT, Winder DG (2013) A corticotropin releasing factor pathway for ethanol regulation of the ventral tegmental area in the bed nucleus of of the stria terminalis. J Neurosci 33:950–960.

Silva B a, Mattucci C, Krzywkowski P, Murana E, Illarionova A, Grinevich V, Canteras NS, Ragozzino D, Gross CT (2013) Independent hypothalamic circuits for social and predator fear. Nat Neurosci 16:1731–1733.

Simerly RB (2002) WIRED FOR REPRODUCTION: Organization and Development of Sexually Dimorphic Circuits in the Mammalian Forebrain. Annu Rev Neurosci 25:507–536.

Singer W (1999) Neuronal synchrony: a versatile code for the definition of relations? Neuron 24:49-65-125.

Singer W (2010) Temporal Coherence: A Versatile Code for the Definition of Relations. In: The Senses: A Comprehensive Reference, pp 1–9.

Sink KS, Walker DL, Yang Y, Davis M (2011) Calcitonin gene-related peptide in the bed nucleus of the stria terminalis produces an anxiety-like pattern of behavior and increases neural activation in anxiety-related structures. J Neurosci 31:1802–1810.

Smith Y, Pare D (1994) Intra-amygdaloid projections of the lateral nucleus in the cat: PHAL anterograde labeling combined with postembedding GABA and glutamate immunocytochemistry. J Comp Neurol 342:232–248.

Sofroniew M V. (1983) Direct reciprocal connections between the bed nucleus of the stria terminalis and dorsomedial medulla oblongata: Evidence from immunohistochemical detection of tracer proteins. J Comp Neurol 213:399–405.

Steriade M, Amzica F, Contreras D (1996) Synchronization of fast (30-40 Hz) spontaneous cortical rhythms during brain activation. J Neurosci 16:392–417.

Steriade M, Llinás RR (1988) The functional states of the thalamus and the associated neuronal interplay. Physiol Rev 68:649–742.

Steriade M, McCormick DA, Sejnowski TJ (1993) Thalamocortical oscillations in the sleeping and aroused brain. Science 262:679–685.

Steriade M, Nuñez a, Amzica F (1993) A novel slow (< 1 Hz) oscillation of neocortical neurons in vivo: depolarizing and hyperpolarizing components. J Neurosci 13:3252–3265.

Steriade M (1997) Synchronized activities of coupled oscillators in the cerebral cortex and thalamus at different levels of vigilance. Cereb Cortex 7:583–588.

Stujenske JM, Likhtik E, Topiwala MA, Gordon JA (2014) Fear and Safety Engage Competing Patterns of Theta-Gamma Coupling in the Basolateral Amygdala. Neuron 83:919–933.

Sullivan GM, Apergis J, Bush DEA, Johnson LR, Hou M, Ledoux JE (2004) Lesions in the bed nucleus of the stria terminalis disrupt corticosterone and freezing responses elicited by a contextual but not by a specific cue-conditioned fear stimulus. Neuroscience 128:7–14.

Sun N, Cassell MD (1993) Intrinsic GABAergic neurons in the rat central extended amygdala. J Comp Neurol 330:381–404.

Swanson LW, Petrovich GD (1998) What is the amygdala? Trends Neurosci 21:323–31.

Tepper JM, Bolam JP (2004) Functional diversity and specificity of neostriatal interneurons. Curr Opin Neurobiol 14:685–692.

Timofeev I, Contreras D, Steriade M (1996) Synaptic responsiveness of cortical and thalamic neurons during various phases of slow sleep oscillation in cat. J. Physiol. 494:265-278.

Tort ABL, Kramer MA, Thorn C, Gibson DJ, Kubota Y, Graybiel AM, Kopell NJ (2008) Dynamic cross-frequency couplings of local field potential oscillations in rat striatum and hippocampus during performance of a T-maze task. Proc Natl Acad Sci U S A 105:20517–20522.

Tort ABL, Scheffer-Teixeira R, Souza BC, Draguhn A, Brankačk J (2013) Theta-associated high-frequency oscillations (110-160Hz) in the hippocampus and neocortex. Prog Neurobiol 100:1–14.

Traub RD, Cunningham MO, Whittington MA (2011) Chemical synaptic and gap junctional interactions between principal neurons: Partners in epileptogenesis. Neural Networks 24:515–525.

Traub RD, Middleton SJ, Knöpfel T, Whittington MA (2008) Model of very fast (> 75 Hz) network oscillations generated by electrical coupling between the proximal axons of cerebellar Purkinje cells. Eur J Neurosci 28:1603–1616.

Tukker JJ, Fuentealba P, Hartwich K, Somogyi P, Klausberger T (2007) Cell type-specific tuning of hippocampal interneuron firing during gamma oscillations in vivo. J Neurosci 27:8184–8189.

Turesson HK, Rodríguez-Sierra OE, Pare D (2013) Intrinsic connections in the anterior part of the bed nucleus of the stria terminalis. J Neurophysiol 109:2438–2450.

Uhlhaas PJ, Mishara AL (2007) Perceptual anomalies in schizophrenia: Integrating phenomenology and cognitive neuroscience. Schizophr Bull 33:142–156.

Van Pett K, Viau V, Bittencourt JC, Chan RKW, Li HY, Arias C, Prins GS, Perrin M, Vale W, Sawchenko PE (2000) Distribution of mRNAs encoding CRF receptors in brain and pituitary of rat and mouse. J Comp Neurol 428:191–212.

Veening JG, Swanson LW, Sawchenko PE (1984) The organization of projections from the central nucleus of the amygdala to brainstem sites involved in central autonomic regulation: A combined retrograde transport-immunohistochemical study. Brain Res 303:337–357.

Waddell J, Morris RW, Bouton ME (2006) Effects of bed nucleus of the stria terminalis lesions on conditioned anxiety: aversive conditioning with long-duration conditional stimuli and reinstatement of extinguished fear. Behav Neurosci 120:324–336.

Walker DL, Davis M (1997) Double dissociation between the involvement of the bed nucleus of the stria terminalis and the central nucleus of the amygdala in startle increases produced by conditioned versus unconditioned fear. J Neurosci 17:9375–9383.

Walker DL, Miles LA, Davis M (2009) Selective participation of the bed nucleus of the stria terminalis and CRF in sustained anxiety-like versus phasic fear-like responses. Prog Neuro-Psychopharmacology Biol Psychiatry 33:1291–1308.

Wang L, Chen IZ, Lin D (2015) Collateral Pathways from the Ventromedial Hypothalamus Mediate Defensive Behaviors. Neuron 85:1344–1358.

Weller KL, Smith DA (1982) Afferent connections to the bed nucleus of the stria terminalis. Brain Res 232:255–270.

Wenzel JM, Cotten SW, Dominguez HM, Lane JE, Shelton K, Su ZI, Ettenberg A (2014) Noradrenergic beta-receptor antagonism within the central nucleus of the amygdala or bed nucleus of the stria terminalis attenuates the negative/anxiogenic effects of cocaine. J Neurosci 34:3467–3474.

Wenzel JM, Waldroup SA, Haber ZM, Su Z-I, Ben-Shahar O, Ettenberg A (2011) Effects of lidocaine-induced inactivation of the bed nucleus of the stria terminalis, the central or the basolateral nucleus of the amygdala on the opponent-process actions of self-administered cocaine in rats. Psychopharmacology (Berl) 217:221–230.

Whittington M a, Traub RD, Jefferys JG (1995) Synchronized oscillations in interneuron networks driven by metabotropic glutamate receptor activation. Nature 373:612–615.

Whittington MA, Traub RD, Kopell N, Ermentrout B, Buhl EH (2000) Inhibition-based rhythms: Experimental and mathematical observations on network dynamics. In: International Journal of Psychophysiology, pp 315–336.

Whittington MA, Traub RD (2003) Interneuron Diversity series: Inhibitory interneurons and network oscillations in vitro. Trends Neurosci 26:676–682.

Wilensky AE, Schafe GE, Kristensen MP, Ledoux JE (2006) Rethinking the Fear Circuit: The Central Nucleus of the Amygdala Is Required for the Acquisition, Consolidation, and Expression of Pavlovian Fear Conditioning. J Neurosci 26:12387–12396.

Wilson, C.J. and Kawaguchi, Y. (1996) The origins of two-state spontaneous membrane potential fluctuations of neostriatal spiny neurons. J. Neurosci. 16:2397-2410.

Yamaguchi T, Danjo T, Pastan I, Hikida T, Nakanishi S (2013) Distinct roles of segregated transmission of the septo-habenular pathway in anxiety and fear. Neuron 78:537–544.

Ylinen A, Bragin A, Nádasdy Z, Jandó G, Szabó I, Sik A, Buzsáki G (1995) Sharp wave-associated high-frequency oscillation (200 Hz) in the intact hippocampus: network and intracellular mechanisms. J Neurosci 15:30–46.

Zemankovics R, Veres JM, Oren I, Hájos N (2013) Feedforward inhibition underlies the propagation of cholinergically induced gamma oscillations from hippocampal CA3 to CA1. J Neurosci 33:12337–12351.